Universidade do Estado do Rio de Janeiro
Centro de Tecnologia e Ciências
Instituto de Química

Milena Mendonça Guimarães

Study of the catalytic conversion of CO_2 to CO by Reverse Water-Gas Shift Reaction (RWGS) as a decarbonization alternative for the petroleum industry

Rio de Janeiro
2024

Milena Mendonça Guimarães

Study of the catalytic conversion of CO_2 to CO by Reverse Water-Gas Shift Reaction (RWGS) as a decarbonization alternative for the petroleum industry

Dissertação apresentada, como requisito parcial para obtenção do título de Mestre, ao Programa de Pós-Graduação em Engenharia Química, da Universidade do Estado do Rio de Janeiro.
Área de concentração: Processos Químicos, Petróleo e Meio-ambiente.

Orientadores: Prof.ª Drª. Fatima Maria Zanon Zotin
Prof. Dr. André Luiz Hemerly Costa
Prof.ª Drª. Lucia Gorenstin Appel

Rio de Janeiro
2024

CATALOGAÇÃO NA FONTE
UERJ / REDE SIRIUS / BIBLIOTECA CTC/Q

G963 Guimarães, Milena Mendonça.

Study of the catalytic conversion of CO2 to CO by Reverse Water-Gas Shift Reaction (RWGS) as a decarbonization alternative for the petroleum industry. – 2024.

111 f.

Orientador (a): Fatima Maria Zanon Zotin
André Luiz Hemerly Costa
Lucia Gorenstin Appel

Dissertação (Mestrado) – Universidade do Estado do Rio de Janeiro. Instituto de Química.

1. Catálise – Teses. I. Zotin, Fatima Maria Zanon. II. Costa, André Luiz Hemerly. III. Appel, Lucia Gorenstin. IV. Universidade do Estado do Rio de Janeiro. Instituto de Química. V. Título.

CDU 541.128

gov.br Documento assinado digitalmente
MILENA MENDONCA GUIMARAES
Data: 26/03/2025 16:42:51-0300
Verifique em https://validar.iti.gov.br

_____
Assinatura

10/10/2024
Data

Milena Mendonça Guimarães

Study of the catalytic conversion of CO_2 to CO by Reverse Water-Gas Shift Reaction (RWGS) as a decarbonization alternative for the petroleum industry

Dissertação apresentada, como requisito parcial para obtenção do título de Mestre, ao Programa de Pós-Graduação em Engenharia Química, da Universidade do Estado do Rio de Janeiro.
Área de concentração: Processos Químicos, Petróleo e Meio Ambiente.

Aprovada em 10 de outubro de 2024.

Banca Examinadora:

Documento assinado digitalmente
gov.br
FATIMA MARIA ZANON ZOTIN
Data: 25/10/2024 07:33:36-0300
Verifique em https://validar.iti.gov.br

_____

Prof.ª Drª. Fatima Maria Zanon Zotin (Orientadora)

Instituto de Química – UERJ

Documento assinado digitalmente
gov.br
ANDRE LUIZ HEMERLY COSTA
Data: 26/10/2024 13:43:12-0300
Verifique em https://validar.iti.gov.br

_____

Prof. Dr. André Luiz Hemerly Costa (Orientador)

Instituto de Química - UERJ

Documento assinado digitalmente
gov.br
LUCIA GORENSTIN APPEL
Data: 27/10/2024 17:24:05-0300
Verifique em https://validar.iti.gov.br

_____

Prof.ª Dr.ª Lucia Gorenstin A

Instituto Nacional de Tecnologia - INT

Documento assinado digitalmente
gov.br
LUZ AMPARO PALACIO SANTOS
Data: 29/10/2024 09:06:25-0300
Verifique em https://validar.iti.gov.br

_____

Prof.ª Drª. Luz Amparo Palacio Santos

Instituto de Química - UERJ

Documento assinado digitalmente
gov.br
ERIKA BATISTA SILVEIRA
Data: 14/03/2025 12:19:07-0300
Verifique em https://validar.iti.gov.br

_____

Prof.ª Drª. Erika Batista Silveira

Instituto Nacional de Tecnologia - INT

Documento assinado digitalmente
gov.br
MONICA ANTUNES PEREIRA DA SILVA
Data: 18/03/2025 22:27:59-0300
Verifique em https://validar.iti.gov.br

_____

Prof.ª Drª. Monica Antunes Pereira da Silva

Escola de Química - UFRJ

Rio de Janeiro

2024

DEDICATÓRIA

Dedico esse trabalho a Deus, à minha família e aos meus orientadores, com toda a alegria e gratidão.

AGRADECIMENTOS

A Deus, digno de toda a honra e toda a glória, por Seu infinito amor, que faz o impossível em minha vida, segundo após segundo.

A Jesus Cristo, meu Senhor e Salvador, minha força e minha luz, por sua graça incomparável e pela esperança inabalável da vida eterna.

Ao Espírito Santo, por me orientar, inspirar, capacitar, renovar e nunca me deixar só.

À minha mãe, Cleidimar Guimarães, que me alfabetizou e sempre entrega tudo de si pela minha vida em cuidado, ensino, exemplo e oração.

Ao meu pai, Claudio Guimarães, que sempre faz tudo o que estiver ao alcance para eu me tornar continuamente a minha melhor versão.

À minha avó materna, Olivete Mendonça, grande exemplo de resiliência, que sempre marca presença nos meus momentos mais especiais.

Ao meu avô materno, Alexandre Mendonça (*in memoriam*), cuja tranquilidade e bom humor me inspiram até hoje.

À minha avó paterna, Sirlei Guimarães (*in memoriam*), que por mim orava continuamente e tinha profundo carinho.

Ao meu avô paterno, Ildefonso Guimarães (*in memoriam*), que mesmo o fato de não o ter conhecido não impediu que fosse fundamental na minha história.

Ao meu tio, Anderson Mendonça, figura marcante e muito querida na minha vida.

Aos meus três orientadores, cuja direção foi imprescindível para a realização deste trabalho, e que sempre terão minha admiração e gratidão por todo o seu apoio, suporte e paciência: Professora Fatima Zotin, que me acompanha desde minha segunda iniciação científica, e venturosamente me apresentou às particularidades desta reação tão fascinante que é a RWGS; Professor André Hemerly, que me aconselhou e incentivou na continuidade dos estudos logo após o fim da graduação, decisão que hoje é motivo de grande satisfação; e Professora Lucia Appel, que tão gentilmente contribuiu com este projeto, estreitando a duradoura parceria de sucesso entre o INT e a UERJ.

A toda a equipe do Laboratório de Catálise em Petróleo e Meio Ambiente (LCPMA/IQ/UERJ), cuja supervisão e auxílio foram fundamentais na realização de

todos os testes catalíticos, em especial Samara Montani, que me ensinou a vivenciar as glórias e dores da ciência experimental com persistência e bom ânimo, e João Carlos Soares, que me ensinou que um dos itens mais importantes da metodologia de toda pesquisa científica é a curiosidade.

A Daniela Trespalacios, que tão solicitamente me acompanhou e auxiliou quando comecei a me aventurar no mundo da pesquisa experimental de pós-graduação.

Ao Laboratório de Materiais em Engenharia Química (LabMEQ/IQ/UERJ), de cuja estrutura também usufruí na parte experimental deste trabalho, e a toda a sua amável e acolhedora equipe.

A toda a equipe do Laboratório Multiusuário de Difração de Raios X (LMDRX/IQ/UERJ), que com excelência realizou as análises de DRX apresentadas.

Ao Instituto Nacional de Tecnologia (INT) e a toda a sua equipe, que, além de nos ceder o catalisador estudado nesta dissertação, me recebeu com grande cortesia em minha visita de 12 de agosto de 2024.

A toda a equipe do Colégio Santamarinha, que me proporcionou uma sólida base educacional para ir muito mais longe do que jamais imaginei. Aos Professores Manuel Simão Santamarinha e Vania Santamarinha, que sempre me inspiraram e acreditaram em mim, e a toda a sua família. A todos os professores e colegas que tive no Ensino Fundamental, que guardo com carinho no coração.

A toda a equipe da Fundação de Apoio à Escola Técnica (FAETEC), onde tive um tempo muito proveitoso e agradável. A todos os professores e colegas que tive no Ensino Técnico, que fizeram meu início de adolescência bastante especial.

A toda a equipe do Colégio Pedro II, onde meu amor pelas Ciências Exatas foi confirmado e nutrido, embora minha experiência com outras disciplinas também tenha sido bastante enriquecedora. A todos os professores e colegas que tive no Ensino Médio, que me incentivaram muito e tornaram minha adolescência feliz e recheada de aprendizado.

A toda a equipe da Universidade do Estado do Rio de Janeiro, que desde a minha adolescência sacramenta a mudança da minha vida através da busca do conhecimento. A todos os meus professores e colegas na Graduação, tendo cada um deixado uma contribuição muito especial para que o presente momento se concretizasse.

Às Professoras Lílian de Senna e Deborah César, que me concederam a oportunidade de participar do meu primeiro projeto de Iniciação Científica, no Laboratório de Eletroquímica e Corrosão (LEC/IQ/UERJ), experiência que foi preciosa no meu desenvolvimento acadêmico e pessoal.

A Antonio de Castro, cuja prestimosa ajuda foi crucial nos primeiros passos de minha trajetória científica, assim como a de Ana Bauerfeldt, Thaís Lima, William Beruth, Camila Santos e toda a equipe do LEC, da qual tenho memórias muito felizes.

Aos Professores Fatima Zotin, José Zotin, José Zanon Zotin e Luz Palacio, que me concederam a oportunidade de participar do meu segundo projeto de Iniciação Científica, em parceria com o Centro Federal de Educação Tecnológica Celso Suckow da Fonseca (CEFET/RJ), guiando-me na exploração do fantástico universo da modelagem computacional, no qual quero muito continuar me aprofundando daqui em diante.

A toda a equipe do Programa de Pós-Graduação em Engenharia Química da UERJ (PPG-EQ/UERJ), pela oportunidade de usufruir de sua formidável estrutura, que tem me proporcionado contínuo aprimoramento profissional e acadêmico, bem como aprofundamento em questões altamente relevantes no campo da Engenharia Química, possibilitando o desenvolvimento do presente trabalho.

À Coordenação do PPG-EQ/UERJ, Professora Cristiane Henriques e Professor André Hemerly, pelo diuturno empenho no desenvolvimento do Programa.

À Secretaria do PPG-EQ/UERJ, Francisco Júnior e Renata Ximenes, de quem nada escapa na organização do dia-a-dia do Programa, sempre muito antenados, gentis e atenciosos.

Aos Professores Eduardo Lima, Lílian de Senna, Mariana Marques, André Alberton, Fatima Zotin, Márcio Paredes, André Hemerly e Nathalia Vernin, que me orientaram nas disciplinas do mestrado, e a todos os colegas que me acompanham ao longo desta incrível e inestimável jornada.

A toda a equipe do Programa Línguas para Comunidade (Licom/ILE/UERJ), em especial à Coordenadora do Projeto em Línguas Adicionais (PLA), Professora Sabrina de Oliveira, e ao Professor Flavio Souza, que ministrou o Curso de Inglês com Fins Acadêmicos, que teve um papel decisivo no meu contato com a literatura científica ao longo do mestrado e até hoje produz frutos na minha vida acadêmica, propiciando a redação desta dissertação em língua inglesa.

Aos amigos que fazemos pelo caminho, como Rayssa Cardoso, Kaio Tavares e Douglas Igor, que me proporcionaram tanta alegria nos dias tranquilos e ajuda nos dias difíceis (e vice-versa).

Aos meus irmãos em Cristo, que oraram por mim e me deram força e encorajamento ao longo de minha trajetória acadêmica e espiritual.

À Banca Examinadora, que, além de dedicar tempo e energia à avaliação deste trabalho, me concedeu a honra de sua presença em minha defesa de dissertação de mestrado.

Ao apoio financeiro do Programa de Recursos Humanos da Agência Nacional do Petróleo, Gás Natural e Biocombustíveis – PRH-ANP, suportado com recursos provenientes do investimento de empresas petrolíferas qualificadas na Cláusula de P, D&I da Resolução ANP nº 50/2015.

Ao Coordenador do PRH 24.1, Professor Márcio Paredes, aos Pesquisadores Visitantes Marcos José da Silva e Walmir dos Santos e ao Apoio Técnico de Maxwell Schiavon e Camilla Vianna; a toda a equipe do PRH 24.1, por seu incansável trabalho em prol dos bolsistas, mantendo constantemente um canal de comunicação transparente e eficiente com os alunos desse programa que vem sendo grandemente edificante e importante em minha vida profissional e acadêmica desde a graduação.

Este sistema belíssimo do Sol, planetas e cometas só pode ter surgido do conselho e domínio de um Ser inteligente e poderoso.

Sir Isaac Newton

RESUMO

GUIMARÃES, M. M. *Study of the catalytic conversion of CO_2 to CO by Reverse Water-Gas Shift Reaction (RWGS) as a decarbonization alternative for the petroleum industry*. 2024. 111 f. Dissertação (Mestrado em Engenharia Química) – Instituto de Química, Universidade do Estado do Rio de Janeiro, Rio de Janeiro, 2024.

O aumento contínuo da concentração de gases do efeito estufa na atmosfera desde a Revolução Industrial é a origem das mudanças climáticas que acometem o planeta. A resolução dessa questão passa pela redução das emissões antropogênicas de CO_2; desta forma, torna-se importante desenvolver alternativas para aproveitar o CO_2 como matéria-prima para a obtenção de produtos de interesse comercial. A reação de deslocamento gás-água reversa (bastante conhecida pelo seu nome em inglês, *reverse water-gas shift*, comumente abreviado como RWGS), apontada como uma rota promissora nos esforços direcionados à descarbonização, consiste na hidrogenação do dióxido de carbono, dando origem a água e monóxido de carbono, que, por sua vez, é amplamente empregado na indústria química para a fabricação de uma grande variedade de produtos. No entanto, a existência de reações competitivas e a natureza endotérmica da reação RWGS fazem com que sua aplicação em escala industrial exija o desenvolvimento de catalisadores mais ativos e seletivos, processo que necessariamente envolve a busca por um conhecimento mais profundo da cinética da reação. Nesse contexto, o presente trabalho tem o objetivo de estudar o desempenho do catalisador comercial de $CuO/ZnO/Al_2O_3$ sob diferentes condições operacionais e obter valores de parâmetros cinéticos para as expressões de taxa de reação disponíveis na literatura. Para esse fim, foram realizados testes em temperaturas fixas de 330 °C, 380 °C e 430 °C (testes em patamares de temperatura) sob diferentes velocidades espaciais (18 $m^3\ kg^{-1}\ h^{-1}$, 30 $m^3\ kg^{-1}\ h^{-1}$ e 42 $m^3\ kg^{-1}\ h^{-1}$) e razões molares H_2/CO_2 (1:1, 2.5:1 e 4:1), além de testes em rampa de temperatura (testes de *light-off*) da temperatura ambiente até 500 °C. A seletividade a monóxido de carbono obtida foi de 100% em todos os experimentos. Os testes em patamares de temperatura permitiram verificar que maiores temperaturas, maiores razões H_2/CO_2 e menores velocidades espaciais proporcionam conversões de CO_2 mais altas. Os parâmetros cinéticos foram ajustados a partir dos dados experimentais das curvas de *light-off* fornecidas pelos testes em rampa de temperatura, devido à concordância observada entre essas curvas e os resultados dos testes isotérmicos. Os parâmetros foram estimados usando um modelo pseudo-homogêneo de reator de leito fixo em estado estacionário, aplicando as expressões de taxa de reação propostas por três diferentes grupos de pesquisa. A simulação das curvas de *light-off* com os parâmetros obtidos forneceu uma previsão satisfatória das tendências observadas experimentalmente, indicando que as curvas de *light-off* podem ser uma abordagem prática para a extração de informações cinéticas de uma forma mais simples e com menor número de experimentos necessários.

Palavras-chave: CO_2; catálise; descarbonização; reação de deslocamento gás-água reversa; modelagem.

ABSTRACT

GUIMARÃES, M. M. *Study of the catalytic conversion of CO_2 to CO by Reverse Water-Gas Shift Reaction (RWGS) as a decarbonization alternative for the petroleum industry*. 2024. 111 f. Dissertação (Mestrado em Engenharia Química – Instituto de Química, Universidade do Estado do Rio de Janeiro, Rio de Janeiro, 2024.

The continuous increase in the concentration of greenhouse gases in the atmosphere since the Industrial Revolution is the origin of the climate change that affects the planet. The solution to this issue involves reducing anthropogenic CO_2 emissions; therefore, it is important to develop alternatives for employing the CO_2 as a raw material to obtain products with commercial interest. The reverse water-gas shift reaction (commonly abbreviated as RWGS), identified as a promising route in efforts aimed at decarbonization, consists of the hydrogenation of carbon dioxide, giving rise to water and carbon monoxide, which, in turn, is widely used in the chemical industry to manufacture a broad variety of products. However, the existence of competitive reactions and the endothermic nature of the RWGS reaction mean that its application on an industrial scale requires the development of more active and selective catalysts, a process that necessarily involves the search for a deeper understanding of the reaction kinetics. In this scenario, the present work aims to study the performance of the commercial $CuO/ZnO/Al_2O_3$ catalyst under different operating conditions and to obtain kinetic parameter values for reaction rate expressions available in the literature. For this purpose, tests were performed at fixed temperatures of 330 °C, 380 °C and 430 °C (tests at temperature levels) under different space velocities (18 $m^3\ kg^{-1}\ h^{-1}$, 30 $m^3\ kg^{-1}\ h^{-1}$ and 42 $m^3\ kg^{-1}\ h^{-1}$) and H_2/CO_2 molar ratios (1:1, 2.5:1 and 4:1), in addition to temperature ramp tests (light-off tests) from room temperature to 500 °C. The selectivity to carbon monoxide obtained was 100% in all experiments. The fixed-temperature tests allowed verifying that higher temperatures, higher H_2/CO_2 ratios, and lower space velocities provide higher CO_2 conversions. The kinetic parameters were fitted from the experimental data of the light-off curves provided by the temperature ramp tests, due to the agreement observed between these curves and the results of the isothermal tests. The parameters were estimated using a pseudo-homogeneous model of a steady-state fixed-bed reactor, applying the reaction rate expressions proposed by three different research groups. The simulation of the light-off curves with the obtained parameters provided a satisfactory prediction of the experimentally observed trends, indicating that the light-off curves can be a practical approach for the extraction of kinetic information in a simpler way and with a smaller number of experiments required.

Keywords: CO_2; catalysis; decarbonization; reverse water-gas shift reaction; modeling.

LISTA DE FIGURAS

LISTA DE TABELAS

LISTA DE ABREVIATURAS E SIGLAS

CCS	Carbon Capture and Storage
CCU	Carbon Capture and Utilization
CCUS	Carbon Capture, Utilisation and Storage
FTS	Fischer-Tropsch Synthesis
GHSV	Gas Hourly Space Velocity
IBP	Instituto Brasileiro de Petróleo e Gás
IEA	International Energy Agency
IPCC	Intergovernmental Panel on Climate Change
ECMWF	European Center for Medium-Range Weather Forecasts
NIST	National Institute of Standards and Technology
RWGS	Reverse Water-Gas Shift
WGS	Water-Gas Shift

LISTA DE SÍMBOLOS

$\Delta G°_{298\ K}$	Standard Gibbs free energy of formation at 298 K (kJ mol^{-1})
$\Delta H°_{R,\ 298\ K}$	Standard enthalpy of reaction at 298 K (kJ mol^{-1})
S	Vacant active sites (dimensionless)
r_j	Rate of reaction j (mol g^{-1} h^{-1}, mol kg^{-1} s^{-1})
k_1	Rate constant of the RWGS reaction (atm^{-1} h^{-1}, mol kg^{-1} s^{-1} bar^{-1}, mol kg^{-1} s^{-1} $bar^{-0.5}$)
L_0	Concentration of active sites of fresh catalyst (mol g^{-1})
P_i	Partial pressure of component i (Pa, atm, bar)
K_1	Equilibrium constant of the RWGS reaction (dimensionless)
K_8*	Equilibrium constant of reaction (8) (atm^{-1})
K_{24}*	Equilibrium constant of reaction (24) (atm)
K_{H2O}	Adsorption equilibrium constant for H_2O (bar^{-1})
K_{H2}	Adsorption equilibrium constant for H_2 (bar^{-1})
K_{15}*	Equilibrium constant of reaction (15) (dimensionless)
K_{16}*	Equilibrium constant of reaction (16) (dimensionless)
T	Temperature (°C, K)
R	Universal gas constant (J mol^{-1} K^{-1}, kcal mol^{-1} K^{-1}, L atm mol^{-1} K^{-1})
S_1	Site where CO and CO_2 adsorb competitively (dimensionless)
S_2	Site where H_2 and H_2O adsorb competitively (dimensionless)
K_{CO}	Adsorption equilibrium constant for CO (bar^{-1})
K_{CO2}	Adsorption equilibrium constant for CO_2 (bar^{-1})
f_i	Parcial fugacity of component i (bar)
$k_{1,0}$	Pre-exponential factor (atm^{-1} h^{-1})

$E_{a,1}$	Apparent activation energy of RWGS reaction (kJ mol^{-1}, kcal mol^{-1})
W	Catalyst mass (kg, g)
F_i	Molar flow rate of component i (mol s^{-1}, mol h^{-1})
R_i	Generation or consumption rate of component i per mass of catalyst (mol s^{-1} kg^{-1})
dW	Catalyst mass element (kg)
ν_i	Stoichiometric coefficient of component i in the RWGS reaction (dimensionless)
m	Dimensionless mass
W_0	Total catalyst mass used in the experiment (kg, g)
y_i	Molar fraction of component i in the gas phase (dimensionless)
P	Pressure (Pa, atm, bar)
A	Dimensionless parameter A
B	Dimensionless parameter B
D	Dimensionless parameter D
E	Dimensionless parameter E
G	Dimensionless parameter G
H	Dimensionless parameter H
I	Dimensionless parameter I
J	Dimensionless parameter J
L	Dimensionless parameter L
N	Dimensionless parameter N
Q	Dimensionless parameter Q
q	Volumetric flow rate (m^3 s^{-1}, mL min^{-1}, L h^{-1})
f_P	Correction factor for pressure (bar Pa^{-1})
f_{obj}	Objective function (dimensionless)

X_{CALC}	Calculated CO_2 conversion (dimensionless)
X_{EXP}	Experimental CO_2 conversion (dimensionless)
X	CO_2 conversion (dimensionless)
ΔG_R	Gibbs free energy of reaction (J mol^{-1})
$\Delta G°_R$	Standard Gibbs free energy of reaction (J mol^{-1})
$\Delta H°_R$	Standard enthalpy of reaction (J mol^{-1})
R^2	Coefficient of determination (dimensionless)
V	Volume (m^3, L)
n	Number of moles (mol)
F_T	Total molar flow rate (mol s^{-1}, mol h^{-1})
X_{eq}	CO_2 conversion at equilibrium (dimensionless)
P^0_i	Partial pressure of component i at the inlet (atm)
P^{eq}_i	Partial pressure of component i at equilibrium (atm)

SUMMARY

INTRODUCTION

In recent decades, our planet has been passing through a series of climate changes, associated with rising sea levels, global average temperatures, and ocean acidification (United States Global Change Research Program, 2017). According to the Intergovernmental Panel on Climate Change (IPCC) in its Sixth Assessment Report on Climate Change (2023), the planet's temperature increased between 1970 and 2020 at a rate greater than in any other 50-year period in at least the last two millennia. From 2013 to 2022, the global surface temperature was approximately 1.15 °C above that corresponding to the period between 1850 and 1900 (IPCC, 2023). The 2023 year was confirmed as the hottest on record (Poynting; Rivault, 2024), exceeding the average pre-industrial level by 1.48 °C, as attested at the beginning of 2024 by the European Center for Medium-Range Weather Forecasts (ECMWF).

Such observed warming has been caused by anthropogenic action, mainly due to the progressive greenhouse gases concentration increasing in the Earth's atmosphere (IPCC, 2023). Without the greenhouse effect, the global average temperature would be -18 °C, making life unfeasible on the planet (Casagrande; Silva Junior; Mendonça, 2011; Ambrizzi *et al*., 2021). Nevertheless, climate system changes, driven by greenhouse gases emissions from human activities, have manifested themselves through the frequency and magnitude of extreme weather events, representing a risk to humanity (IPCC, 2023).

CO_2 accounts for the majority of anthropogenic greenhouse gas emissions, with 74.1% by mass; in second place comes CH_4, with 17.3%, followed by N_2O (6.2%) and fluorinated gases (2.4%) (Climate Watch, 2022a). For this reason, reducing CO_2 emissions becomes an urgent need (Shekari *et al*., 2023). In order to achieve this goal, three main alternatives arise.

The first option involves reducing the amount of CO_2 produced, which requires improvements in energy efficiency and prioritization of less carbon-intensive energy sources, such as renewable energy and hydrogen, to the detriment of burning fossil fuels. This complete change represents a difficult challenge to be met on a time scale of at least decades (Ghodoosi; Khosravi-Nikou; Shariati, 2017; Pöhlmann; Jess, 2016; Ravanchi; Sahebdelfar, 2021; Okonkwo; Yablonsky; Biswas, 2020; Pérez-Alonso *et al*., 2008). The second option involves CO_2 Capture and Storage (CCS),

which consists of CO_2 separation and its transporting to remote locations for subsequent long-term storage, in order to avoid its release into the atmosphere (Ghodoosi; Khosravi-Nikou; Shariati, 2017; Ateka *et al*., 2022; Wang *et al*., 2022; Oshima *et al*., 2014; Suescum-Morales; Jiménez; Fernández-Rodríguez, 2022; Tawalbeh *et al*., 2023; Elsernagawy *et al*., 2020; Ravanchi; Sahebdelfar, 2021; Daza *et al*., 2016; Pöhlmann; Jess, 2016). The CCS strategy has already proven itself technically viable, with the potential to mitigate global CO_2 emissions by nearly 20% until 2050 (Kamkeng *et al*., 2021; Suescum-Morales; Jiménez; Fernández-Rodríguez, 2022; Tawalbeh *et al*., 2023; Cao *et al*., 2020; Daza; Kuhn, 2016). Nonetheless, as CCS develops, it will be progressively restricted by the existence of natural safe storage alternatives (Pahija *et al*., 2022). Besides, these technologies have high energy consumption (which could result in even more emissions) and a high cost of investment, transport and storage, which makes their commercial implementation on a large scale difficult and curbs their contribution to mitigating climate change (Kamkeng *et al*., 2021; Cao *et al*., 2020; Kaiser *et al*., 2013; Daza; Kuhn, 2016) Therefore, CCS by itself is unable to reduce carbon dioxide emissions (Pahija *et al*., 2022). The third option is the capture and usage of CO_2 (approach commonly abbreviated as CCU, an acronym for Carbon Capture and Utilization) (Ghodoosi; Khosravi-Nikou; Shariati, 2017; Shekari *et al*., 2023; Suescum-Morales; Jiménez; Fernández-Rodríguez, 2022; Pöhlmann; Jess, 2016). Similarly, as in CCS, CCU aims to capture CO_2 from several sources (e.g. industries and power plants) and to avert its emission (Ravanchi; Sahebdelfar, 2021). However, in CCU carbon dioxide is employed as feedstock for processes that transform it into different compounds (Kaiser *et al*., 2013; Ravanchi; Sahebdelfar, 2021). Thereby, in addition to acting on climate change mitigation, CCU utilizes the hugely plentiful CO_2 to obtain value-added products, such as alcohols, aromatics, olefins and fuels (Suescum-Morales; Jiménez; Fernández-Rodríguez, 2022; Daza; Kuhn, 2016; Nezam *et al*., 2021). The fact that such an approach provides a continuous supply of carbon-based compounds, generating profitability and minimizing the depletion of fossil fuels, has attracted the attention of researchers in catalysis, process design and materials (Daza *et al*., 2016; Okonkwo; Yablonsky; Biswas, 2020; Nezam *et al*., 2021). For this reason, the term CCS gave way to CCUS (Carbon Capture, Utilisation and Storage) in which the economic value of captured CO_2 is enhanced by its application (Kamkeng *et al*., 2021).

Since the beginning of the millennium, the energy sector's share of global greenhouse gas emissions has remained above 70% (Climate Watch, 2022b); the report The Oil and Gas Industry in Net Zero Transitions (2023), published by the International Energy Agency (IEA), states that, of the total emissions corresponding to this sector, in turn, almost 15% originate from oil and gas production, transport and processing. To transform this reality, Carbon Capture, Utilization, and Storage technologies represent a valuable tool for the oil and gas industry, being a source of opportunities both in financial and technological terms, as emphasized by the Brazilian Oil and Gas Institute in its publication Carbon Capture and Storage Technologies (CCUS) and its Importance for the Energy Transition in Brazil (IBP, 2023).

Meanwhile, CO_2 is a linear molecule in which the four carbon electrons are involved in covalent double bonds with oxygen atoms. Due to the strength of these bonds between oxygen and carbon, the carbon dioxide molecule is characterized by high stability and an intrinsic thermodynamic inertia that makes its direct conversion difficult (Kamkeng *et al*., 2021; Liu *et al*., 2017; Su *et al*., 2017). On the other hand, H_2 is considered a high-energy electron donor, and its standard Gibbs free energy ($\Delta G^\circ_{298\ K}$ (H_2) = 0) is higher than that of CO_2 ($\Delta G^\circ_{298\ K}$ (CO_2) = -394.389 kJ mol^{-1}), thus carbon dioxide can be activated through its reduction by H_2 (Dai *et al*., 2017; Kamkeng *et al*., 2021; Chase, Jr., 1998). This fact may explain the broad interest in the catalytic hydrogenation of CO_2 as a promising way to provide added value to CO_2, through the production of a variety of products, including carbon monoxide (CO), much more reactive than CO_2 (Desgagnés; Iliuta, 2023; Braga; Vidinha; Rossi, 2020; Liu *et al*., 2020a; Bahmanpour *et al*., 2020; Su *et al*., 2017). CO is a building block widely used in the chemical industry to obtain fuels, polymers, chemicals, and hydrocarbons (Desgagnés; Iliuta, 2023; Pahija *et al*., 2022).

Examples of hydrogenation reactions comprise methanation, reverse water-gas shift (RWGS), and methanol synthesis. Among them, the RWGS reaction emerges as the most attractive approach, being an essential intermediate stage in the direct thermochemical CO_2 conversion processes (Dai *et al*., 2017; Su *et al*., 2017; Liu *et al*., 2020b; Chen *et al*., 2020). In the RWGS reaction, carbon dioxide reacts with hydrogen, thus generating water and carbon monoxide, as shown in equation (1):

$$H_2 + CO_2 \rightleftharpoons CO + H_2O \quad (1)$$

The chemical equilibrium of this reaction is pressure-independent, and therefore capable of operating at atmospheric pressure, reducing investment and operational costs without compromising carbon monoxide yield (Desgagnés; Iliuta, 2023; Chen *et al*., 2020; Bown *et al*., 2021). CO, in turn, can be employed in a mixture with H_2 (denominated synthesis gas, or "syngas"), as a reagent in methanol, ethanol, dimethyl ether, and Fischer-Tropsch fuels production (Bown *et al*., 2021; Gandara-Loe *et al*., 2021; Liu *et al*., 2020b). Hence, the RWGS reaction stands out as an interesting option in Carbon Capture, Utilization, and Storage, allowing, more practically and effectively, the transition of CO_2 to added value products as hydrocarbon chains (Chen *et al*., 2020; Chen *et al*., 2021; Gandara-Loe *et al*., 2021; Su *et al*., 2017).

Despite this, the RWGS reaction still has some problems to overcome before establishing itself as an industrial-scale CCUS alternative. As a result of the low chemical reactivity of CO_2, its conversion processes have a high energy activation to be surpassed (Liu *et al*., 2017; Kamkeng *et al*., 2021; Gandara-Loe *et al*., 2021). Furthermore, this reaction is moderately endothermic ($\Delta H°_{R,\ 298\ K}$ = +41.2 kJ mol^{-1}), being thermodynamically favored at elevated temperatures, necessary for the cleavage of the chemical bonds between carbon and oxygen (Desgagnés; Iliuta, 2023; Liu *et al*., 2020a; Liu *et al*., 2020b; Gandara-Loe *et al*., 2021). Whereas a lower reaction temperature allows for lower capital costs and energy expenditures, it is essential to develop ways to operate the process under these conditions (Braga; Vidinha; Rossi, 2020; Su *et al*., 2017). However, CO methanation and Sabatier reaction are instances of side reactions that can take part under similar reaction conditions, competing with RWGS for the available H_2 (Gandara-Loe *et al*., 2021). In this case, the exothermic nature of these reactions favors them to occur at low temperatures (Gandara-Loe *et al*., 2021; Liu *et al*., 2020a).

There is a clear need to design catalysts that are not only highly active, in order to allow the use of the RWGS reaction at lower temperatures, but also highly selective to carbon monoxide, in addition to presenting availability and low cost, ensuring a commercially viable large-scale process (Bown *et al*., 2021; Gandara-Loe *et al*., 2021; Kamkeng *et al*., 2021). To achieve this purpose, it is necessary to

acquire greater knowledge about the RWGS reaction mechanism and its kinetic over commercial and novel catalysts (Su *et al*., 2017).

However, even for commercial catalysts, the availability of kinetic studies of RWGS reaction is scarce. This is closely related to the fact that the production of a kinetic study is a difficult and time-consuming process that requires dozens – or even hundreds – of experiments, using several different combinations of operating conditions. Still, the scope of accuracy of the kinetic parameters provided by these studies is limited by the range of conditions used, especially with regard to temperature. This path would be greatly facilitated if it were possible to extract kinetic data from light-off curves. If the kinetic parameters could be obtained from the CO_2 conversion data along a temperature ramp (light-off curves), this process would be quite facilitated experimentally, because the number of tests required would be much smaller. In addition, this could enhance the accuracy of the model due to the large number of temperatures evaluated.

In this context, the present work aims to study the performance of the commercial catalyst $CuO/ZnO/Al_2O_3$ in the RWGS reaction and carry out a kinetic study, in order to obtain parameter values for reaction rate expressions available in the literature that provides a satisfactory adjust to the experimental data (light-off curves). This information is expected to provide more tools for increasing the degree of maturity of the RWGS technology, taking into account the trade-off between energy demands and thermodynamic restraints of the reaction, thus contributing to decarbonization efforts (Dai *et al*., 2018; Galhardo *et al*., 2021).

1 **LITERATURE REVIEW**

1.1 **Catalysts for RWGS reaction**

Catalysts used in heterogeneous catalysis for the RWGS reaction consist typically of well-dispersed metals supported on high surface area metal oxides (Villora-Picó *et al*., 2024; Zhang *et al*., 2022). Regarding the metal sites, literature reports both noble metals (Pt, Pd, Rh, Ru, Au) and non-noble metals (Fe, Mo, Cu, Co, Ni) (Bown *et al*., 2021; Zhang *et al*., 2022).

Noble metal catalysts have been widely investigated in RWGS reaction, presenting high activity and selectivity, and higher reaction rates (Su *et al*., 2017; González-Castaño; Dorneanu; Arellano-García, 2021). Nevertheless, these metals are relatively scarce, and their costs are elevated, hindering the application of such materials for large-scale CO_2 utilization (Su *et al*., 2017; Vu *et al*., 2022; Bown *et al*., 2021). In this sense, several efforts have been invested in the design and study of catalysts that present good catalytic performance and cost-effectiveness, an issue in which non-noble metals have shown to be promising alternatives (Su *et al*., 2017; Vu *et al*., 2022; González-Castaño; Dorneanu; Arellano-García, 2021).

Nickel is also an economical and highly active non-noble metal (Chen *et al*., 2021). These features, together with its well-doing on the forward water-gas shift (WGS) reaction, make this material a focus of wide interest for studies of the RWGS reaction (Liu *et al*., 2020a). Wolf, Jess, and Kern (2016) used a commercial steam reforming catalyst (Ni-Al_2O_3) and obtained CO_2 conversions close to equilibrium, observing considerable stability at 900 °C. With a Ni/CeO_2-Al_2O_3 catalyst, Yang *et al*. (2018) obtained CO_2 conversions above 60% at temperatures from 600 °C onwards. Conversely, Ni-based catalysts are also known to face problems such as the deactivation by coke deposition and the occurrence of undesired methanation reactions, (2) and (3) (Chen *et al*., 2021; Lalinde *et al*., 2020). These reactions are exothermic ($\Delta H°_{R,\ 298\ K}$ = -165.0 kJ mol^{-1} for reaction (2) and $\Delta H°_{R,\ 298\ K}$ = -206.1 kJ mol^{-1} for reaction (3)), thus an elevated selectivity toward CH_4 is favored at low temperatures (particularly below 500 °C), more than with noble metals (Vu *et al*., 2022; Reinikainen *et al*., 2022; Meng *et al*., 2018).

$$4\,H_2 + CO_2 \rightleftharpoons CH_4 + 2\,H_2O \quad (2)$$

$$3\,H_2 + CO \rightleftharpoons CH_4 + H_2O \quad (3)$$

Some of the properties that make Fe-based catalysts reputed among the most successful at high temperatures include good adsorption of intermediates, sintering tolerance, thermal stability, and elevated oxygen mobility (Kamkeng *et al*., 2021; Pastor-Pérez *et al*., 2017). In the literature, iron is described as an active metal capable of providing reasonable CO_2 conversions and CO selectivities (González-Castaño; Dorneanu; Arellano-García, 2021). Chou, Loiland, and Lobo (2019) studied an unsupported iron catalyst derived from magnetite (Fe_2O_3) between 450 °C and 500 °C at atmospheric pressure, obtaining elevated CO formation rate and stability, in addition to selectivity greater than 99% under a 1:1 H_2/CO_2 ratio. Under low temperature (150 °C), Yamaoka *et al*. (2024) investigated a series of Fe-supported catalysts (Fe/CeO_2, $Fe/Ce_{0.5}Zr_{0.5}O_2$ and $Fe/Ce_{0.4}Al_{0.1}Zr_{0.5}O_2$) with an electric field, reporting high CO_2 conversions and selectivities of about 100%.

On the other hand, Cu-based catalysts still stand out as the most studied for the RWGS reaction, being reported as highly active, selective, and cost-effective catalysts, with promising potential to replace noble metals (Vu *et al*., 2022; Reinikainen *et al*., 2022; Reina; Odriozola; Arellano-Garcia, 2021). In fact, copper catalysts achieve high CO_2 conversions without CH_4 formation, in addition to being more suitable than iron catalysts for operating at low temperatures (Chen *et al*., 2021; Kamkeng *et al*., 2021). Pahija *et al*. (2022) described copper as an abundant metal with an affinity for CO_2 and H_2 adsorption. Moreover, copper catalysts have already commercial applications in WGS and methanol synthesis processes and have shown great stability under high carbon dioxide concentrations (Su *et al*., 2017; Elsernagawy *et al*., 2020). At high temperatures, however, copper nanoparticles tend to sinter (Reina; Odriozola; Arellano-Garcia, 2021). Another issue is the oxidation of part of the metallic Cu by CO_2, causing agglomeration with consequent loss of metal surface area and, therefore, activity and stability over time (Reina; Odriozola; Arellano-Garcia, 2021; Liu *et al*, 2020b; Bown *et al*., 2021). Consequently, research have been directed to enhance the activity and stability of copper RWGS catalysts (Reina; Odriozola; Arellano-Garcia, 2021; Liu *et al*, 2020b). Some of the strategies employed in this regard include dispersion of the active copper on several supports,

search for improvement of parameters that influence catalytic performance (such as morphology, Cu content, and surface area), and use of promoters (Reina; Odriozola; Arellano-Garcia, 2021).

Chen, Cheng, and Lin (2004) studied the RWGS reaction over Cu/SiO_2 catalysts under H_2/CO_2 flow in a 1:1 ratio, concluding that the addition of a small amount of iron as a promoter (0.3% Fe to 10% Cu/SiO_2) was enough to upgrade the performance and stability appreciably. The catalyst presented an elevated conversion, at 600 °C and atmospheric pressure, for over 120 h without deactivation (Chen; Cheng; Lin, 2004). Ai *et al*. (2022) prepared supported $Cu/\gamma\text{-}Al_2O_3$ by wet impregnation and by grinding, achieving a reaction rate of $1.85 \cdot 10^{-5}$ mol g_{cat}^{-1} s^{-1} with the catalyst made by wet impregnation and a reaction rate of $2.12 \cdot 10^{-5}$ mol g_{cat}^{-1} s^{-1} for the catalyst obtained by the grinding method. The authors reported that the grinding method provided higher content and dispersion of metallic Cu on the surface of the catalyst (Ai *et al*., 2022).

Jurković *et al*. (2017) investigated the effect of the support on Cu-based catalysts, analyzing Al_2O_3, CeO_2, SiO_2, TiO_2, and ZrO_2. All the catalysts were prepared by deposition-precipitation method and evaluated in the temperature range from 280 °C to 360°C (Jurković *et al*., 2017). Alumina was reported to be the support that provides the highest Cu dispersion, and also the greatest catalyst activity (Jurković *et al*., 2017). There is a linear dependence between activity and surface area of Cu^0, thereby this oxide may boost the reaction rate (Su *et al*., 2017).

Cu-based catalysts are also widely used in conjunction with ZnO. In these catalysts, copper acts as the main active metal, while zinc is a promoter; the interface between CuO and ZnO plays a pivotal role in the proceeding of the reaction, therefore it is essential to choose a preparation method that provides a good dispersion of the phases on the catalyst surface (Jurković *et al*., 2017). ZnO supplies active sites for hydrogen spillover, in addition to influencing Cu^0 dispersion (Reina; Odriozola; Arellano-Garcia, 2021). The performance is described in the literature as being better for samples with greater Cu content (Jurković *et al*., 2017; Su *et al*., 2017; Ai *et al*., 2022). Besides, ZnO shows more efficiency in the presence of other oxides such as alumina and zirconia (Reina; Odriozola; Arellano-Garcia, 2021).

Cu/Al_2O_3 and $Cu/ZnO/Al_2O_3$ are often used in RWGS due to their attractive price, as well as good activity and selectivity to CO at low temperatures (between 170 – 250 °C) (Vu *et al*., 2022; Elsernagawy *et al*., 2020). The high surface area of

alumina makes CuO and ZnO crystallite size smaller, and the copper dispersion is also favored for higher Cu/Zn ratios (Reina; Odriozola; Arellano-Garcia, 2021; Stone; Waller, 2003). Jadhav, Joshi and Vaidya (2020) synthesized Cu/ZnO/Al_2O_3 catalysts by hydrothermal and combustion methods, testing the samples in a temperature range from 280 °C to 300 °C and H_2/CO_2 ratio of 3. In all cases, no coke formation was observed, and the authors concluded that the catalyst prepared by the hydrothermal technique was more stable than that obtained by the combustion technique, with the former providing a consistent activity for the 20 h of the test, because of the ability of the hydrothermal method to provide catalysts with strongly crystalline nature (Jadhav; Joshi; Vaidya; 2020).

1.2 **RWGS mechanism**

In order to design more effective catalysts, it is important to clarify the elementary steps of RWGS over catalytic surface (Su *et al*., 2017; González-Castaño; Dorneanu; Arellano-García, 2021). Several in-situ techniques and density functional theory (DFT) calculations have provided kinetic data that supports the search for a deeper understanding of the RWGS pathway, still a subject under discussion (Pahija *et al*., 2022; Su *et al*., 2017; Ateka *et al*., 2022; González-Castaño; Dorneanu; Arellano-García, 2021). For the reaction, there are two categories of mechanisms usually accepted: the surface redox mechanism and the associative mechanism (Gu *et al*., 2021; Liu *et al*, 2020a; Chen *et al*., 2020). These pathways differ mainly regarding the participation or not of the dissociated H_2 in the production of carbonaceous intermediates (Chen *et al*., 2020; Su *et al*., 2017; González-Castaño; Dorneanu; Arellano-García, 2021).

In the redox mechanism (also called dissociative or regenerative mechanism), CO_2 dissociates to CO, oxidizing the metal (González-Castaño; Dorneanu; Arellano-García, 2021; Reina; Odriozola; Arellano-Garcia, 2021). Next, H_2 reduces the active site to its initial state (Pahija *et al*., 2022; González-Castaño; Dorneanu; Arellano-García, 2021). The H species does not take part in CO_2 dissociation (González-Castaño; Dorneanu; Arellano-García, 2021). The redox mechanism requires two key conditions: the catalyst surface must be able to be reduced by H_2 and, once partially

reduced, it must be able to be efficiently reoxidized by CO_2 at RWGS conditions (Reina; Odriozola; Arellano-Garcia, 2021).

The redox mechanism was originally described over Cu-based catalysts, as indicated below (Chen *et al*., 2020; Ginés; Marchi; Apesteguía, 1997; Reina; Odriozola; Arellano-Garcia, 2021; Zhu; Ge; Zhu, 2020):

$$CO_{2\,(g)} + 2\,Cu^{0}_{(s)} \rightarrow CO_{(g)} + Cu_2O_{(s)} \quad (4)$$

$$H_{2\,(g)} + Cu_2O_{(s)} \rightarrow H_2O_{(g)} + 2\,Cu^{0}_{(s)} \quad (5)$$

Cu^0 is the active site that facilitates the dissociation of CO_2 and undergoes consecutive oxidation and reduction by carbon monoxide and hydrogen, respectively (Chen *et al*., 2020; Ginés; Marchi; Apesteguía, 1997; Reina; Odriozola; Arellano-Garcia, 2021). This scheme shows CO_2 oxidizing metallic copper, forming Cu^+ and carbon monoxide, while H_2 reduces Cu^+ to Cu^0, originating water (Chen *et al*., 2020).

Ginés, Marchi, and Apesteguía (1997) carried out a kinetic study over $CuO/ZnO/Al_2O_3$, corroborating this mechanism. Online gas analysis during CO_2/H_2 cycles at 230 °C and 1 atm showed that the CO_2 addition to the reactor generated only CO. Further addition of H_2 to the reactor generated only water. Furthermore, through quantitative gravimetric data, the authors found that the catalyst weight gain after the introduction of the CO_2-containing atmosphere represented an atomic ratio of around 0.4-0.5 between the oxygen and the copper on the surface, which is a likely value in agreement with the reaction (4). This suggests a coverage of adsorbed oxygen atoms on the copper surface of 50%. Moreover, the weight gain was also almost equal to the weight loss of the catalyst during the subsequent introduction of H_2. The authors still detailed the mechanism through the reactions (6) to (10), assuming active sites are identical and no interaction between adsorbed species:

$$CO_{2\,(g)} + 2\,S \rightleftharpoons CO_{(a)} + O_{(a)} \quad (6)$$

$$CO_{(a)} \rightleftharpoons CO_{(g)} + S \quad (7)$$

$$H_{2\,(g)} + 2\,S \rightleftharpoons 2\,H_{(a)} \quad (8)$$

$$2\,H_{(a)} + O_{(a)} \rightleftharpoons H_2O_{(a)} + 2\,S \quad (9)$$

$$H_2O_{(a)} \rightleftharpoons H_2O_{(g)} + S \quad (10)$$

where *S* represents the vacant active sites, and the subscript *(a)* denotes adsorbed species. In the same work, the authors ruled out possible support effects on hydrogen chemisorption after observing that H_2 chemisorption in Al_2O_3 and ZnO samples at 230 °C was negligible, indicating selective adsorption in the metallic copper phase (Ginés; Marchi; Apesteguía, 1997). The dissociative adsorption of CO_2 is the rate-determining step under H_2-rich conditions, whereas, at H_2-lean conditions, both the CO_2 dissociation and the water formation are rate-determining steps (Ginés; Marchi; Apesteguía, 1997).

In the associative mechanism, CO_2 adsorbs on the surface of the catalyst, reacts with adsorbed H from the previous dissociative adsorption of H_2, and produces intermediate species like carboxyl and formate (Gu *et al*., 2021; Pahija *et al*., 2022). Whatever the intermediate species, it decomposes to produce CO and H_2O (Gu *et al*., 2021; Pahija *et al*., 2022; Chen *et al*., 2020). In this case, CO_2 adsorption and H_2 dissociation are found the essential elementary steps (Gu *et al*., 2021).

In the formate-mediated mechanism, a formate intermediate species, $HCOO_{(a)}$, is generated through a hydrogenation of the adsorbed carbon dioxide, dissociating instantaneously. The reaction can be explained by the following scheme (Chen *et al*., 2020):

$$H_{2\,(g)} + 2\,S \rightleftharpoons 2\,H_{(a)} \quad (8)$$

$$CO_{2\,(g)} + S \rightleftharpoons CO_{2\,(a)} \quad (11)$$

$$CO_{2\,(a)} + H_{(a)} \rightleftharpoons HCOO_{(a)} + S \quad (12)$$

$$HCOO_{(a)} + S \rightleftharpoons HCO_{(a)} + O_{(a)} \quad (13)$$

$$HCO_{(a)} + S \rightleftharpoons CO_{(a)} + H_{(a)} \quad (14)$$

$$H_{(a)} + O_{(a)} \rightleftharpoons OH_{(a)} + S \quad (15)$$

$$H_{(a)} + OH_{(a)} \rightleftharpoons H_2O_{(a)} + S \quad (16)$$

$$H_2O_{(a)} \rightleftharpoons H_2O_{(g)} + S \quad (17)$$

$$CO_{(a)} \rightleftharpoons CO_{(g)} + S \quad (18)$$

In the carboxyl-mediated mechanism, a carboxyl intermediate species, $COOH_{(a)}$, is formed as shown in reactions (8), (11) and (19), with H assisting the dissociation of the C–O bond, and the carboxyl instantly decomposes into CO,

sequence that can take place through two different pathways, being one described by the following scheme (Chen *et al*., 2020):

$$H_{2\,(g)} + 2\,S \rightleftharpoons 2\,H_{(a)} \quad (8)$$

$$CO_{2\,(g)} + S \rightleftharpoons CO_{2\,(a)} \quad (11)$$

$$CO_{2\,(a)} + H_{(a)} \rightleftharpoons COOH_{(a)} + S \quad (19)$$

$$COOH_{(a)} + S \rightleftharpoons CO_{(a)} + OH_{(a)} \quad (20)$$

$$H_{(a)} + OH_{(a)} \rightleftharpoons H_2O_{(a)} + S \quad (16)$$

$$H_2O_{(a)} \rightleftharpoons H_2O_{(g)} + S \quad (17)$$

$$CO_{(a)} \rightleftharpoons CO_{(g)} + S \quad (18)$$

The other proposed pathway is presented below (Chen *et al*., 2020):

$$H_{2\,(g)} + 2\,S \rightleftharpoons 2\,H_{(a)} \quad (8)$$

$$CO_{2\,(g)} + S \rightleftharpoons CO_{2\,(a)} \quad (11)$$

$$CO_{2\,(a)} + H_{(a)} \rightleftharpoons COOH_{(a)} + S \quad (19)$$

$$COOH_{(a)} + S \rightleftharpoons HCO_{(a)} + O_{(a)} \quad (21)$$

$$HCO_{(a)} + S \rightleftharpoons CO_{(a)} + H_{(a)} \quad (22)$$

$$H_{(a)} + O_{(a)} \rightleftharpoons OH_{(a)} + S \quad (15)$$

$$H_{(a)} + OH_{(a)} \rightleftharpoons H_2O_{(a)} + S \quad (16)$$

$$H_2O_{(a)} \rightleftharpoons H_2O_{(g)} + S \quad (17)$$

$$CO_{(a)} \rightleftharpoons CO_{(g)} + S \quad (18)$$

It is noteworthy that, in reactions (21) and (22), the $COH_{(a)}$ intermediate could be found instead of $HCO_{(a)}$, although $COH_{(a)}$ is reported to be less stable than its isomer over several metal surfaces (Chen *et al*., 2017).

The nature and quantity of formed intermediates vary according to the metal and the support (Reina; Odriozola; Arellano-Garcia, 2021). On reducible supports, the oxygen vacancies might play the role of active sites allowing CO_2 reduction and the C=O bond cleavage (González-Castaño; Dorneanu; Arellano-García, 2021). Temperature can also influence the rate of decomposition of intermediates, leading to different reaction pathways (González-Castaño; Dorneanu; Arellano-García, 2021).

Chen, Cheng and Lin (2000) studied the mechanism of CO formation over Cu/Al_2O_3, concluding that a redox mechanism could not completely elucidate the reaction pathway. They deduced that H_2 plays a key role in carbon monoxide formation by associating with adsorbed CO_2 to produce reaction intermediates, and proposed formate species as the dominant intermediate.

Dietz, Piccinin and Maestri (2015) carried out DFT calculations on (111) surfaces of Pt, Rh, Ni, Cu, Ag and Pd, demonstrating that the dominant mechanism of the RWGS reaction varies according to the metal, due to the influence of its interaction with oxygen adatom on the activation energy of the dissociation. The authors state that, whereas the dissociation of CO_2 is favored on metals with greater oxygen affinity, CO_2 hydrogenation is favored as the interaction between O and the metal weakens. They also report the preponderance of the surface redox mechanism over Rh, Ni and Cu, and the carboxyl-mediated associative mechanism over Pt, Pd and Ag.

Regardless the sort of the predominant mechanism, an active catalyst for CO_2 reduction must be able to provide the chemisorption of carbon dioxide molecules and cleavage of one of its C–O bonds, as well as dissociation of H_2 with subsequent hydrogenation of O to originate water (González-Castaño; Dorneanu; Arellano-García, 2021; Zhu; Ge; Zhu, 2020; Chen *et al*., 2020). Nevertheless, for such a catalyst to also be selective, it must present a moderate C–O dissociation capacity and a weak CO adsorption ability, in order to avoid the dissociation of this CO and its eventual additional hydrogenation, causing the formation of methane and methanol (Zhu; Ge; Zhu, 2020). Hence, there is a balance that needs to be achieved between C–O bond dissociation and hydrogenation, allowing the catalyst to not only provide high CO_2 conversions under milder conditions but also be selective toward the desired product. Such properties clearly depend on the characteristics of metals, supports and promoters, as well as the interactions between them (Zhu; Ge; Zhu, 2020).

1.3 **Thermodynamic and kinetic behavior of the system**

An important tool in the design and improvement of the RWGS process, in general, is the thermodynamic analysis, which allows evaluation of the tendency of the reaction to proceed or not, as well as the extent of the reaction at the equilibrium

according to parameters like temperature, pressure and feed composition (Santos *et al*., 2023).

An excess of H_2 (relative to CO_2) increases CO_2 conversion at equilibrium (Daza; Kuhn, 2016). The same occurs with increasing temperature, because of the kinetic favoring and the endothermicity of the RWGS reaction (Daza; Kuhn, 2016; Elsernagawy *et al*., 2020). Furthermore, at lower temperatures, RWGS suffers from competition with methanation (González-Castaño; Dorneanu; Arellano-García, 2021; Pastor-Pérez *et al*., 2017). Despite this, from a practical point of view, it is well-known that higher temperatures result in higher energy consumption and higher capital cost, in addition to being potentially harmful to catalysts (González-Castaño; Dorneanu; Arellano-García, 2021; Su *et al*., 2017). Similarly, to work with higher H_2/CO_2 molar ratios in the feed, a greater quantity of hydrogen is required, which is the most expensive raw material in the process (Santos *et al*., 2023). In the same way, the decrease in space velocity represents an increase in residence time that is expected to provide higher conversions, but it is also associated with larger reactor volumes, resulting in an expressive rise in capital cost (Pastor-Pérez *et al*., 2017). Regarding total pressure, a substantial effect on the equilibrium composition is not expected for the RWGS reaction, because the number of moles is the same for the products and reactants, as seen in reaction (1). However, the methanation reactions (2) and (3), which are volume contraction processes, are favored by an increase in pressure (Bulfin *et al*., 2023).

Santos *et al*. (2023) simulated RWGS reaction in ASPEN Plus (v10.0) and investigated the response to different operation conditions (Annex, Figure 18). At 1 bar with a 1:1 H_2/CO_2 molar ratio for the inlet stream, it was observed that CH_4 is the predominant product below 520 °C. CO assumes this position above 700 °C, and from 825 °C the molar fraction of this compound in the product stream is higher than that of CO_2 and H_2. Regarding the feed molar ratio (H_2/CO_2), a range between 0.5 and 1.5 was evaluated. CO_2 conversion was higher above 1.2 but CO selectivity increased above 0.8. Therefore, 0.8 was considered the appropriate value for the molar ratio to contribute to better cost-effectiveness. The authors also remarked on the negative effect of pressure on the CO concentration downstream. Even so, they proposed 20 bar as a suitable pressure for the process, because the desired selectivity can be obtained with an appropriate catalyst. Besides, such pressure is

commercially employed for FTS (Fischer-Tropsch Synthesis) and can facilitate the integration between these processes.

Utilizing the software ASPEN Plus (v10.0), Elsernagawy *et al*. (2020) carried out a thermo-economic analysis through a steady-state simulation of RWGS reaction followed by methanol synthesis both at higher (940 °C) and lower (450 °C) temperatures. A Cu-ZnO/Al_2O_3 was considered for a lower temperature approach, and Ni/Al_2O_3 was considered for operating at higher temperatures. The results showed that the performance of both approaches was quite similar. Although the lower temperature corresponded to lower energy consumption, this approach required higher recycling ratios, and thus bigger volumes of reactors and higher amounts of catalyst to reach the same production, increasing the production cost. On the other hand, the higher temperature approach presented a better environmental performance evidenced by a larger negative carbon footprint, and was considered more advantageous. The authors further explored the effect of the H_2/CO_2 ratio at 500 °C and 10 bar, finding an optimal feed ratio of 3:1 due to the higher CO_2 and H_2 conversions obtained under these conditions.

Reinikainen *et al*. (2022) simulated CO_2 conversion in the RWGS reactor as a function of GHSV at 850 °C in the software ASPEN Plus v11 (Annex, Figure 19). They also investigated the effect of H_2/CO_2 feed ratio, observing that, at the lowest GHSV values, the conversion was quite near to equilibrium. Moreover, the more the space velocity increased, the further the conversions were moved away from equilibrium values. The work also highlighted the strong influence of the inlet H_2/CO_2 molar ratio on the composition of the product stream, monitoring a range between 1 and 3. A linear dependence of the selectivity to CH_4 concerning the H_2/CO_2 ratio was observed since methanation consumes the excess hydrogen available in the medium.

1.4 **Kinetic studies**

In their kinetic study over CuO/ZnO/Al_2O_3 catalysts, Ginés, Marchi and Apesteguía (1997) analyzed the RWGS considering a surface redox mechanism, summarized by following reactions, where *S* represents the vacant active sites, and the subscript *(a)* denotes adsorbed species.

$$CO_{2\,(g)} + S \rightleftharpoons CO_{(g)} + O_{(a)} \quad (23)$$

$$H_{2\,(g)} + 2\,S \rightleftharpoons 2\,H_{(a)} \quad (8)$$

$$2\,H_{(a)} + O_{(a)} \rightleftharpoons H_2O_{(g)} \quad (24)$$

Assuming (23) as the rate-determining step, the authors proposed the reaction rate equation (25), obtained through Langmuir-Hinshelwood kinetics:

$$r_{RWGS} = \frac{k_1 L_0 \left(P_{CO_2} P_{H_2} - \frac{P_{CO}^2}{K_1}\right)}{P_{H_2} + \sqrt{K_8^*} \cdot P_{H_2}^{1.5} + \frac{1}{K_8^* K_{24}^*} \cdot P_{CO}} \quad (25)$$

in which r_{RWGS} is the RWGS reaction rate in mol h^{-1} g^{-1}, k_1 is the forward reaction constant of reaction (23) in atm^{-1} h^{-1}, L_0 indicates the concentration of active sites of fresh catalyst in mol g^{-1}, P_i represents the partial pressure of component *i* in atm, K_1 is the equilibrium constant of the RWGS reaction (dimensionless), K_8* is the equilibrium constant of the dissociative hydrogen adsorption (8) in atm^{-1}, and K_{24}* is the equilibrium constant of reaction (24), also in atm.

Vanden Bussche and Froment (1996) developed a steady-state kinetic model for the RWGS reaction over a commercial $Cu/ZnO/Al_2O_3$ catalyst, also considering a redox mechanism, expressed by the following reactions:

$$H_{2\,(g)} + 2\,S \rightleftharpoons 2\,H_{(a)} \quad (8)$$

$$CO_{2\,(g)} + S \rightleftharpoons CO_{(g)} + O_{(a)} \quad (23)$$

$$H_{(a)} + O_{(a)} \rightleftharpoons OH_{(a)} + S \quad (15)$$

$$H_{(a)} + OH_{(a)} \rightleftharpoons H_2O_{(a)} + S \quad (16)$$

$$H_2O_{(a)} \rightleftharpoons H_2O_{(g)} + S \quad (17)$$

The authors considered the dissociative adsorption of CO_2 as the rate-determining step and presented the reaction rate indicated in equation (26):

$$r_{RWGS} = \frac{k_1 \cdot P_{CO_2} \cdot \left(1 - \left(\frac{1}{K_1}\right) \cdot \left(\frac{P_{H_2O} \cdot P_{CO}}{P_{CO_2} \cdot P_{H_2}}\right)\right)}{\left(1 + \left(\frac{K_{H_2O}}{K_{15}^* K_{16}^* K_{H_2}}\right)\left(\frac{P_{H_2O}}{P_{H_2}}\right) + \sqrt{K_{H_2} \cdot P_{H_2}} + K_{H_2O} \cdot P_{H_2O}\right)} \quad (26)$$

where r_{RWGS} is the reaction rate in mol kg^{-1} s^{-1}, k_1 the reaction rate constant in mol kg^{-1} s^{-1} bar^{-1}, P_i the partial pressure of component *i* in bar, K_1 the RWGS equilibrium constant (dimensionless), K_{H2O} the adsorption equilibrium constant for H_2O in bar^{-1}, K_{H2} the adsorption equilibrium constant for H_2 in bar^{-1}, K_{15}* is the equilibrium constant of reaction (15) (dimensionless) and K_{16}* is the equilibrium constant of reaction (16) (dimensionless). Indeed, k_1 is a compounded constant, expressed by equation (27):

$$k_1 = k_{23} \cdot c_t \quad (27)$$

where k_{23} is the rate constant of reaction (23) and c_t is the total number of active sites. The equilibrium constant of RWGS reaction, K_1, is determined through equation (28), from Graaf *et al*. (1986), applicable at low pressures:

$$K_1 = 10^{\left(-\frac{2073}{T} + 2.029\right)} \quad (28)$$

where T is the temperature in K. The other kinetic and adsorption equilibrium constants can be calculated by the equations (29) to (32):

$$k_1 = A_{k_1} \cdot exp\left(\frac{B_{k_1}}{R \cdot T}\right) \quad (29)$$

$$K_{H_2O} = A_{K_{H_2O}} \cdot exp\left(\frac{B_{K_{H_2O}}}{R \cdot T}\right) \quad (30)$$

$$\frac{K_{H_2O}}{K_{15}^* K_{16}^* K_{H_2}} = A_{K_{H_2O}/K_{15}^* K_{16}^* K_{H_2}} \cdot exp\left(\frac{B_{K_{H_2O}/K_{15}^* K_{16}^* K_{H_2}}}{R \cdot T}\right) \quad (31)$$

$$\sqrt{K_{H_2}} = A_{\sqrt{K_{H_2}}} \cdot exp\left(\frac{B_{\sqrt{K_{H_2}}}}{R \cdot T}\right) \quad (32)$$

where A_{k1} (mol kg^{-1} s^{-1} bar^{-1}), B_{k1} (J mol^{-1}), A_{KH2O} (bar^{-1}), B_{KH2O} (J mol^{-1}), $A_{KH2O/K15*K16*KH2}$ (dimensionless), $A_{\sqrt{KH2}}$ (bar$^{-0,5}$) and $B_{\sqrt{KH2}}$ (J mol^{-1}) are the seven

parameters to be fitted for this model since $B_{KH2O/K15*K16*KH2}$ is set to zero by the authors and R is the universal gas constant (equal to 8.314 J mol^{-1} K^{-1}) (NIST, 2024).

Graaf, Stamhuis and Beenackers (1988) studied the kinetics of low-pressure methanol synthesis over a commercial Cu/ZnO/Al_2O_3 catalyst, considering a dual-site adsorption mechanism. On one site (represented as S_1), CO and CO_2 adsorb competitively, while, at the other site (represented as S_2), H_2 and H_2O adsorb competitively. They presented the following reaction scheme for RWGS reaction:

$$CO_{2\,(g)} + S_1 \rightleftharpoons CO_{2\,(a)} \tag{33}$$

$$H_{2\,(g)} + 2\,S_2 \rightleftharpoons 2\,H_{(a)} \tag{34}$$

$$CO_{2\,(a)} + H_{(a)} \rightleftharpoons HCO_{2\,(a)} + S_2 \tag{35}$$

$$HCO_{2\,(a)} + H_{(a)} \rightleftharpoons CO_{(a)} + H_2O_{(a)} \tag{36}$$

$$CO_{(a)} \rightleftharpoons CO_{(g)} + S_1 \tag{37}$$

$$H_2O_{(a)} \rightleftharpoons H_2O_{(g)} + S_2 \tag{38}$$

The authors proposed a rate equation for RWGS reaction, expressed by equation (39):

$$r_{RWGS} = \frac{k_1 \cdot K_{CO_2} \cdot \left(f_{CO_2} \cdot f_{H_2} - \frac{f_{H_2O} \cdot f_{CO}}{K_1}\right)}{\left(1 + K_{CO} \cdot f_{CO} + K_{CO_2} \cdot f_{CO_2}\right)\left(f_{H_2}^{0.5} + f_{H_2O} \cdot \left(\frac{K_{H_2O}}{K_{H_2}^{0.5}}\right)\right)} \tag{39}$$

where K_i is the adsorption equilibrium constant of component i in bar^{-1}, f_i is the partial fugacity of component i in bar, K_1 is the equilibrium constant of RWGS reaction (dimensionless) and k_1 is the rate constant, which contains the adsorption equilibrium constant of hydrogen and is expressed in mol s^{-1} kg^{-1} bar$^{-0.5}$.

K_1 and k_1 are determined through equations (28) and (29), respectively, while the adsorption equilibrium constants are calculated by equations (40) to (42):

$$K_{CO} = A_{K_{CO}} \cdot exp\left(\frac{B_{K_{CO}}}{R \cdot T}\right) \tag{40}$$

$$K_{CO_2} = A_{K_{CO_2}} \cdot exp\left(\frac{B_{K_{CO_2}}}{R \cdot T}\right) \quad (41)$$

$$\frac{K_{H_2O}}{K_{H_2}^{0.5}} = A_{K_{H_2O}/K_{H_2}^{0.5}} \cdot exp\left(\frac{B_{K_{H_2O}/K_{H_2}^{0.5}}}{R \cdot T}\right) \quad (42)$$

therefore A_{k1} (mol s^{-1} kg^{-1} $bar^{-0.5}$), B_{k1} (J mol^{-1}), A_{KCO} (bar^{-1}), B_{KCO} (J mol^{-1}), A_{KCO2} (bar^{-1}), B_{KCO2} (J mol^{-1}), $A_{KH2O/\sqrt{}KH2}$ ($bar^{-0,5}$) and $B_{KH2O/\sqrt{}KH2}$ (J mol^{-1}) are the eight parameters to be fitted for this kinetic model.

1.5 **Final considerations**

Given all that has been exposed, it is possible to observe that copper-based catalysts represent a promising perspective toward the industrial application of the RWGS reaction. However, the simulations reported in the literature indicated that the RWGS process is favored under conditions generally associated with high investment and operating costs, such as low space velocities, high temperatures, and H_2/CO_2 ratios. Therefore, it is desirable to develop catalysts that promote the highest possible conversion of CO_2 to the product of interest, carbon monoxide. This objective requires a deeper understanding of how the reaction occurs on the catalytic surface since the reaction mechanism is still a topic under constant discussion. Nevertheless, the development of a new kinetic study can be a very challenging task. The studies in the literature were based on kinetic data obtained in a steady state, requiring at least one catalytic run for each set of operating conditions. Thus, this process demands considerable experimental effort due to the large number of tests, consuming a lot of time and resources.

Furthermore, the accuracy of the original parameters of these models may drop considerably in the case of extrapolation outside the temperature window used. Although there is the possibility that temperature ramp tests may be able to provide kinetic data in less time, in a simpler manner, and cover a wider temperature range, there is a lack of studies in the literature exploring this alternative. Also, no studies were found that compare the accuracy of the estimates provided by the available kinetic models for the RWGS reaction under experimental conditions different from

those employed in its acquisition. Therefore, the present work has the following general objectives:

a) Study the kinetics of the RWGS reaction on a commercial $CuO/ZnO/Al_2O_3$ catalyst;
b) To evaluate the possible use of light-off curves (in temperature ramp) as a replacement for the conventional procedure (in steady state – constant temperature levels) to obtain the kinetic parameters, thus contributing to the development of more effective catalysts for the RWGS reaction.

The specific objectives are:

a) Evaluate diffusional effects on the catalytic bed;
b) Analyze the effect of different experimental conditions on CO_2 conversion through RWGS reaction over a commercial $CuO/ZnO/Al_2O_3$ catalyst for kinetic studies;
c) Obtain kinetic parameter values for the RWGS reaction rate expressions present in the literature based on experimental data of CO_2 conversion along a temperature ramp (light-off curves);
d) Compare the kinetic models of Ginés, Marchi, and Apesteguía (1997), Vanden Bussche and Froment (1996), and Graaf, Stamhuis, and Beenackers (1988) from the point of view of accuracy in modeling the experimental light-off curves;
e) Compare the fit quality to experimental data of parameters obtained from light-off curves and parameters adjusted by the conventional procedure with steady-state data.

2 **METHODOLOGY**

2.1 **Catalyst**

The $CuO/ZnO/Al_2O_3$ used in this study is a commercial catalyst provided by Prosint (a methanol producer in Brazil that is now out of business). It was calcined at 500 °C for 3 h, at a 10 °C min^{-1} rate before use.

2.2 **Catalyst characterization**

X-ray diffraction (XRD) analysis was performed on a Bruker D8 Advance diffractometer employing a CuK_α radiation source. The 2θ range employed was 10–70º, scanning speed of 4° min^{-1}, step size of 0.02° and step time of 0.3 s. The qualitative analysis of the resulting patterns was accomplished based on the JCPDS database (Joint Committee on Powder Diffraction Standards) and literature information.

Temperature-Programmed Reduction (TPR), with H_2 as the reducing agent (H_2-TPR), was performed in a Micromeritics AutoChem II 2920 instrument, furnished with a Thermal Conductivity Detector (TCD). 51.6 mg of catalyst were placed into the U-shaped quartz fixed bed reactor. First, the sample was pretreated at 150 °C, with a heating rate of 10 °C min^{-1} from room temperature, remaining at this temperature for 10 min, under a 50 mL min^{-1} argon flow. After returning to room temperature, the catalyst was reduced under 50 mL min^{-1} of 10% H_2/Ar mixture (ramp of 10 °C min^{-1} up to 500 °C).

2.3 **Catalytic evaluation**

The RWGS catalytic tests were performed at atmospheric pressure in a Pyrex U-shaped fixed bed reactor placed into a multipurpose unit coupled to an Agilent 7890A gas chromatograph equipped with a thermal conductivity detector (TCD), a

front inlet detector (FID), GS – GASPRO and HP – MOLESIEVE capillary column. A catalyst sample of 50 mg was diluted with silicon carbide in a 1:1 mass ratio, in order to increase the thermal homogeneity of the bed, minimize the occurrence of hot spots within the reactor, and thus ensuring the reproducibility of the tests. A pretreatment was carried-out under H_2 flow, at 500 °C (heating rate of 10 °C min^{-1}) for 1 h. The following mixtures, with different H_2/CO_2 molar ratios, were used in the tests: mixture 1 (0.10:0.10, and balance in He), mixture 2 (0.25:0.10, and balance in He) and mixture 3 (0.40:0.10, and balance in He).

2.3.1 Light-off tests

The light-off curve of a catalytic reaction is a plot of conversion versus temperature. These curves are commonly used in catalyst development since they allow evaluating the catalytic activity (Duprat, 2022). Three light-off curves relating CO_2 conversion to reaction temperature were obtained using the three mixtures, with different H_2/CO_2 molar ratios. In all the experiments, after the pretreatment previously defined, a heating rate of 5 °C min^{-1} was applied, from room temperature to 500 °C, with a space velocity of 30 m^3 kg^{-1} h^{-1}.

The objective of these tests is to generate a large set of kinetic data in a single experiment.

2.3.2 Evaluation of possible diffusional effects

In order to verify whether the contribution of internal mass transfer is significant for the reactor modeling, three temperature ramp tests (light-off tests) were performed with mixture 3 (H_2/CO_2 molar ratio of 4) at 30 m^3 kg^{-1} h^{-1}. The calcined catalyst was sieved through A Bronzinox sieves to produce three samples (50 mg) with different particle sizes in the ranges of 0.180-0.250 mm, 0.250-0.425 mm, and 0.425-0.850 mm. Each sample was used in a temperature ramp test (light-off test) from room temperature to 500 °C, applying a heating rate of 5 °C min^{-1}.

External diffusion limitations were evaluated through three temperature ramp tests (light-off tests) from room temperature to 500 °C, with a heating rate of 5 °C min^{-1}, using a catalyst with particle size between 0.250 mm and 0.425 mm. The space velocity was 30 m^3 kg^{-1} h^{-1} in the three tests, but different volumetric flow rates and catalyst masses were used in each test. In the first test, the volumetric flow rate was 25 mL min^{-1} and the mass 50 mg; in the second test, the volumetric flow rate was 35 mL min^{-1} and the mass 70 mg; in the third test, the volumetric flow rate was 45 mL min^{-1} and the mass 90 mg.

2.3.3 Stability test

In the RWGS reaction, copper catalysts can deactivate mainly due to sintering and reoxidation (Bahmanpour *et al*., 2019). Thus, a long-term test was performed to analyze the stability of the catalyst. After pretreatment, the sample was heated at a rate of 5 °C min^{-1} until 500 °C, maintaining this temperature for more than 9 hours under the flow of mixture 1 (H_2/CO_2 molar ratio of 1) at 18 m^3 kg^{-1} h^{-1}.

2.3.4 Catalytic tests at fixed temperatures

Aiming at evaluating the CO_2 conversion in the RWGS reaction, avoiding interferences arising from the dynamics of the catalytic system (that may occur on the same time scale as the heating rate), catalytic tests were also performed at fixed temperatures. In such experiments, CO_2 conversion data were obtained after the catalyst activity reached a steady state. Three temperature levels were applied: 330 °C, 380 °C, and 430 °C. In order to achieve these temperatures, the samples were subjected to a heating rate of 5 °C min^{-1} after the pretreatment. CO_2 conversion was also investigated under different space velocities and inlet composition conditions. The space velocities applied were 18 m^3 kg^{-1} h^{-1}, 30 m^3 kg^{-1} h^{-1} and 42 m^3 kg^{-1} h^{-1}, and the feed composition effect was observed performing the tests at fixed

temperatures with mixture 1 (H_2/CO_2 molar ratio of 1), mixture 2 (H_2/CO_2 molar ratio of 2.5) and mixture 3 (H_2/CO_2 molar ratio of 4).

In each condition, the catalyst was exposed to the reaction mixture until stable conversion was achieved.

The objective of these experiments is to check if the curves obtained at temperature ramp tests can provide results equivalent to conventional catalytic tests.

2.4 **Kinetic modeling**

Among the different kinetic studies available in the literature involving the RWGS reaction, three were chosen to be studied, based on the type of catalyst and reactor used. The first model investigated was proposed by Ginés, Marchi and Apesteguía (1997):

$$r_{RWGS} = \frac{k_1 L_0 \left(P_{CO_2} P_{H_2} - \frac{P_{CO}^2}{K_1} \right)}{P_{H_2} + \sqrt{K_8^*} \cdot P_{H_2}^{1.5} + \frac{1}{K_8^* K_{24}^*} \cdot P_{CO}} \tag{25}$$

Since the authors do not specify an expression for determining the equilibrium constant K_1, it was calculated through the equation (28), the same expression used in the other two models studied in the present work.

$$K_1 = 10^{\left(-\frac{2073}{T} + 2.029\right)} \tag{28}$$

It is possible to observe that, in reaction (25), there is a set of parameters to adjust in order to determine the reaction rate. k_1 and L_0 were taken as a single parameter, to be fitted together with K_8* and K_{24}*.

However, the parameters by Ginés, Marchi, and Apesteguía (1997) are temperature-dependent, so each temperature has its own set of associated parameters. Intending to obtain temperature-independent parameters, the present work took the initiative of adapting the parameters k_1L_0, K_8^*, and K_{24}^*, considering a

temperature dependence pattern described by the Arrhenius expression, so that $k_1 L_0$ becomes:

$$k_1 \cdot L_0 = k_{1,0} \cdot L_0 \cdot e^{-\frac{E_{a,1}}{R \cdot T}} \tag{43}$$

in which $k_{1,0}$ is the pre-exponential factor in $atm^{-1}\ h^{-1}$, $E_{a,1}$ is the apparent activation energy in kcal mol^{-1}, R is the universal gas constant in kcal $K^{-1}\ mol^{-1}$, and T is the temperature in K.

It was also assumed that a rate constant k_2 governs the forward reaction (8), while in the reverse direction, the constant is k_{-2}. Similarly, the forward reaction (24) has k_3 as the rate constant, and the reverse reaction has a rate constant k_{-3}. Therefore, the equilibrium constants K_8^* and the product of constants $K_8^* \cdot K_{24}^*$ can be written as:

$$K_8^* = \frac{k_2}{k_{-2}} \tag{44}$$

$$K_8^* \cdot K_{24}^* = \frac{k_2}{k_{-2}} \cdot \frac{k_3}{k_{-3}} \tag{45}$$

Nevertheless, these rate constants can be expressed in terms of the Arrhenius expression as well:

$$K_8^* = \frac{k_{2,0} \cdot e^{-\frac{E_{a,2}}{R \cdot T}}}{k_{-2,0} \cdot e^{-\frac{E_{a,-2}}{R \cdot T}}} \tag{46}$$

$$K_8^* \cdot K_{24}^* = \frac{k_{2,0} \cdot e^{-\frac{E_{a,2}}{R \cdot T}}}{k_{-2,0} \cdot e^{-\frac{E_{a,-2}}{R \cdot T}}} \cdot \frac{k_{3,0} \cdot e^{-\frac{E_{a,3}}{R \cdot T}}}{k_{-3,0} \cdot e^{-\frac{E_{a,-3}}{R \cdot T}}} \tag{47}$$

where $k_{2,0}$ represents the pre-exponential factor of forward reaction (8), $k_{-2,0}$ is the pre-exponential factor of reverse reaction (8), $E_{a,2}$ is the apparent activation energy of the forward reaction (8), $E_{a,-2}$ is the apparent activation energy of reverse reaction (8), $k_{3,0}$ represents the pre-exponential factor of forward reaction (24), $k_{-3,0}$ is the pre-exponential factor of reverse reaction (24), $E_{a,3}$ is the apparent activation energy of

the forward reaction (24) and $E_{a,-3}$ is the apparent activation energy of reverse reaction (24). Therefore, equations (46) and (47) can be written as:

$$K_8^* = \frac{k_{2,0}}{k_{-2,0}} \cdot e^{-\left(\frac{E_{a,2}}{R \cdot T} - \frac{E_{a,-2}}{R \cdot T}\right)} \tag{48}$$

$$K_8^* \cdot K_{24}^* = \frac{k_{2,0}}{k_{-2,0}} \cdot e^{-\left(\frac{E_{a,2}}{R \cdot T} - \frac{E_{a,-2}}{R \cdot T}\right)} \cdot \frac{k_{3,0}}{k_{-3,0}} \cdot e^{-\left(\frac{E_{a,3}}{R \cdot T} - \frac{E_{a,-3}}{R \cdot T}\right)} \tag{49}$$

Giving rise to:

$$K_8^* = \frac{k_{2,0}}{k_{-2,0}} \cdot e^{-\frac{\left(E_{a,2} - E_{a,-2}\right)}{RT}} \tag{50}$$

$$K_8^* \cdot K_{24}^* = \frac{k_{2,0}}{k_{-2,0}} \cdot e^{-\frac{\left(E_{a,2} - E_{a,-2}\right)}{RT}} \cdot \frac{k_{3,0}}{k_{-3,0}} \cdot e^{-\frac{\left(E_{a,3} - E_{a,-3}\right)}{RT}} \tag{51}$$

Defining parameters $k_{4,0}$ in atm^{-1}, $k_{5,0}$ (dimensionless), and the activation energy differences $\Delta E_{a,4}$ and $\Delta E_{a,5}$, both in kcal mol^{-1}:

$$k_{4,0} = \frac{k_{2,0}}{k_{-2,0}} \tag{52}$$

$$k_{5,0} = \frac{k_{2,0} \cdot k_{3,0}}{k_{-2,0} \cdot k_{-3,0}} \tag{53}$$

$$\Delta E_{a,4} = E_{a,2} - E_{a,-2} \tag{54}$$

$$\Delta E_{a,5} = \left(E_{a,2} + E_{a,3}\right) - \left(E_{a,-2} + E_{a,-3}\right) \tag{55}$$

At last, the equilibrium constants turn into:

$$K_8^* = k_{4,0} \cdot e^{-\left(\frac{\Delta E_{a,4}}{R \cdot T}\right)} \tag{56}$$

$$K_8^* \cdot K_{24}^* = k_{5,0} \cdot e^{-\left(\frac{\Delta E_{a,5}}{R \cdot T}\right)} \tag{57}$$

Accordingly, the modeling of a RWGS reactor through the rate equation proposed by Ginés, Marchi and Apesteguía requires the fitting of six parameters: $k_{1,0}$, $E_{a,1}$, $k_{4,0}$, $\Delta E_{a,4}$, $k_{5,0}$ and $\Delta E_{a,5}$.

The second model studied was the model of Vanden Bussche and Froment (1996), given by equation (26). A new fitting based on the same parameters presented by the authors was conducted.

$$r_{RWGS} = \frac{k_1 \cdot P_{CO_2} \cdot \left(1 - \left(\frac{1}{K_1}\right) \cdot \left(\frac{P_{H_2O} \cdot P_{CO}}{P_{CO_2} \cdot P_{H_2}}\right)\right)}{\left(1 + \left(\frac{K_{H_2O}}{K_{15}^* K_{16}^* K_{H_2}}\right)\left(\frac{P_{H_2O}}{P_{H_2}}\right) + \sqrt{K_{H_2} \cdot P_{H_2}} + K_{H_2O} \cdot P_{H_2O}\right)} \quad (26)$$

The third model studied was the model of Graaf, Stamhuis and Beenackers (1988), also adjusting the parameters originally proposed by the authors.

$$r_{RWGS} = \frac{k_1 \cdot K_{CO_2} \cdot \left(f_{CO_2} \cdot f_{H_2} - \frac{f_{H_2O} \cdot f_{CO}}{K_1}\right)}{\left(1 + K_{CO} \cdot f_{CO} + K_{CO_2} \cdot f_{CO_2}\right)\left(f_{H_2}^{0.5} + f_{H_2O} \cdot \left(\frac{K_{H_2O}}{K_{H_2}^{0.5}}\right)\right)} \quad (39)$$

2.5 **Reactor modeling**

A one-dimensional pseudo-homogeneous fixed bed reactor model was developed to provide CO_2 conversion as a function of the mass of the catalyst in contact with the fluid flowing through the bed. This system has the catalyst mass, *W* in kg, as an independent variable. The dependent variables, in turn, are the molar flow rates of each component, F_{CO2}, F_{H2}, F_{CO}, F_{H2O} and F_{He}, which can be expressed by F_i in mol s^{-1}. The following simplifying assumptions were assumed:

a) Uniform and constant cross-sectional area;
b) Isothermal system;
c) Unidirectional flow;
d) Uniform flow at the catalyst inlet;
e) No diffusion limitations;
f) Ideal gas behavior;
g) Steady-state;

h) Uniform axial velocity;

i) Isobaric system.

Neither energy balance nor momentum balance were considered, as a result of hypotheses (b), (c), (h) and (i). A differential material balance was carried out according to:

$$\{input\} - \{output\} + \{generation\} = \{accumulation\} \tag{58}$$

The input term, in this case, is given by $F_i|_W$, which is the molar flow rate of component *i* at a given mass of catalyst *W* along the bed, while the output term is expressed by $F_i|_{W+dW}$, which consists of the molar flow rate of component *i* after the reaction mixture has already passed through a corresponding mass of catalyst to *W+dW*. The accumulation term is equal to zero, as a consequence of having assumed hypothesis (g). The generation term is given by $R_i \cdot dW$ and is expressed by equation (59):

$$R_i = \nu_i \cdot r_{RWGS} \tag{59}$$

where R_i indicates the generation or consumption rate of component *i* in mol s^{-1} kg^{-1}, ν_i is the stoichiometric coefficient of component *i* in the RWGS reaction (dimensionless, negative for reactants and positive for products), and r_{RWGS} represents the rate of RWGS reaction in mol s^{-1} kg^{-1}.

Therefore, the complete material balance is given by:

$$0 = F_i|_W - F_i|_{W+dW} + R_i \cdot dW \tag{60}$$

Dividing both sides of the equation by *dW*:

$$0 = \frac{F_i|_W - F_i|_{W+dW}}{dW} + R_i \tag{61}$$

Let $dW \rightarrow 0$, then:

$$0 = \frac{-dF_i}{dW} + R_i \tag{62}$$

Therefore, the material balance for each component is given by:

$$\frac{dF_{CO_2}}{dW} = -r_{RWGS} \tag{63}$$

$$\frac{dF_{H_2}}{dW} = -r_{RWGS} \tag{64}$$

$$\frac{dF_{CO}}{dW} = r_{RWGS} \tag{65}$$

$$\frac{dF_{H_2O}}{dW} = r_{RWGS} \tag{66}$$

$$\frac{dF_{He}}{dW} = 0 \tag{67}$$

After that, the rate equations were introduced into the balance and a dimensionless version of each set of equations was proposed (the details of the derivation of each model are shown in Appendix A), as follows:

Model of Ginés, Marchi and Apesteguía (1997):

$$\frac{dy_{CO_2}}{dm} = -\frac{A \cdot \left(y_{CO_2} \cdot y_{H_2} - \frac{y_{CO}^2}{K_1}\right)}{y_{H_2} + B \cdot y_{H_2}^{1.5} + D \cdot y_{CO}} \tag{68}$$

$$\frac{dy_{H_2}}{dm} = -\frac{A \cdot \left(y_{CO_2} \cdot y_{H_2} - \frac{y_{CO}^2}{K_1}\right)}{y_{H_2} + B \cdot y_{H_2}^{1.5} + D \cdot y_{CO}} \tag{69}$$

$$\frac{dy_{CO}}{dm} = \frac{A \cdot \left(y_{CO_2} \cdot y_{H_2} - \frac{y_{CO}^2}{K_1}\right)}{y_{H_2} + B \cdot y_{H_2}^{1.5} + D \cdot y_{CO}} \tag{70}$$

$$\frac{dy_{H_2O}}{dm} = \frac{A \cdot \left(y_{CO_2} \cdot y_{H_2} - \frac{y_{CO}^2}{K_1}\right)}{y_{H_2} + B \cdot y_{H_2}^{1.5} + D \cdot y_{CO}} \tag{71}$$

$$\frac{dy_{He}}{dm} = 0 \tag{72}$$

Model of Vanden Bussche and Froment (1996):

$$\frac{dy_{CO_2}}{dm} = -\frac{E \cdot y_{CO_2}\left(1-\left(\frac{1}{K_1}\right)\cdot\left(\frac{y_{H_2O}\cdot y_{CO}}{y_{CO_2}\cdot y_{H_2}}\right)\right)}{\left(1+G\left(\frac{y_{H_2O}}{y_{H_2}}\right)+H\cdot\sqrt{y_{H_2}}+I\cdot y_{H_2O}\right)} \quad (73)$$

$$\frac{dy_{H_2}}{dm} = -\frac{E \cdot y_{CO_2}\left(1-\left(\frac{1}{K_1}\right)\cdot\left(\frac{y_{H_2O}\cdot y_{CO}}{y_{CO_2}\cdot y_{H_2}}\right)\right)}{\left(1+G\left(\frac{y_{H_2O}}{y_{H_2}}\right)+H\cdot\sqrt{y_{H_2}}+I\cdot y_{H_2O}\right)} \quad (74)$$

$$\frac{dy_{CO}}{dm} = \frac{E \cdot y_{CO_2}\left(1-\left(\frac{1}{K_1}\right)\cdot\left(\frac{y_{H_2O}\cdot y_{CO}}{y_{CO_2}\cdot y_{H_2}}\right)\right)}{\left(1+G\left(\frac{y_{H_2O}}{y_{H_2}}\right)+H\cdot\sqrt{y_{H_2}}+I\cdot y_{H_2O}\right)} \quad (75)$$

$$\frac{dy_{H_2O}}{dm} = \frac{E \cdot y_{CO_2}\left(1-\left(\frac{1}{K_1}\right)\cdot\left(\frac{y_{H_2O}\cdot y_{CO}}{y_{CO_2}\cdot y_{H_2}}\right)\right)}{\left(1+G\left(\frac{y_{H_2O}}{y_{H_2}}\right)+H\cdot\sqrt{y_{H_2}}+I\cdot y_{H_2O}\right)} \quad (76)$$

$$\frac{dy_{He}}{dm} = 0 \quad (77)$$

Model of Graaf, Stamhuis and Beenackers (1988):

$$\frac{dy_{CO_2}}{dm} = -\frac{J\cdot N\cdot\left(y_{CO_2}\cdot y_{H_2}-\frac{y_{H_2O}\cdot y_{CO}}{K_1}\right)}{\left(1+L\cdot y_{CO}+N\cdot y_{CO_2}\right)\left(\sqrt{y_{H_2}}+y_{H_2O}\cdot Q\right)} \quad (78)$$

$$\frac{dy_{H_2}}{dm} = -\frac{J\cdot N\cdot\left(y_{CO_2}\cdot y_{H_2}-\frac{y_{H_2O}\cdot y_{CO}}{K_1}\right)}{\left(1+L\cdot y_{CO}+N\cdot y_{CO_2}\right)\left(\sqrt{y_{H_2}}+y_{H_2O}\cdot Q\right)} \quad (79)$$

$$\frac{dy_{CO}}{dm} = \frac{J\cdot N\cdot\left(y_{CO_2}\cdot y_{H_2}-\frac{y_{H_2O}\cdot y_{CO}}{K_1}\right)}{\left(1+L\cdot y_{CO}+N\cdot y_{CO_2}\right)\left(\sqrt{y_{H_2}}+y_{H_2O}\cdot Q\right)} \quad (80)$$

$$\frac{dy_{H_2O}}{dm} = \frac{J\cdot N\cdot\left(y_{CO_2}\cdot y_{H_2}-\frac{y_{H_2O}\cdot y_{CO}}{K_1}\right)}{\left(1+L\cdot y_{CO}+N\cdot y_{CO_2}\right)\left(\sqrt{y_{H_2}}+y_{H_2O}\cdot Q\right)} \quad (81)$$

$$\frac{dy_{He}}{dm} = 0 \quad (82)$$

Dimensionless variables:

m is the dimensionless mass, given by:

$$m = \frac{W}{W_0} \tag{83}$$

where W_0 is the total catalyst mass.

y_i is the molar fraction of the component *i*:

$$y_i = \frac{P_i}{P} \tag{84}$$

where P_i is the partial pressure of the component *i*, and *P* is the total pressure.

Dimensionless model parameters:

$$A = \frac{k_1 L_0 \cdot R \cdot T \cdot W_0}{q} \tag{85}$$

$$B = \sqrt{K_8^* \cdot P} \tag{86}$$

$$D = \frac{1}{K_8^* K_{24}^*} \tag{87}$$

$$E = \frac{k_1 \cdot R \cdot T \cdot f_P \cdot W_0}{q} \tag{88}$$

$$G = \frac{K_{H_2O}}{K_{15}^* K_{16}^* K_{H_2}} \tag{89}$$

$$H = \sqrt{K_{H_2} \cdot P} \tag{90}$$

$$I = K_{H_2O} \cdot P \tag{91}$$

$$J = \frac{k_1 \cdot R \cdot T \cdot f_P \cdot W_0 \cdot \sqrt{P}}{q \cdot P} \tag{92}$$

$$L = K_{CO} \cdot P \tag{93}$$

$$N = K_{CO_2} \cdot P \tag{94}$$

$$Q = \frac{K_{H_2O} \cdot \sqrt{P}}{K_{H_2}^{0.5}} \tag{95}$$

in which *q* is the volumetric flow rate, and f_P is a correction factor for pressure, with value of 10^{-5} bar Pa^{-1}.

2.6 **Reactor simulation and kinetic parameter estimation**

The reactor model was implemented through a computational routine in Python language. The conservation equations were integrated using the LSODA solver through the odeint package in the SciPy module. The integration was carried out for 1000 points between m = 0 and m = 1, with the following initial conditions:

$$y_{CO_2}\big|_{m=0} = 0.1 \tag{96}$$

$$y_{H_2}\big|_{m=0} = y_{H_2}^0 \tag{97}$$

$$y_{CO}\big|_{m=0} = 0 \tag{98}$$

$$y_{H_2O}\big|_{m=0} = 0 \tag{99}$$

$$y_{He}\big|_{m=0} = 1 - \left[0.1 + \left(y_{H_2}\big|_{m=0}\right)\right] \tag{100}$$

where y_{H2}^0 is the molar fraction of H_2 in the feed (0.10 for mixture 1, 0.25 for mixture 2 and 0.40 for mixture 3).

The determination of the kinetic parameters was conducted through a parameter estimation procedure based on an optimization problem solved with the Scipy module through the Differential Evolution method, presented by Storn and Price (1997), which, for each model, returned the respective set of parameters capable of minimizing the following objective function:

$$f_{obj} = \sum_{d} \left(X_{CALC_d} - X_{EXP_d}\right)^2 \tag{101}$$

where *d* is the pool of all the different sets of operational conditions, composed by temperature, space velocity and H_2/CO_2 molar ratio, $X_{CALC,d}$ is the CO_2 conversion predicted by the model for certain operational conditions, and $X_{EXP,d}$ is the experimental CO_2 conversion obtained under the same conditions. The CO_2 conversion is given by:

$$X = \frac{y^0_{CO_2} - y_{CO_2}}{y^0_{CO_2}} \tag{102}$$

being X the CO_2 conversion and y^0_{CO2} is the molar fraction of CO_2 in the feed. The upper and lower limits used in the search for the global optimum were within the order of magnitude of the respective parameters described in the literature for each model.

3 **RESULTS AND DISCUSSIONS**

3.1 **Catalyst characterization**

The commercial $CuO/ZnO/Al_2O_3$ catalyst used in the present work has a mass composition of 71% CuO, 24% ZnO and 5% Al_2O_3, as determined in previous research by our team (Gonzalez, 2017). In Figure 1, which shows the X-ray diffractogram of the calcined $CuO/ZnO/Al_2O_3$, the presence of CuO and ZnO is confirmed by the occurrence of their characteristic diffraction peaks. A diffraction peak characteristic of graphite also appears, probably due to the addition of 1.5% by mass of additive during the tableting of the catalyst (Gonzalez, 2017; Chu *et al*., 2013). The non-detection of alumina by X-ray diffraction is probably because its presence occurs in the amorphous phase.

Figure 1 – Diffractogram of the calcined catalyst

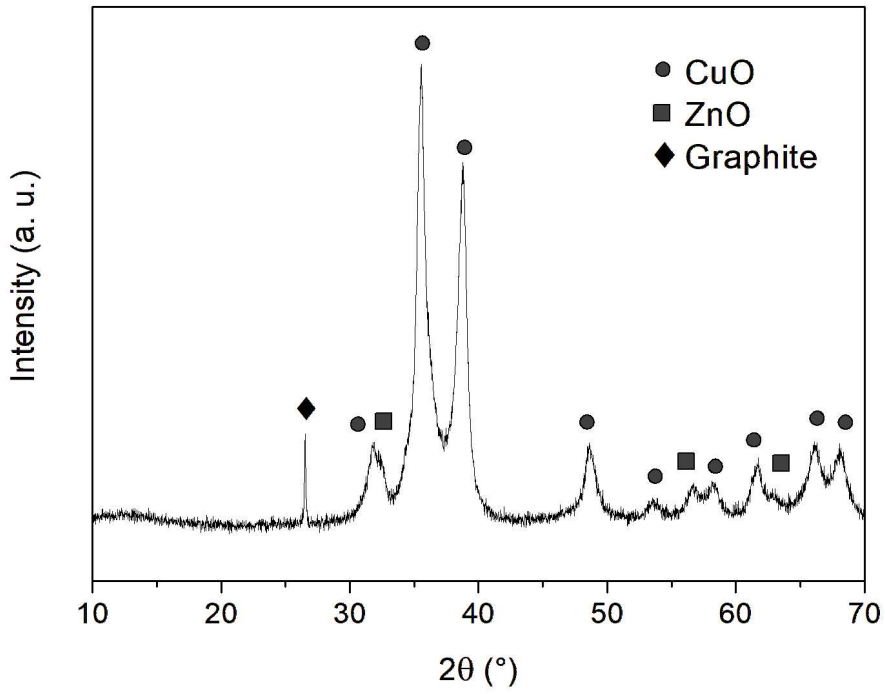

Source: The author, 2024.

The results of the TPR test are presented in Figure 2, in which a peak close to 207 °C can be observed. This maximum represents the reduction of CuO to metallic copper. Table 1 provides a comparison between the experimental H_2 consumption and the theoretical value, determined by the catalyst composition.

Figure 2 – TPR profile of the calcined catalyst

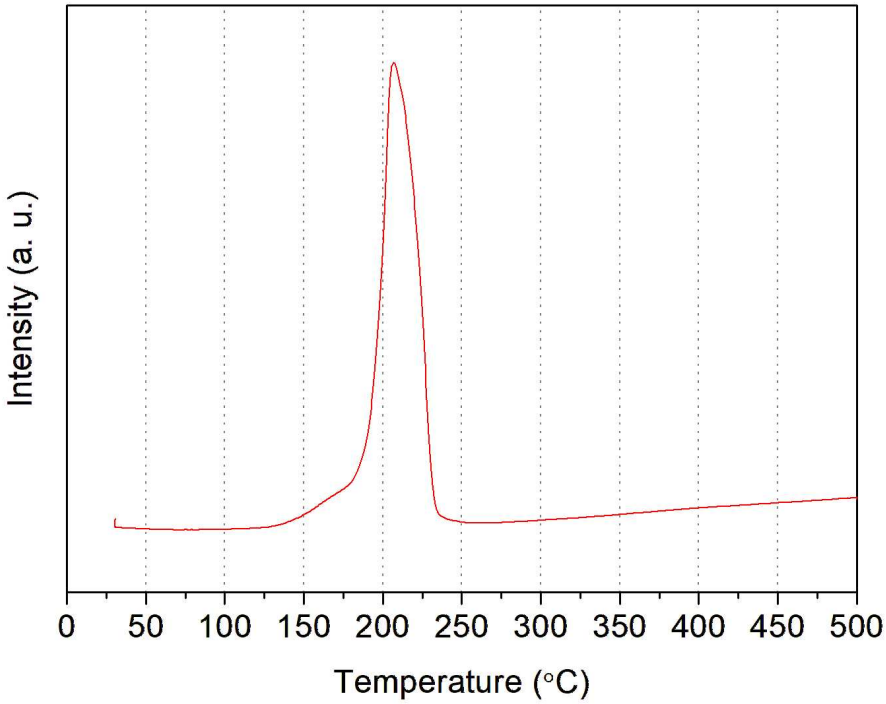

Source: The author, 2024.

Table 1 – Experimental and theoretical consumption of H_2

Experimental H_2 consumption (mmol g_{cat}^{-1})	Theoretical H_2 consumption (mmol g_{cat}^{-1})	Ratio between experimental and theoretical H_2 consumption (%)
8.647	8.926	97

Source: The author, 2024.

The theoretical consumption of H_2 was calculated considering a molar mass of 79.545 g/mol for CuO and a stoichiometric ratio of 1:1 between CuO and H_2 in the reduction of copper oxide, according to the equation (103).

$$\frac{1\ mol\ H_2}{1\ mol\ CuO} \cdot \frac{1\ mol\ CuO}{79.545\ g} \cdot \frac{71\ g}{100\ g\ sample} = \frac{8.926 \cdot 10^{-3}\ mol\ H_2}{g\ sample} \quad (103)$$

From the ratio between the experimental H_2 consumption and the theoretical value, it is possible to conclude that practically all copper oxide was reduced to metallic copper (Gonzalez, 2017; Blanco *et al*., 2019; Dasireddy *et al*., 2018).

3.2 **Analysis of diffusional effects**

Figure 3 presents the results of the evaluation of possible diffusional effects. The outcomes obtained under the different conditions were quite close, within a tolerance range, concluding that it was possible to disregard internal and external diffusional limitations under the conditions used in the tests of the present work. This means the system is under chemical kinetic control (Zhang *et al*., 2019). Thus, the applicability of hypothesis (e) (no diffusion limitations) to the modeling of the reactor was confirmed.

Figure 3 – CO_2 conversion versus temperature during the experiments for evaluation of diffusional limitations, at 30 m³ kg^{-1} h^{-1}, with H_2:CO_2 molar ratio of 4:1

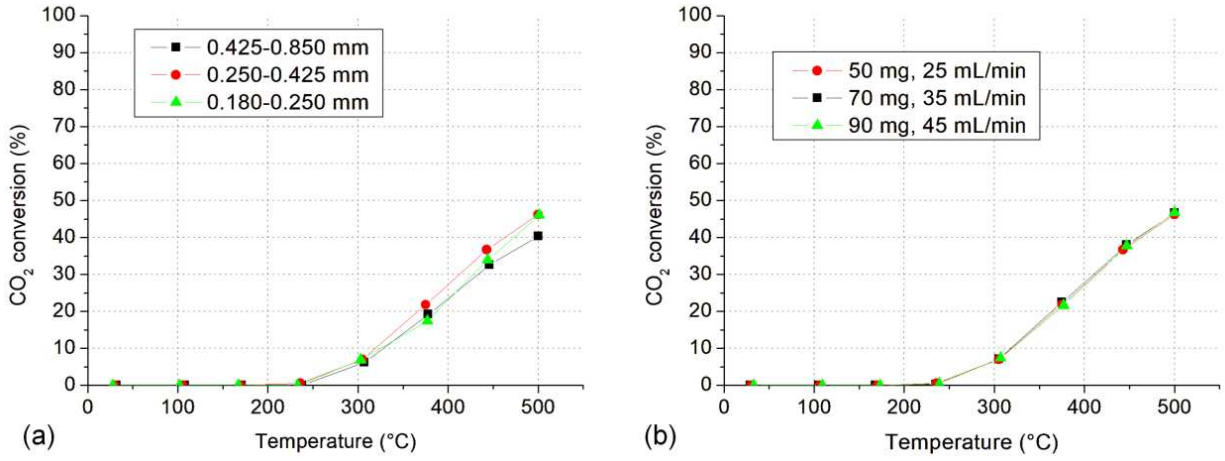

Legend: (a) – Evaluation of internal diffusional effects; (b) – Evaluation of external diffusional effects, with particle size range between 0.250 mm and 0.425 mm.

Source: The author, 2024.

3.3 **Stability evaluation**

Figure 4 presents the results of the stability evaluation. It is possible to observe that the commercial catalyst presented consistent performance, maintaining CO_2 conversion at around 28% for more than nine hours. Therefore, this indicates no meaningful catalyst deactivation under the test conditions. No significant methane formation was detected.

Figure 4 – CO_2 conversion versus time during the stability test at 500 °C, 18 $m^3\ kg^{-1}\ h^{-1}$ and H_2:CO_2 = 1:1

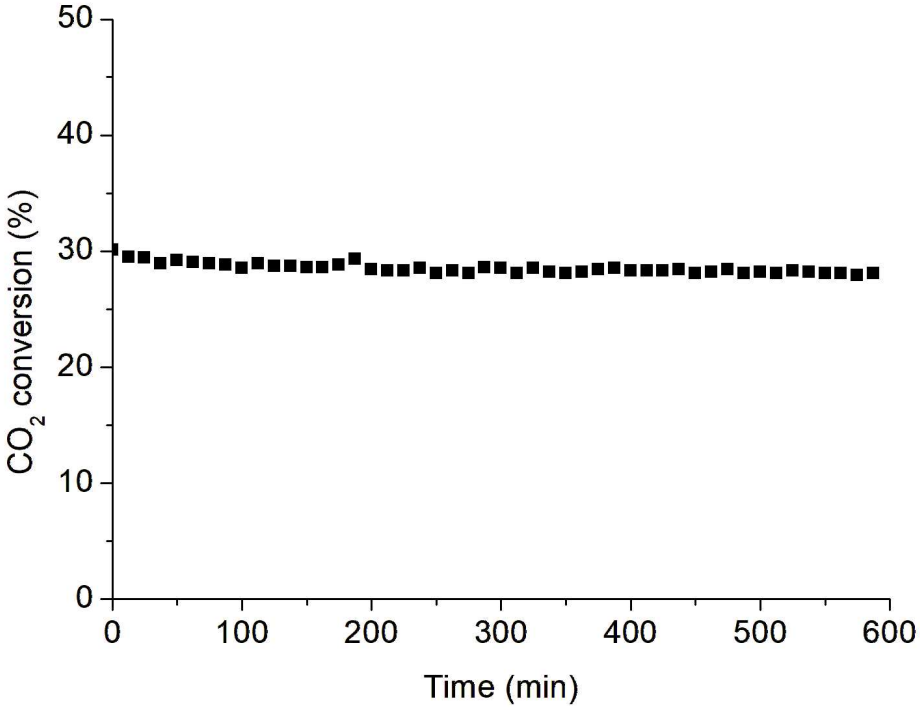

Source: The author, 2024.

In the same way, carbon monoxide was the only carbon-containing compound produced in all the light-off and fixed-temperature tests carried out in this work, pointing out that the catalyst performs 100% selectivity to CO.

3.4 **Thermodynamic modeling**

The equation (28) by Graaf *et al*. (1986) allows the calculation of the chemical equilibrium constant of the RWGS equation and, therefore, of the equilibrium CO_2 conversion as a function of temperature.

$$K_1 = 10^{\left(-\frac{2073}{T} + 2.029\right)} \tag{28}$$

The same equation was applied to calculate the equilibrium conversion through a computational routine in Python language, using the fsolve solver from the optimize library in the SciPy module. The mathematical procedure adopted is detailed in Appendix B.

Figure 5 shows the variation of K_1 as a function of temperature, confirming the expected trend for the constant to increase with increasing temperature due to the endothermicity of the reaction.

Figure 5 – RWGS equilibrium constant K_1 versus temperature

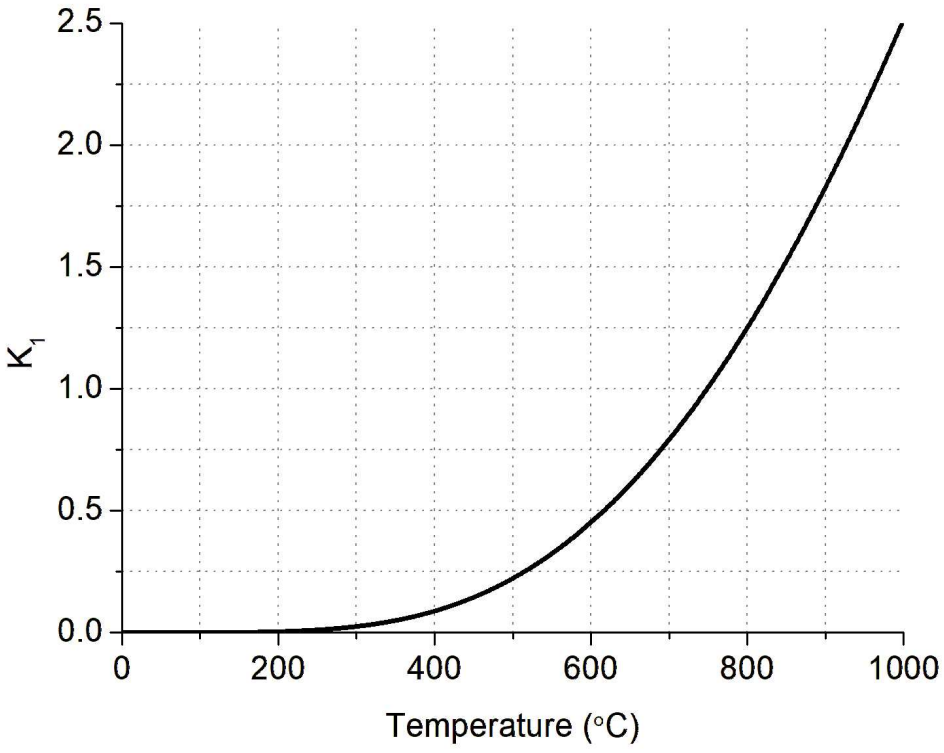

Source: The author, 2024.

Figure 6 presents the simulation results of carbon dioxide conversion at equilibrium as a function of temperature for the three H_2/CO_2 molar ratios studied. The thermodynamic curve points to two main trends: the increase in equilibrium conversion with increasing temperature, motivated by the rise in the K_1 constant, and, for the same temperature, a higher equilibrium conversion for higher H_2/CO_2 ratios, due to the presence of more reagent in the medium shifting the equilibrium towards CO_2 conversion.

Figure 6 – CO_2 conversion at equilibrium versus temperature

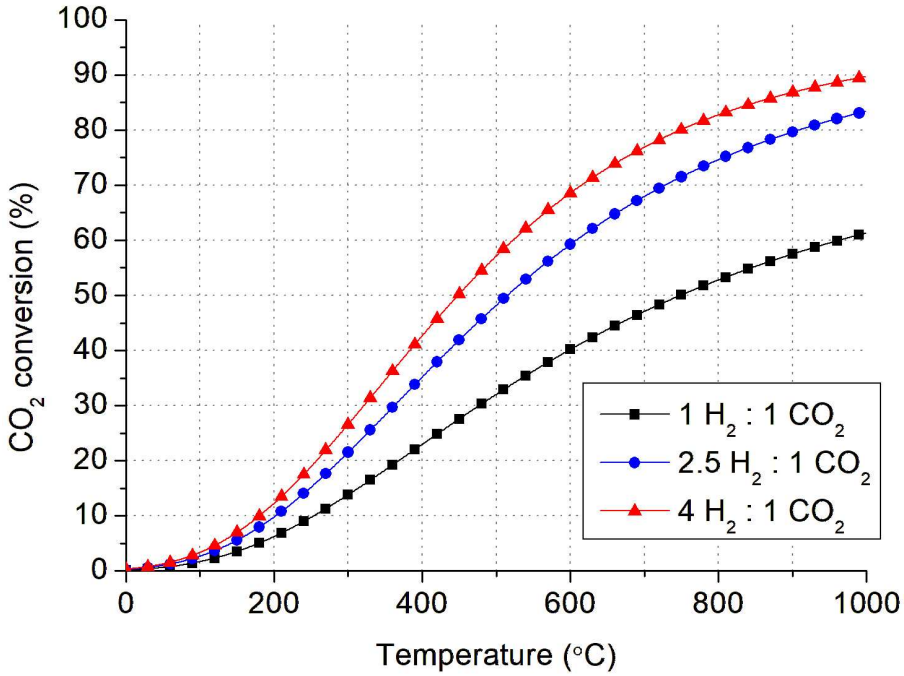

Source: The author, 2024.

If Gibbs free energy (ΔG_R) of the reaction is negative, RWGS tends to occur spontaneously. If, however, ΔG_R is greater than zero, the forward WGS reaction tends to occur. At constant temperature and pressure, ΔG_R is expressed by (Atkins; Jones, 2006):

$$\Delta G_R = \Delta G^\circ_R + RT \cdot \ln Q_1 \tag{104}$$

where ΔG°_R is the Standard Gibbs Free Energy of reaction, R is the universal gas constant, T is the temperature and Q_1 is given by (Atkins; Jones, 2006):

$$Q_1 = \frac{P_{CO} \cdot P_{H_2O}}{P_{CO_2} \cdot P_{H_2}} \quad (105)$$

At equilibrium, the equilibrium constant K_1 is equal to Q_1 and $\Delta G_R = 0$, thus equation (104) turns into (Atkins; Jones, 2006):

$$\Delta G°_R = -RT \cdot \ln K_1 \quad (106)$$

Otherwise, using a feed mixture with a H_2/CO_2 molar ratio greater than 1 means working with a reaction quotient Q_1 lower than K_1, because the reactants are in the denominator of Q_1. Therefore, the reaction will proceed in the direction of the formation of CO and H_2O, so that Q_1 increases until it equals K_1. The higher the H_2/CO_2 ratio, the lower the value of Q_1 and the more the equilibrium will be shifted towards the consumption of CO_2. This helps to understand that the conversions achieved were higher with larger excesses of H_2 (Atkins; Jones, 2006).

The effect of the temperature in the equilibrium can be explained through Le Châtelier Principle, expressed through van't Hoff equation, (107) (Atkins; Jones, 2006):

$$\ln \frac{K_2}{K_1} = \frac{\Delta H°_R}{R} \cdot \left(\frac{1}{T_1} - \frac{1}{T_2}\right) \quad (107)$$

where K_2 is the equilibrium constant at temperature T_2, K_1 is the equilibrium constant at temperature T_1 and $\Delta H°_R$ is the standard enthalpy of reaction. RWGS reaction is endothermic, then $\Delta H°_R > 0$. If T_2 is higher than T_1, $1/T_2$ will be smaller than $1/T_1$, thereby the term between parenthesis will be positive. Therefore, $\ln(K_2/K_1)$ is necessarily positive, which means the constant K_2 is greater than K_1. Thus, using a higher temperature favors CO_2 and H_2 consumption, as well as CO and H_2O formation (Atkins; Jones, 2006).

3.5 **Effects of composition, space velocity, and temperature in catalytic tests conducted at a fixed temperature**

Figures 7, 8 and 9 show the results of the tests at a fixed temperature. The conversion data presented are the average CO_2 conversion values recorded after reaching a steady state, gathered in Appendix C. To better guide the discussion, each graph shows the CO_2 conversion at a given constant operating condition (space velocity, temperature, H_2:CO_2 ratio in the feed), showing the different outcomes obtained with the variation of the other two conditions.

3.5.1 Effect of the feed composition

Figure 7 illustrates the direct relation that the H_2:CO_2 molar ratio in the feed has with CO_2 conversion, for the same space velocity. The results at 430 °C were chosen because they provide a clearer view, but at 330 °C and 380 °C the effect is equivalent.

Figure 7 – Experimental results of CO_2 conversion at 430 °C for different H_2:CO_2 molar ratios at the three space velocities

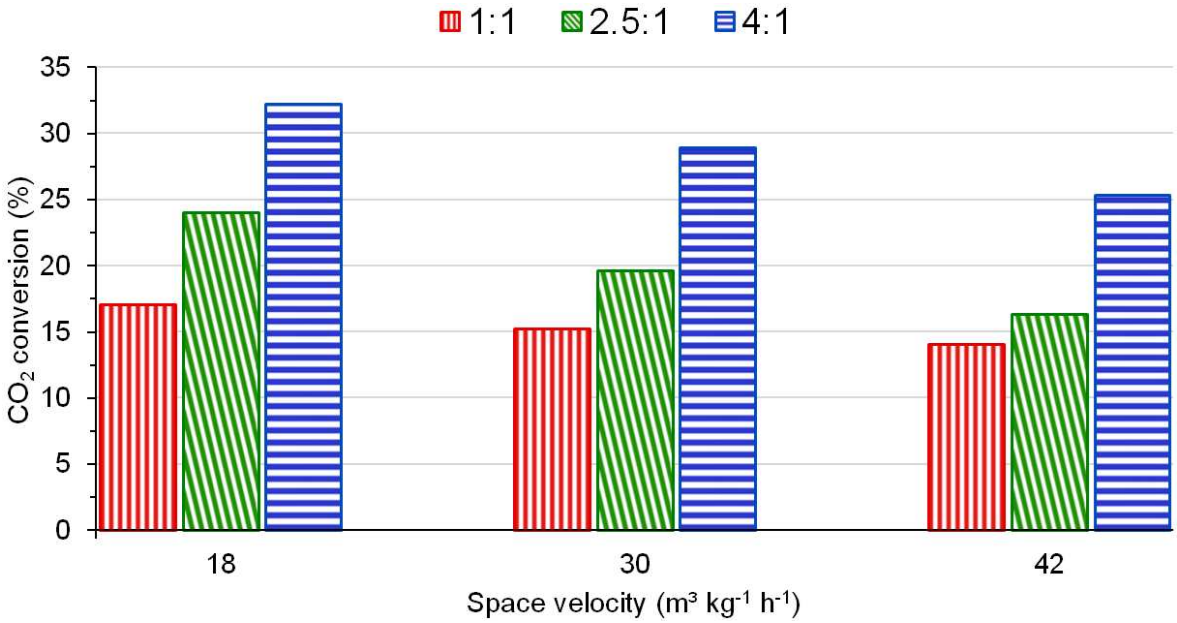

Source: The author, 2024.

From a kinetic point of view, higher H_2 partial pressures may be associated with a higher hydrogen coverage and a higher adsorption capacity on the catalyst surface. In H_2-poor reaction mixtures, preferential adsorption of CO_2 may lead to a CO_2-rich surface, reducing the chances of the reactants interacting. This is mitigated when higher H_2 partial pressures are used (Reina; Odriozola; Arellano-Garcia, 2021). Ginés, Marchi, and Apesteguía (1997) studied the effect of the inlet composition on the initial reaction rate with $CuO/ZnO/Al_2O_3$ catalysts, changing the H_2/CO_2 molar ratio between 0.3 and 9.0. They stated that a reconstruction of the copper surface takes place at ratios of 3 or over, making the surface more reactive to dissociative CO_2 adsorption.

3.5.2 Effect of the space velocity

The effect of the space velocity can be observed in Figure 8. The results with mixture 3 (H_2:CO_2 molar ratio of 4:1) were chosen because they provide a clearer view, but with mixtures 1 and 2 the effect is equivalent.

Figure 8 – Experimental results of CO_2 conversion with 4 H_2:1 CO_2 molar ratio for different space velocities at the three temperatures

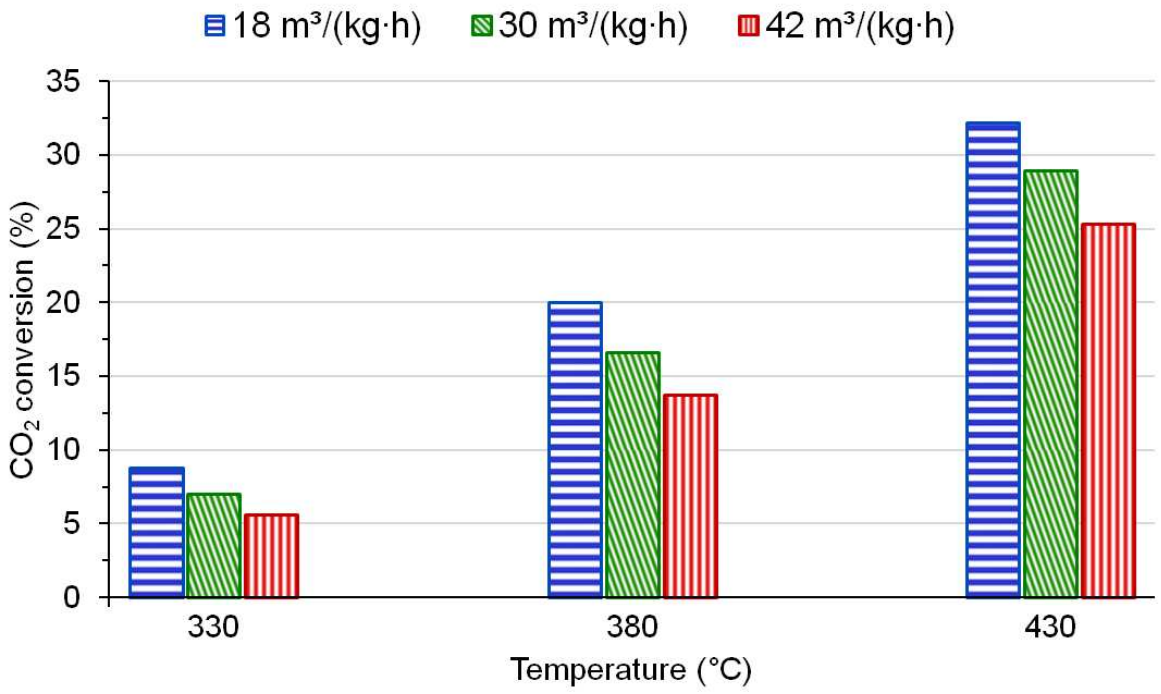

Source: The author, 2024.

Lower space velocities lead to higher CO_2 conversions, for the same temperature. For each of the temperature levels studied, the conversion at 18 $m^3\ kg^{-1}\ h^{-1}$ is always higher than that at 30 $m^3\ kg^{-1}\ h^{-1}$, which, in turn, is higher than the conversion at 42 $m^3\ kg^{-1}\ h^{-1}$. This effect is related to the fact that a higher spatial velocity causes the residence time to be shorter. Therefore, the contact time provided between the reactants and the catalytic surface is shorter, leading to a decrease in conversion (Park *et al.*, 2014; Ojeda, 2022).

3.5.3 Effect of the temperature

In Figure 9, is possible to observe the influence of temperature on RWGS reaction for the same space velocity. The results at 18 $m^3\ kg^{-1}\ h^{-1}$ were chosen because they provide a clearer view, but at 30 $m^3\ kg^{-1}\ h^{-1}$ and 42 $m^3\ kg^{-1}\ h^{-1}$ the effect is equivalent.

Figure 9 – Experimental results of CO_2 conversion at 18 $m^3\ kg^{-1}\ h^{-1}$ for different temperatures at the three H_2/CO_2 molar ratios

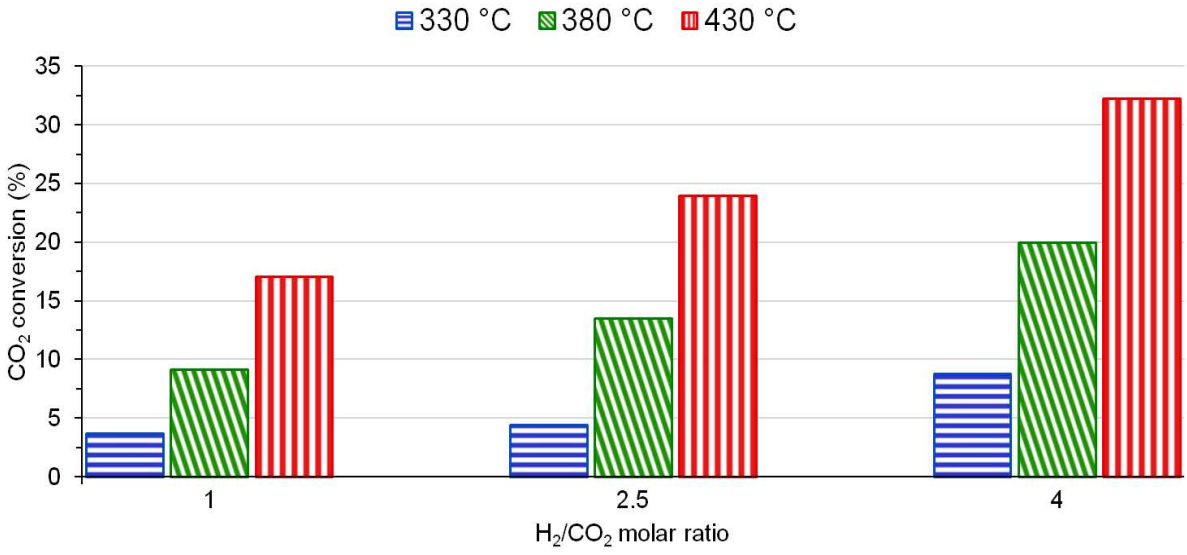

Source: The author, 2024.

The difference in temperature affects the kinetic constant, as shown by the Arrhenius equation:

$$\ln k_1 = \ln k_{1,0} - \frac{E_{a,1}}{R \cdot T} \tag{108}$$

As can be seen in equation (108), the higher the value of *T*, the lower the magnitude of the negative term. As a result, the value of ln(k_1) will be higher, thus k_1 will be larger as well, leading to a higher rate constant and, consequently, a higher reaction rate.

3.6 **Comparison between light-off tests and fixed temperature tests**

Figure 10 presents the results of the light-off tests carried out at 30 $m^3\ kg^{-1}\ h^{-1}$ with H_2/CO_2 molar ratios of 1:1, 2.5:1, and 4:1. The conversion and temperature data obtained from these tests are listed in Appendix D. The same graph also shows the CO_2 conversion obtained through the catalytic runs at fixed temperatures with the three molar ratios studied at 30 $m^3\ kg^{-1}\ h^{-1}$. The highest conversion is obtained with the molar ratio 4 H_2:1 CO_2, while the lowest conversion at the same temperature is associated with the reaction mixture with a molar ratio of 1:1. As expected, Mixture 2, with an intermediate H_2/CO_2 ratio, provided intermediate conversion values.

Figure 10 – Experimental results of CO_2 conversion vs. temperature at 30 m^3 kg^{-1} h^{-1} with different H_2/CO_2 molar ratios in light-off tests and fixed-temperature tests

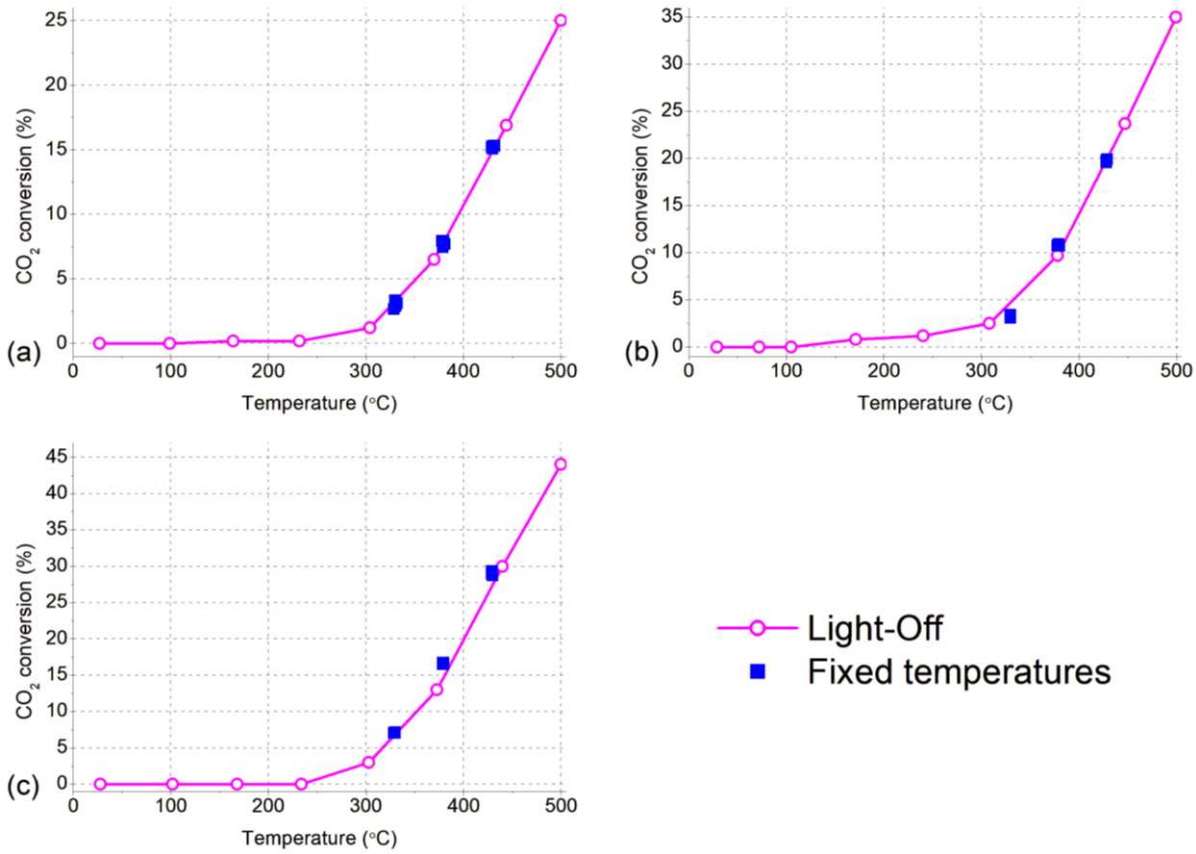

Legend: (a) – H_2/CO_2 molar ratio of 1:1; (b) – H_2/CO_2 molar ratio of 2.5:1; (c) – H_2/CO_2 molar ratio of 4:1.

Source: The author, 2024.

It is also possible to identify in Figure 10 a significant consistency between the values obtained by light-off tests and tests at fixed temperatures. This indicates that, on the commercial $CuO/ZnO/Al_2O_3$ catalyst, there is no significant influence of possible transient processes in CO_2 conversion along the temperature ramp under the conditions defined for the experiments. Therefore, obtaining kinetic parameters from data provided by light-off curves turns out to be a concrete possibility that will be applied in the following sections.

3.7 **Light-off curves simulation with kinetic parameters from the literature**

The simulation of the light-off curves was conducted using the values of the kinetic parameters originally reported in the literature. Because one of the parameters of the Ginés, Marchi, and Apesteguía (1997) model was not reported in the original paper, it was not possible to simulate the light-off curve using this model.

Vanden Bussche and Froment (1996) carried out 276 experiments, varying the temperature between 180 and 280 °C, the CO/CO_2 ratio between 0 and 4.1, and the total pressure between 15 and 51 bar to produce the kinetic data used to fit the parameters of their kinetic model for methanol synthesis on a commercial $CuO/ZnO/Al_2O_3$ catalyst. The values of the parameters reported in the original paper are listed in Table 2.

Table 2 – Kinetic parameters obtained by Vanden Bussche and Froment (1996)

Parameter	Value
$A_{\sqrt{KH2}}$ ($bar^{-0,5}$)	0.499
$B_{\sqrt{KH2}}$ (J mol^{-1})	17197
A_{KH2O} (bar^{-1})	$6.62 \cdot 10^{-11}$
B_{KH2O} (J mol^{-1})	124119
$A_{KH2O/K15*K16*KH2}$	3453.38
A_{k1} (mol kg^{-1} s^{-1} bar^{-1})	$1.22 \cdot 10^{10}$
B_{k1} (J mol^{-1})	-94765

Source: Vanden Bussche; Froment, 1996.

In their kinetic study of low-pressure methanol synthesis over a commercial Cu–Zn–Al catalyst, Graaf, Stamhuis, and Beenackers (1988) carried out a series of experiments under steady-state conditions. Temperatures between 210.4 °C and 243.6 °C were applied, at total pressures of 15 bar, 30 bar and 50 bar, space velocities between 0.1 m^3 s^{-1} kg^{-1} and 7 m^3 s^{-1} kg^{-1}, CO/CO_2 molar ratios between 0 and 5.7 in the feed, and H_2/CO_2 molar ratios between 2.6 and 40.9 in the feed. They obtained the parameters shown in Table 3.

Table 3 – Kinetic parameters obtained by Graaf, Stamhuis and Beenackers (1988)

Parameter	Value
A_{k1} (mol s^{-1} kg^{-1} $bar^{-0.5}$)	$(7.31 \pm 4.90)\cdot10^{8}$
B_{k1} (J mol^{-1})	-123400 ± 1600
A_{KCO} (bar)	$(7.99 \pm 1.28)\cdot10^{-7}$
B_{KCO} (J mol^{-1})	58100 ± 600
A_{KCO2} (bar)	$(1.02 \pm 0.16)\cdot10^{-7}$
B_{KCO2} (J mol^{-1})	67400 ± 600
$A_{KH2O\sqrt{}KH2}$ ($bar^{-0,5}$)	$(4.13 \pm 1.51)\cdot10^{-11}$
$B_{KH2O\sqrt{}KH2}$ (J mol^{-1})	104500 ± 1100

Source: Graaf; Stamhuis; Beenackers, 1988.

Riquelme (2020) adjusted the model of Vanden Bussche and Froment and the model of Graaf, Stamhuis and Beenackers to kinetic data obtained at 20 bar with two sets of temperatures, 240°C and 260°C, over a commercial $Cu/ZnO/Al_2O_3$ catalyst (CuO 63.5%, ZnO 24.7%, Al_2O_3 10%, and MgO 1.3%) and a $Cu/ZnO/Al_2O_3$ catalyst synthesized in the laboratory (CuO 60%, ZnO 30%, and Al_2O_3 10%). The parameters found by the author are in Tables 4 and 5.

Table 4 – Kinetic parameters obtained by Riquelme (2020) with the kinetic model of Vanden Bussche and Froment (1996)

Parameter	Value estimated for synthesized catalyst	Value estimated for commercial catalyst
$A_{\sqrt{}KH2}$ ($bar^{-0,5}$)	0.644	0.376
$B_{\sqrt{}KH2}$ (J mol^{-1})	21719	23183
A_{KH2O} (bar^{-1})	$3.31\cdot10^{-7}$	$3.31\cdot10^{-7}$
B_{KH2O} (J mol^{-1})	96829	88741
$A_{KH2O/K15*K16*KH2}$	1064.90	2716.61
A_{k1} (mol kg^{-1} s^{-1} bar^{-1})	$5.90\cdot10^{9}$	$1.88\cdot10^{10}$
B_{k1} (J mol^{-1})	-48144	-70605

Source: Riquelme, 2020.

Table 5 – Kinetic parameters obtained by Riquelme (2020) with the kinetic model of Graaf, Stamhuis and Beenackers (1988)

Parameter	Value estimated for synthesized catalyst	Value estimated for commercial catalyst
A_{k1} (mol s^{-1} kg^{-1} $bar^{-0.5}$)	$1.96 \cdot 10^{9}$	$2.26 \cdot 10^{10}$
B_{k1} (J mol^{-1})	-189348	-292083
A_{KCO} (bar)	$4.87 \cdot 10^{-2}$	$7.62 \cdot 10^{-2}$
B_{KCO} (J mol^{-1})	86017	64162
A_{KCO2} (bar)	$1.04 \cdot 10^{-2}$	$1.01 \cdot 10^{-2}$
B_{KCO2} (J mol^{-1})	31623	33224
$A_{KH2O\sqrt{}KH2}$ ($bar^{-0,5}$)	$2.90 \cdot 10^{-5}$	$2.21 \cdot 10^{-6}$
$B_{KH2O\sqrt{}KH2}$ (J mol^{-1})	9.32	67795

Source: Riquelme, 2020.

Dehghanpoor *et al*. (2022), in their feasibility study of the conversion of petrochemical off-gas streams to methanol over a commercial $CuO/ZnO/Al_2O_3$ catalyst, evaluated parameters for the model of Graaf, Stamhuis, and Beenackers (1988) using real plant data. They reported the parameters presented in Table 6.

Table 6 – Kinetic parameters obtained by Dehghanpoor *et al*. (2022) with the kinetic model of Graaf, Stamhuis and Beenackers (1988)

Parameter	Value
A_{k1} (mol s^{-1} kg^{-1} $bar^{-0.5}$)	$9.64 \cdot 10^{11}$
B_{k1} (J mol^{-1})	-152900.00
A_{KCO} (bar)	$2.14 \cdot 10^{-5}$
B_{KCO} (J mol^{-1})	47120.51
A_{KCO2} (bar)	$7.92 \cdot 10^{-7}$
B_{KCO2} (J mol^{-1})	62148.78
$A_{KH2O\sqrt{}KH2}$ ($bar^{-0,5}$)	$4.39 \cdot 10^{-9}$
$B_{KH2O\sqrt{}KH2}$ (J mol^{-1})	84350.46

Source: Dehghanpoor *et al*., 2022.

The model of Vanden Bussche and Froment (1996) was employed for the simulation of the light-off curves using the values of the kinetic parameters reported

in the original paper and using the parameters estimated by Riquelme (2020). The model of Graaf, Stamhuis, and Beenackers (1988) was employed using the original parameters and the parameters proposed by the works of Riquelme (2020) and Dehghanpoor *et al*. (2022). The results of these simulations are presented in Figures 11 and 12, compared with the experimental data.

Figure 11 – Comparison between the experimental light-off curves at 30 $m^3\ kg^{-1}\ h^{-1}$ and the simulation through the Vanden Bussche and Froment model with original parameters

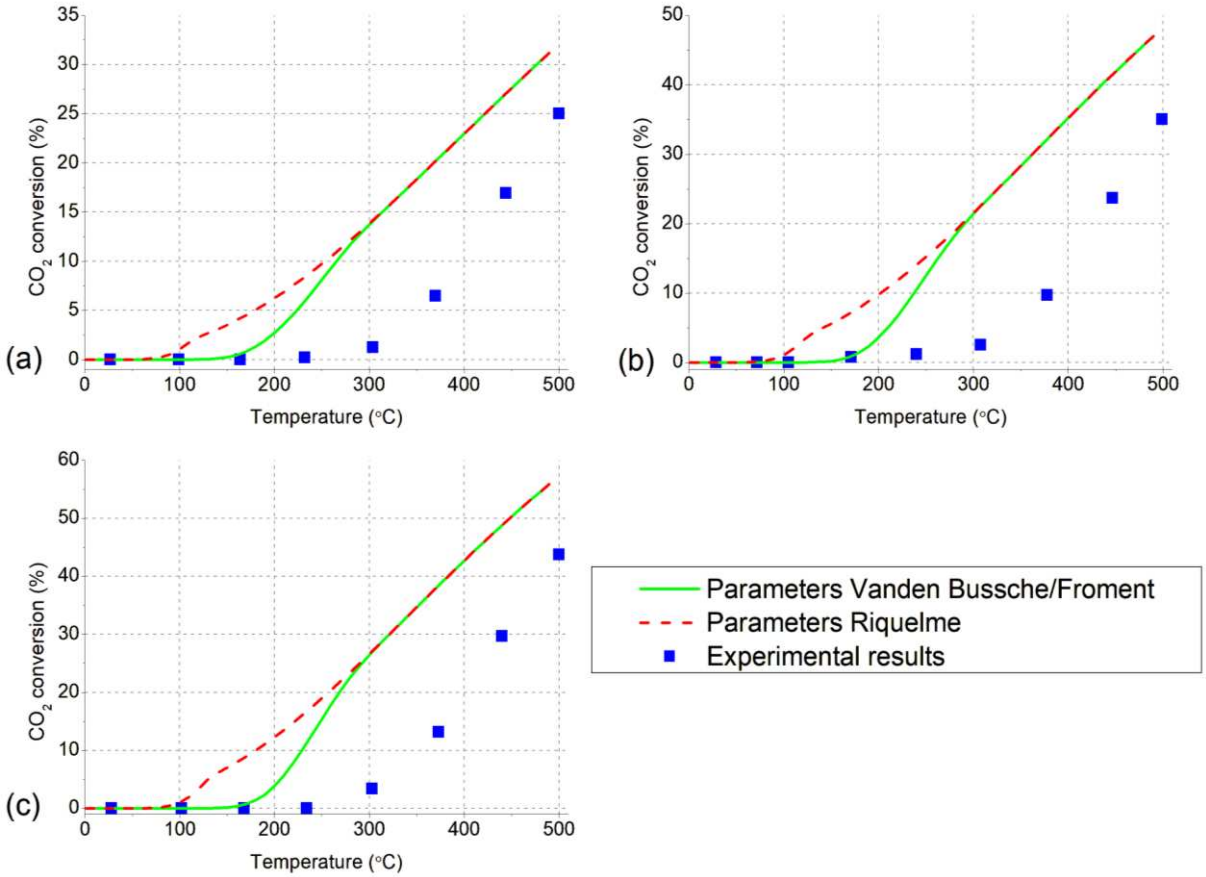

Legend: (a) – H_2/CO_2 molar ratio of 1:1; (b) – H_2/CO_2 molar ratio of 2.5:1; (c) – H_2/CO_2 molar ratio of 4:1.
Source: The author, 2024.

Figure 11 shows that the introduction of the original Vanden Bussche and Froment parameters into the reactor model for the conditions used in the light-off tests was not able to reproduce the behavior observed in the catalytic tests faithfully, predicting conversions higher than the experimental conversions from 160 °C onwards for all compositions analyzed. The parameters provided by Riquelme (2020) led to a result very similar to that observed with the Vanden Bussche and Froment

parameters, except in the range between 100 °C and 300 °C, where the Riquelme (2020) parameters produce higher conversions than the original parameters.

Figure 12 – Comparison between the experimental light-off curves at 30 $m^3\ kg^{-1}\ h^{-1}$ and the simulation through the Graaf, Stamhuis, and Beenackers model with original parameters

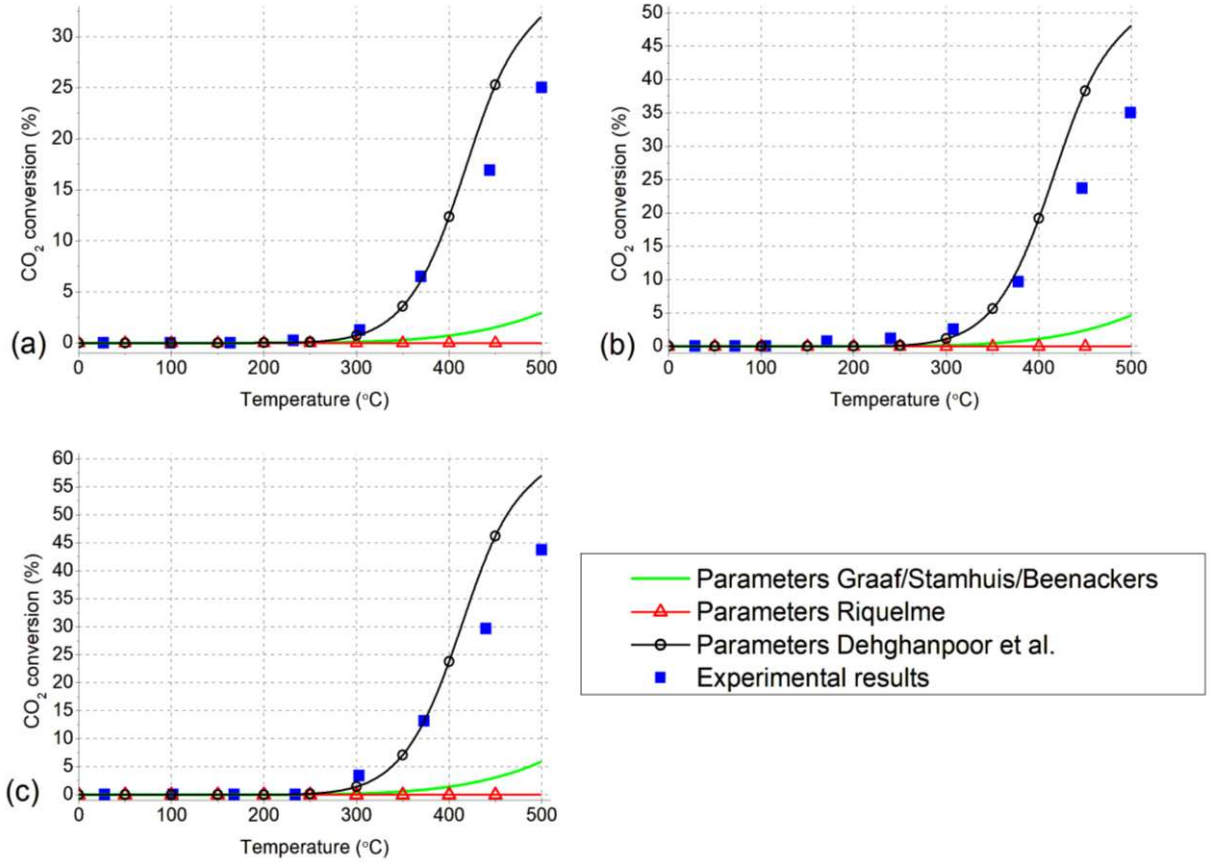

Legend: (a) – H_2/CO_2 molar ratio of 1:1; (b) – H_2/CO_2 molar ratio of 2.5:1; (c) – H_2/CO_2 molar ratio of 4:1.
Source: The author, 2024.

Figure 12 shows that the original parameters of Graaf, Stamhuis, and Beenackers provide significantly lower conversions than those obtained experimentally. The simulation using the parameters reported by Riquelme (2020) underestimates even more significantly the CO_2 conversion. While these two sets of parameters predict a very late onset of CO_2 conversion along the temperature ramp, the parameters of Dehghanpoor (2022), in turn, manage to reasonably reproduce the trend of the experimental data up to approximately 370 °C, when the calculated conversion starts to be quite above the experimental values.

The large difference in the fit of the reactor model to the experimental data using the parameters from the literature reflects the difficulty of extrapolating the use of kinetic parameters to different experimental conditions. In the studies by Vanden Bussche and Froment (1996), Riquelme (2020), and Graaf, Stamhuis, and Beenackers (1988), experiments were carried out at pressures between 15 and 51 bar and in a temperature range from 180 °C to 280 °C. The specific experimental conditions used by Dehghanpoor *et al*. (2022) in adjusting the parameters were not explained. This temperature window is narrow compared to the range covered by the light-off tests, which may help to explain the wide deviation from the experimental conversions when these parameters are used to model the reactor. Other possible causes for the discrepancy observed between the experimentally observed behavior and the predictions obtained with kinetic parameters from the literature involve possible differences in formulation and/or preparation technique of the catalysts and the significant distance between the pressure levels applied in the kinetic studies analyzed and the atmospheric pressure used in the present work.

3.8 **Kinetic parameter estimation**

The reactor model with the reaction rate proposed by Ginés, Marchi, and Apesteguía (1997) was fitted to the light-off experimental data obtained in this work. Table 7 lists the values obtained for the proposed parameters.

Table 7 - Parameters estimated using the kinetic model of Ginés, Marchi, and Apesteguía (1997)

Parameter	Value
$k_{1,0} \cdot L_0$ (mol h^{-1} g^{-1} atm^{-1})	$1.034 \cdot 10^{9}$
$E_{a,1}$ (kcal mol^{-1})	22.82
$k_{4,0}$ (atm^{-1})	5.131
$\Delta E_{a,4}$ (kcal mol^{-1})	2.014
$k_{5,0}$ (atm^{-1})	$6.963 \cdot 10^{-5}$
$\Delta E_{a,5}$ (kcal mol^{-1})	0.0491

Source: The author, 2024.

The same procedure was adopted for the models of Vanden Bussche and Froment (1996) and Graaf, Stamhuis, and Beenackers (1988), providing the estimation of the parameters shown in Tables 8 and 9.

Table 8 – Parameters estimated using the kinetic model of Vanden Bussche and Froment (1996)

Parameter	Value
$A_{\sqrt{KH2}}$ ($bar^{-0,5}$)	0.300
$B_{\sqrt{KH2}}$ (J mol^{-1})	10030.7
A_{KH2O} (bar^{-1})	$1.00 \cdot 10^{-11}$
B_{KH2O} (J mol^{-1})	91163.8
$A_{KH2O/K15*K16*KH2}$	3991.59
A_{k1} (mol kg s^{-1} bar^{-1})	$1.00 \cdot 10^{9}$
B_{k1} (J mol^{-1})	-111053.8

Source: The author, 2024.

Table 9 – Parameters estimated using the kinetic model of Graaf, Stamhuis, and Beenackers (1988)

Parameter	Value
A_{k1} (mol s^{-1} kg^{-1} $bar^{-0.5}$)	$3.16 \cdot 10^{8}$
B_{k1} (J mol^{-1})	-92897.6
A_{KCO} (bar)	$2.29 \cdot 10^{-6}$
B_{KCO} (J mol^{-1})	89986.3
A_{KCO2} (bar)	$2.21 \cdot 10^{-7}$
B_{KCO2} (J mol^{-1})	53564.6
$A_{KH2O\sqrt{KH2}}$ ($bar^{-0,5}$)	$9.71 \cdot 10^{-9}$
$B_{KH2O\sqrt{KH2}}$ (J mol^{-1})	109957.8

Source: The author, 2024.

Performing catalytic runs in an integral reactor at 1 atm in the 493–523 °C temperature range, with a 2–40 g h mol^{-1} contact time range and a H_2/CO_2 molar ratio of 6 in the feed, Ginés, Marchi, and Apesteguía (1997) obtained kinetic data to fit the parameters of their kinetic model, presented in Table 10. They plotted the $\ln(k_1 L_0)$ values as a function of the inverse of the temperature to calculate the

apparent activation energy of the RWGS reaction, presented in Table 11, together with other values available in the literature and the value of $E_{a,1}$ found in the present work through the kinetic model of Ginés, Marchi, and Apesteguía (1997). It can be observed that the estimated value is within the range of reported values.

Table 10 – Kinetic parameters obtained by Ginés, Marchi, and Apesteguía (1997) in their kinetic model, according to the temperature

Temperature (K)	k_1L_0 (mol h^{-1} g^{-1} atm^{-1})	K_8* (atm^{-1})
493	0.0200 ± 0.0015	0.060 ± 0.008
503	0.0487 ± 0.0044	0.051 ± 0.004
513	0.0711 ± 0.0070	0.041 ± 0.007
523	0.1287 ± 0.0077	0.039 ± 0.002

Source: Ginés; Marchi; Apesteguía, 1997.

Table 11 – Apparent activation energy values reported in the literature

Reference	Apparent activation energy (kJ mol^{-1})	Catalyst
Ginés, Marchi and Apesteguía (1997)	100.4	$CuO/ZnO/Al_2O_3$
Van Herwijnen and de Jong (1980)	98.3	Cu/ZnO
Ernst, Campbell and Moretti (1992)	75.3	Cu(110)
Yoshihara and Campbell (1996)	78.0	Cu(110)
Purnama *et al*. (2004)	108.0	$CuO/ZnO/Al_2O_3$
Jadhav and Vaidya (2020)	72.4	$CuO/ZnO/Al_2O_3$
This work (2024)	95.5	$CuO/ZnO/Al_2O_3$

Source: The author, 2024.

The average relative error for each kinetic model was calculated using equation (109):

$$Average\ relative\ error = \frac{\sum\left(\frac{|X_{CALC} - X_{EXP}|}{X_{EXP}}\right) \cdot 100\%}{Number\ of\ catalytic\ runs} \quad (109)$$

The average relative error and the minimum value of the objective function found after optimization are presented in Table 12.

Table 12 – Average relative error and values of f_{obj} after the estimation of the parameters for each kinetic model studied

Model	Average relative error (%)	f_{obj}
Ginés, Marchi and Apesteguía (1997)	16.9	0.0020
Vanden Bussche and Froment (1996)	11.6	0.0039
Graaf, Stamhuis and Beenackers (1988)	12.3	0.0011

Source: The author, 2024.

The results listed in Table 12 indicate a virtually equivalent quality of fit for the three models, with a slight emphasis on the models by Vanden Bussche and Froment (1996) and Graaf, Stamhuis, and Beenackers (1988), which provided the lowest average error and the lowest value for the objective function, respectively.

Regarding the reaction scheme, the three models have in common the fact that they are based on the adsorption of CO_2 and the dissociative adsorption of H_2.

The models by Vanden Bussche and Froment (1996) and Ginés, Marchi, and Apesteguía (1997) present the greatest degree of similarity between them. Both assume a redox mechanism that occurs only on the copper surface, with zinc oxide playing merely a structural promotion role. In this mechanism, metallic copper is the active site consecutively oxidized and reduced by CO_2 and H_2. Furthermore, in both studies, the dissociative adsorption of CO_2 (23) is indicated as the rate-determining step.

$$CO_{2\,(g)} + S \rightleftharpoons CO_{(g)} + O_{(a)} \tag{23}$$

The two models differ concerning water formation and desorption. The reaction route proposed by Ginés, Marchi, and Apesteguía (1997) describes the formation of water in a direct manner, with two individually adsorbed hydrogen atoms combining with an adsorbed oxygen atom to form water, according to the reaction (24):

$$2\,H_{(a)} + O_{(a)} \rightleftharpoons H_2O_{(g)} \tag{24}$$

The reaction route of Ginés, Marchi, and Apesteguía (1997) does not take into account intermediate stages of desorption, neither of water nor of carbon monoxide, because the authors assumed a low coverage of these adsorbates under the temperature and partial pressure conditions used in the work. The mechanism related to the Vanden Bussche and Froment (1996) model also does not involve a CO desorption step but considers the water desorption step, which they describe as relatively slow. Furthermore, the formation of water is assumed to occur in two stages. In the first (15), an adsorbed O atom is hydrogenated, giving rise to an intermediate hydroxyl species; in the second (16), the hydroxyl interacts with a second adsorbed H atom to form water, which is subsequently desorbed in stage (17).

$$H_{(a)} + O_{(a)} \rightleftharpoons OH_{(a)} + S \quad (15)$$

$$H_{(a)} + OH_{(a)} \rightleftharpoons H_2O_{(a)} + S \quad (16)$$

$$H_2O_{(a)} \rightleftharpoons H_2O_{(g)} + S \quad (17)$$

The lower average error obtained with the Vanden Bussche and Froment model indicates that taking into account the intermediate stages of water formation and desorption may have contributed to greater accuracy. Even so, the difference between the errors was relatively small, and it is possible to consider that the assumptions made in the Ginés, Marchi, and Apesteguía model meet a compromise between a simplified mechanism and a faithful representation of the system behavior, even achieving a lower value for f_{obj} with this model.

On the other hand, Graaf, Stamhuis, and Beenackers (1988) assumed a dual-site associative mechanism via formate route, in which CO and CO_2 adsorb competitively on site 1, and H_2 and H_2O adsorb competitively on site 2.

$$CO_{2\,(g)} + S_1 \rightleftharpoons CO_{2\,(a)} \quad (33)$$

$$H_{2\,(g)} + 2\,S_2 \rightleftharpoons 2\,H_{(a)} \quad (34)$$

$$CO_{2\,(a)} + H_{(a)} \rightleftharpoons HCO_{2\,(a)} + S_2 \quad (35)$$

This reaction route considers the ability of ZnO to activate the H_2 molecule through its dissociative adsorption while it is not capable of adsorbing carbon monoxide, as opposed to Cu^+, which can adsorb CO and not H_2. Therefore, the type

2 sites responsible for the scission of the H_2 molecule may be associated with ZnO, while the type 1 sites would be related to Cu^+ and its adjacent oxygen vacancies, capable of promoting the adsorption of CO and CO_2. After a statistical evaluation, Graaf, Stamhuis, and Beenackers pointed out the hydrogenation of the formate intermediate as the rate-determining step, which produces CO adsorbed at site 1 and water adsorbed at site 2 (Graaf; Stamhuis; Beenackers, 1988; Herman *et al*., 1979; Riquelme, 2020).

$$HCO_{2\,(a)} + H_{(a)} \rightleftharpoons CO_{(a)} + H_2O_{(a)} \tag{36}$$

In addition to the form of water generation, the mechanism differs from that observed in the other two models by considering the desorption of both water and carbon monoxide (Graaf; Stamhuis; Beenackers, 1988).

$$CO_{(a)} \rightleftharpoons CO_{(g)} + S_1 \tag{37}$$

$$H_2O_{(a)} \rightleftharpoons H_2O_{(g)} + S_2 \tag{38}$$

The minimum value of the objective function achieved with the Graaf, Stamhuis, and Beenackers (1988) model was lower than with the other two models, indicating that the assumed reaction path may have led to lower absolute errors. However, the average relative error is still higher than that provided by the Vanden Bussche and Froment (1996) model, indicating a slightly greater precision with the redox mechanism.

3.9 **Light-off curves simulation using parameter estimation results**

The parameters obtained from adjusting the experimental data were introduced into the reactor model to simulate the light-off curves. The following graphs compare the calculated curves from 25 °C to 500 °C with the three models studied and the experimental results under the same operational conditions. Figures 13, 14, and 15 are associated with H_2/CO_2 molar ratios of 1:1, 2.5:1, and 4:1

respectively. In all scenarios, the space velocity was the same as that used in the light-off experiments, 30 m^3 kg^{-1} h^{-1}. The graphs reveal a satisfactory agreement between the model predictions and the experimental data. The shape of the experimental curve was represented reasonably well for the three models analyzed, but the joint plotting allows us to observe a better fitting with the model by Vanden Bussche and Froment, which for almost all points is slightly closer to the experimental points than the other two rate equations, highlighting the smaller relative error obtained with the Vanden Bussche and Froment model. Both the effect of temperature variation and the effect of feed composition variation were successfully predicted by the investigated models with the estimated parameters, and it was possible to observe the sharp increase in CO_2 conversion along the temperature ramp and the higher conversion achieved for higher H_2/CO_2 ratios.

Figure 13 – Comparison between the simulated light-off curves and the experimental data with H_2/CO_2 molar ratio of 1:1

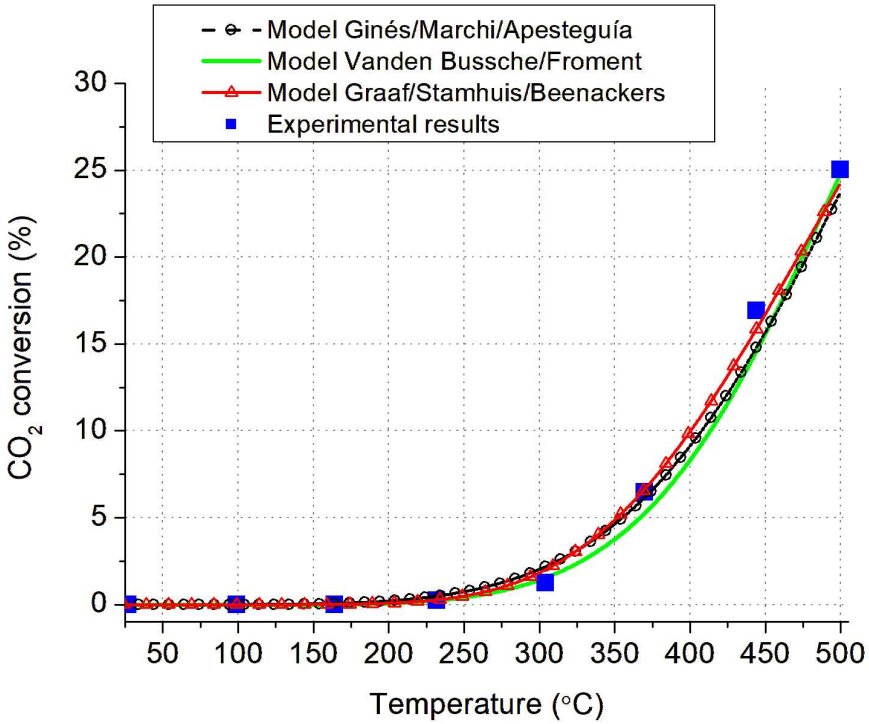

Source: The author, 2024.

Figure 14 – Comparison between the simulated light-off curves and the experimental data with H_2/CO_2 molar ratio of 2.5:1

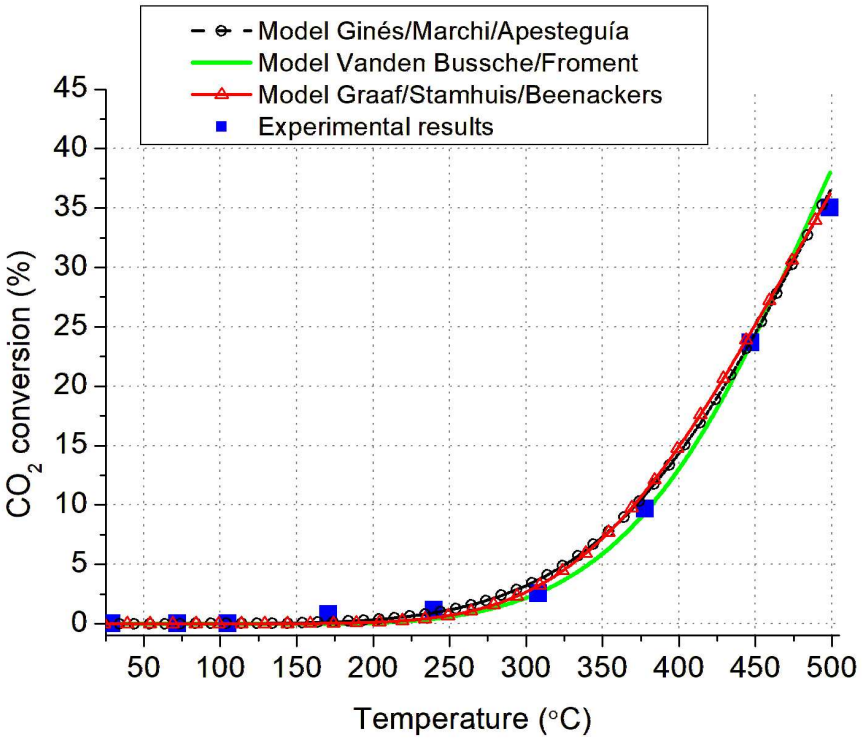

Source: The author, 2024.

Figure 15 – Comparison between the simulated light-off curves and the experimental data with H_2/CO_2 molar ratio of 4:1

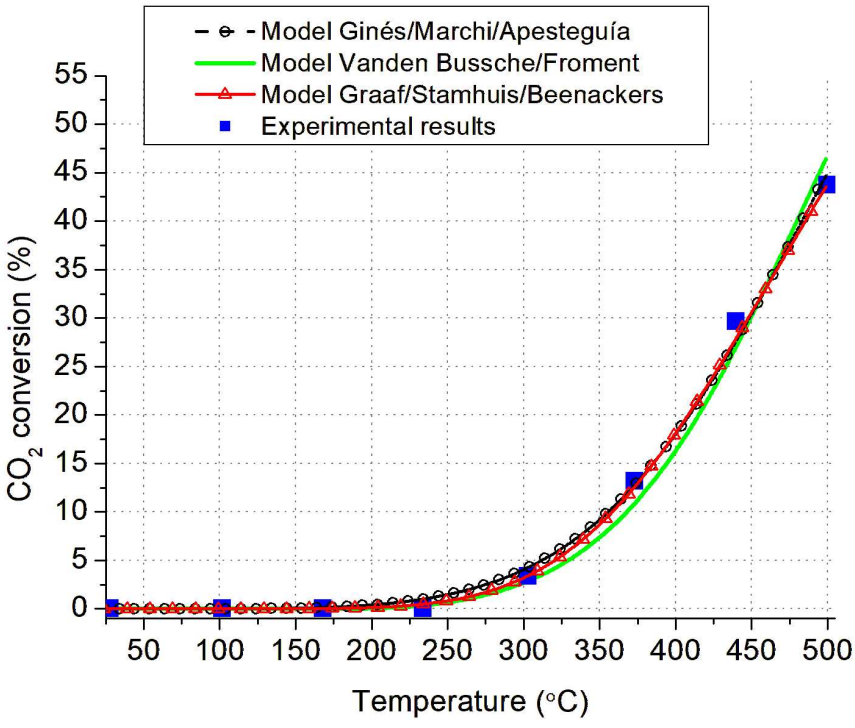

Source: The author, 2024.

Figure 16 presents a parity plot for the carbon dioxide conversion with the three models studied. The proximity of the points to the diagonal line shows the agreement between the measured conversion values, present in the experimental light-off curves, and the model estimates for the corresponding conditions. Furthermore, the absence of trends in the deviations from the bisector indicates that these are random deviations. Table 13 lists the values of the coefficient of determination (R^2) obtained for each model. In all three cases, the value of R^2 is reasonably close to 1, confirming that the three models provided a satisfactory fit to the experimental data. The parity plot with the model by Graaf, Stamhuis, and Beenackers (1988) had the highest coefficient of determination.

Figure 16 – Parity plots for CO_2 conversion in light-off curves

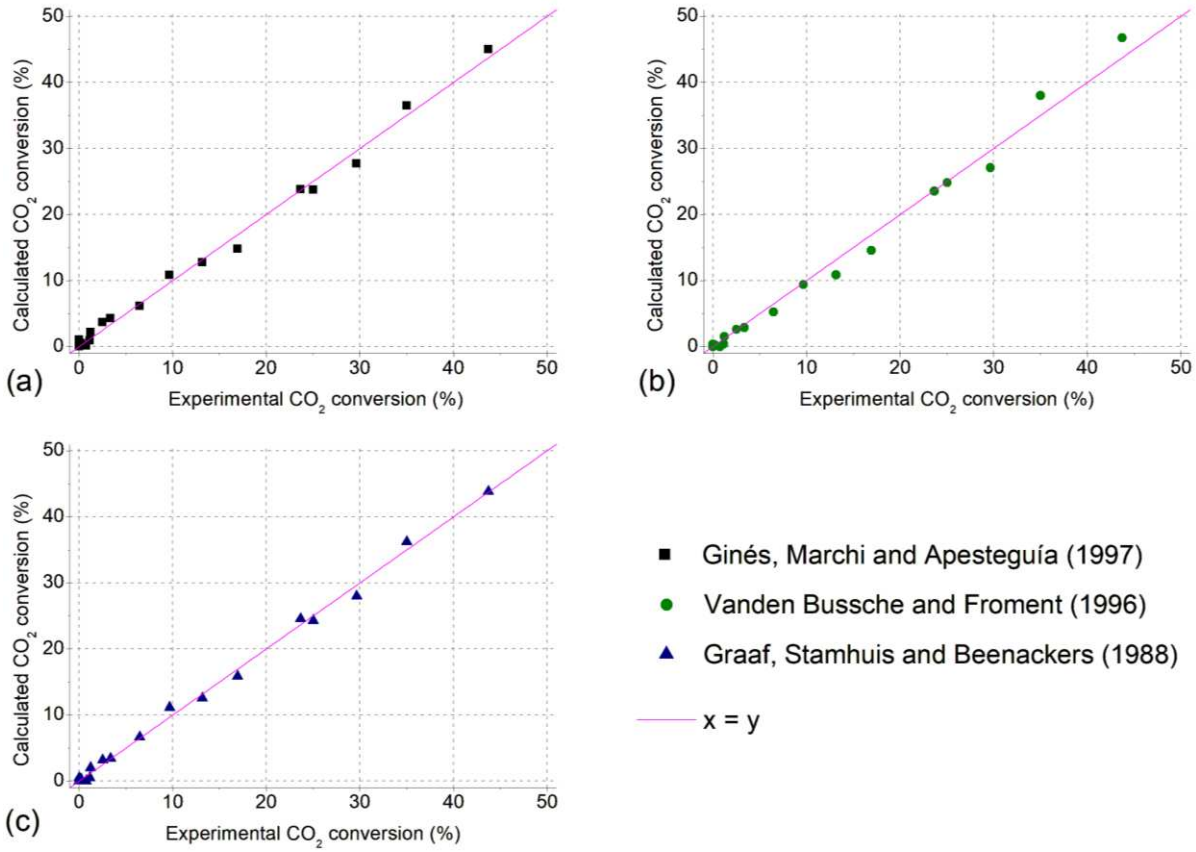

Legend: (a) – Model of Ginés, Marchi and Apesteguía (1997); (b) – Model of Vanden Bussche and Froment (1996); (c) – Model of Graaf, Stamhuis and Beenackers (1988).

Source: The author, 2024.

Table 13 – Coefficient of determination (R^2) of parity plots related to kinetic models

Model	R^2
Ginés, Marchi and Apesteguía (1997)	0.9951
Vanden Bussche and Froment (1996)	0.9917
Graaf, Stamhuis and Beenackers (1988)	0.9971

Source: The author, 2024.

3.10 **Comparison between parameters from light-off curves data and parameters obtained with steady-state data**

The kinetic models studied were applied in a new parameter estimation, now using data from tests at fixed temperatures. For the three models, the results obtained with the data at temperature levels were considerably similar to the results obtained using the light-off curves. However, the model by Vanden Bussche and Froment (1996) stands out due to the similarity of the numerical values of the parameters adjusted in both approaches. Therefore, the results obtained with the model by Vanden Bussche and Froment were selected to be presented in Table 14, which compares the set of parameters adjusted with the data from the light-off curves and the new parameters estimated through the more conventional procedure with data obtained in steady-state, while Table 15 compares the mean relative error and the minimum value for the objective function in the two approaches.

Table 14 – Comparison between the parameters estimated using the model of Vanden Bussche and Froment (1996) with data from tests at temperature levels and data from light-off curves

Parameter	Temperature levels	Light-off curves
$A_{\sqrt{KH2}}$ ($bar^{-0,5}$)	0.250	0.300
$B_{\sqrt{KH2}}$ (J mol^{-1})	10072.1	10030.7
A_{KH2O} (bar^{-1})	$5.00 \cdot 10^{-12}$	$1.00 \cdot 10^{-11}$
B_{KH2O} (J mol^{-1})	90053.5	91163.8
$A_{KH2O/K15*K16*KH2}$	3958.48	3991.59
A_{k1} (mol kg s^{-1} bar^{-1})	$1.00 \cdot 10^{9}$	$1.00 \cdot 10^{9}$
B_{k1} (J mol^{-1})	-109227.3	-111053.8

Source: The author, 2024.

Table 15 – Comparison of average relative error and f_{obj} for parameters estimated using the model by Vanden Bussche and Froment (1996) with data from tests at temperature levels and data from light-off curves

Approach	Average relative error (%)	f_{obj}
Temperature levels	14.8	0.0064
Light-off curves	11.6	0.0039

Source: The author, 2024.

Figure 17 – Comparison between the simulated light-off curves by the model of Vanden Bussche and Froment (1996) using parameters obtained with fixed-temperature tests and experimental light-off curves

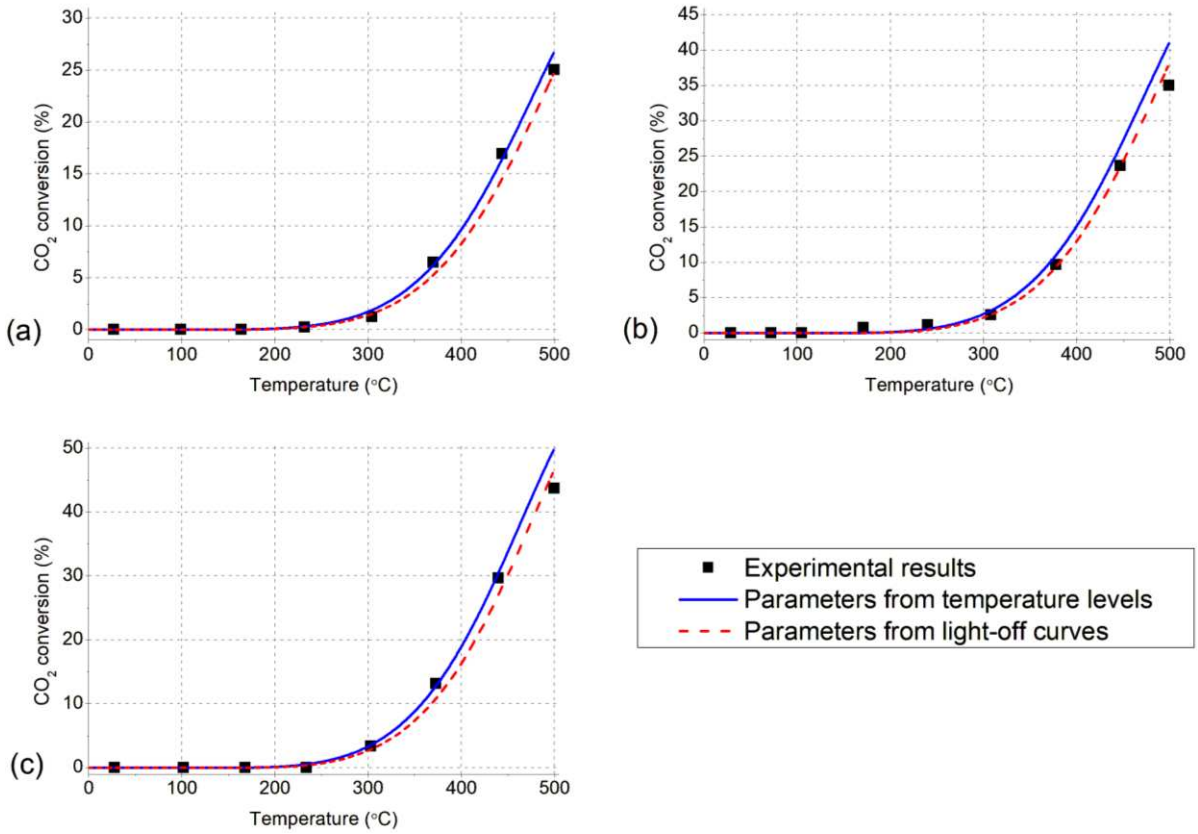

Legend: (a) – H_2/CO_2 molar ratio of 1:1; (b) – H_2/CO_2 molar ratio of 2.5:1; (c) – H_2/CO_2 molar ratio of 4:1.

Source: The author, 2024.

The new parameters fitted through the steady-state experimental data were used to simulate the light-off curves at 30 $m^3\ kg^{-1}\ h^{-1}$ for the three mixtures. Figure 17 presents a comparison between the predictions obtained with the two approaches.

The simulated light-off curves show that the parameters fitted with temperature ramp data are slightly closer to most experimental points, a trend confirmed by the lower values of mean error and f_{obj} found in this approach. Although the fit with the parameters provided by steady-state data was satisfactory, Figure 17 shows that the deviations increase above 430 °C, when the simulation extrapolates the range covered by the tests at temperature levels. The similarity between the estimates in the two approaches also suggests that the heating rate applied in tests at the temperature ramp (5 °C min^{-1}) provided sufficient time to reach a steady state. That is

one of the main conditions required for the use of data from transient tests in the modeling of catalytic reactions. Catalyst deactivation, diffusion limitations, and an excessively high heating rate can affect the prediction provided by temperature ramp data (Duprat, 2002; Mello, 2017).

In addition to light-off curves providing parameters capable of describing the system behavior over a broader temperature range, this approach involves considerably less experimental effort. Obtaining the steady-state kinetic data required 27 experiments, while the experimental light-off curves needed three tests. These results indicate that modeling the kinetics of the RWGS reaction from data extracted from light-off curves is a viable and advantageous possibility in terms of accuracy and use of time, energy, and resources. It is noteworthy that, at the time of carrying out this work, no research was found in the literature evaluating the feasibility of extracting kinetic data from experimental light-off curves for the RWGS reaction.

CONCLUSIONS

The present work studied the conversion of carbon dioxide to carbon monoxide through the reverse gas-water shift (RWGS) reaction as an alternative to reduce the concentration of greenhouse gases in the atmosphere. Catalytic tests were performed over a commercial $CuO/ZnO/Al_2O_3$ catalyst to obtain CO_2 conversion data in temperature ramp experiments (light-off curves) and at fixed temperatures. One of the goals is to determine new values of the kinetic parameters of three rate models available in the literature and identify which model attains the best adherence to the experimental data.

The results of the experiments at fixed temperatures indicated, as expected, that CO_2 conversion is favored under conditions of higher temperature, lower space velocity, and higher molar ratio H_2/CO_2. It was also observed that the experimental values of conversion in temperature ramp were consistent with the steady-state tests, allowing the kinetic parameters to be estimated from the light-off tests. This approach allows obtaining larger sets of data for kinetic studies with a smaller number of experiments required and less time consumption.

The parameters were fitted to the experimental data using the reaction rate expressions proposed by Ginés, Marchi and Apesteguía (1997), Vanden Bussche and Froment (1996) and Graaf, Stamhuis and Beenackers (1988), with an average error of 16.9%, 11.6% and 12.3%, respectively. These results indicate that the model presented by Vanden Bussche and Froment (1996) is associated with the smallest average error.

The comparison between the reactor simulation and the experimental data showed that the estimated parameters provided a good prediction of the CO_2 conversion profile along the temperature ramp, even with the use of a steady-state pseudo-homogeneous reactor model, confirming the validity of the assumed hypotheses and the compatibility of the applied heating rate with the time required to reach steady state.

Simulating the light-off curves with the parameters reported in the literature, it was not possible to faithfully reproduce the experimental data, indicating that extrapolation of the use of kinetic parameters obtained in the steady state outside the range of the experimental conditions employed may compromise the accuracy of the

predictions provided. Extracting kinetic parameters from light-off curves can mitigate this problem, due to the wider temperature range covered by these data.

From the data obtained from the fixed temperature tests, a new set of parameters was fitted using the Vanden Bussche and Froment (1996) model. The parameter values were relatively similar to those obtained from the light-off curves. The simulation of the CO_2 conversion as a function of temperature with both sets of parameters confirmed that the light-off curves were able to lead to a satisfactory prediction of the RWGS reaction over a wider temperature range with less experimental effort.

After all, it was possible to conclude that temperature ramp tests are capable of providing valuable kinetic information to acquire a broader knowledge of the RWGS reaction, enabling an advance in the level of maturity of this technology, which represents a promising alternative towards a decarbonization process.

REFERENCES

AI, X. *et al*. Highly dispersed mesoporous Cu/γ-Al_2O_3 catalyst for RWGS reaction. *International Journal Of Hydrogen Energy*, v. 47, n. 33, p. 14884-14895, abr. 2022. Disponível em: https://doi.org/10.1016/j.ijhydene.2022.03.002. Acesso em: 17 jul. 2024.

AMBRIZZI, T. *et al*. *Mudanças climáticas e a sociedade*. São Paulo: IAG, 2021.

ATEKA, A. *et al*. A review on the valorization of CO_2. Focusing on the thermodynamics and catalyst design studies of the direct synthesis of dimethyl ether. *Fuel Processing Technology*, v. 233, n. 107310, p. 1-29, ago. 2022. Disponível em: https://doi.org/10.1016/j.fuproc.2022.107310. Acesso em: 08 jun. 2024.

ATKINS, P.; JONES, L. *Princípios de Química*: questionando a vida moderna e o meio ambiente. 3. ed. Porto Alegre: Bookman, 2006.

BAHMANPOUR, A. M. *et al*. Cu–Al Spinel as a Highly Active and Stable Catalyst for the Reverse Water Gas Shift Reaction. *ACS Catalysis*, v. 9, n. 7, p. 6243-6251, jun. 2019. Disponível em: https://doi.org/10.1021/acscatal.9b01822. Acesso em: 27 set. 2024.

BAHMANPOUR, A. M. *et al*. Essential role of oxygen vacancies of Cu-Al and Co-Al spinel oxides in their catalytic activity for the reverse water gas shift reaction. *Applied Catalysis B*: Environmental, v. 266, n. 118669, p. 1-8, jun. 2020. Disponível em: https://doi.org/10.1016/j.apcatb.2020.118669. Acesso em: 22 jun. 2024.

BLANCO, H. *et al*. Copper-manganese catalysts with high activity for methanol synthesis. *Applied Catalysis A*: General, v. 579, p. 65-74, jun. 2019. Disponível em: http://dx.doi.org/10.1016/j.apcata.2019.04.021. Acesso em: 09 ago. 2024.

BOWN, R. M. *et al*. Identifying Commercial Opportunities for the Reverse Water Gas Shift Reaction. *Energy Technology*, v. 9, n. 11, p. 1-9, set. 2021. Disponível em: https://doi.org/10.1002/ente.202100554. Acesso em: 22 jun. 2024.

BRAGA, A. H.; VIDINHA, P.; ROSSI, L. M. Hydrogenation of carbon dioxide: from waste to value. *Current Opinion In Green And Sustainable Chemistry*, v. 26, n. 100386, p. 1-7, dez. 2020. Disponível em: https://doi.org/10.1016/j.cogsc.2020.100386. Acesso em: 22 jun. 2024.

BULFIN, B. *et al*. Intensification of the reverse water–gas shift process using a countercurrent chemical looping regenerative reactor. *Chemical Engineering Journal*, v. 461, n. 141896, p. 1-8, abr. 2023. Disponível em: http://dx.doi.org/10.1016/j.cej.2023.141896. Acesso em: 18 jul. 2024.

BUSSCHE, K. M. V.; FROMENT, G. F. A Steady-State Kinetic Model for Methanol Synthesis and the Water Gas Shift Reaction on a Commercial Cu/ZnO/Al_2O_3 Catalyst. *Journal Of Catalysis*, v. 161, n. 1, p. 1-10, jun. 1996. Disponível em: https://doi.org/10.1006/JCAT.1996.0156. Acesso em: 27 jul. 2024.

CAO, C. *et al*. A Review of CO_2 Storage in View of Safety and Cost-Effectiveness. *Energies*, v. 13, n. 3, p. 1-45, jan. 2020. Disponível em: https://doi.org/10.3390/en13030600. Acesso em: 08 jun. 2024.

CASAGRANDE, A.; SILVA JUNIOR, P.; MENDONÇA, F. Mudanças climáticas e aquecimento global: controvérsias, incertezas e a divulgação científica. *Revista Brasileira de Climatologia*, v. 8, jun. 2011. ISSN 2237-8642. Disponível em: https://revistas.ufpr.br/revistaabclima/article/view/25793. Acesso em: 10 dez. 2023.

CHASE, M. W., Jr. *NIST-JANAF Thermochemical Tables*. 4ª ed. Woodbury: American Institute of Physics, 1998.

CHEN, C.-S.; CHENG, W.-H.; LIN, S.-S. Mechanism of CO formation in reverse water–gas shift reaction over Cu/Al_2O_3 catalyst. *Catalysis Letters*, v. 68, n. 1, p. 45-48, ago. 2000. Disponível em: http://dx.doi.org/10.1023/a:1019071117449. Acesso em: 17 jul. 2024.

CHEN, C.-S.; CHENG, W.-H.; LIN, S.-S.. Study of iron-promoted Cu/SiO_2 catalyst on high temperature reverse water gas shift reaction. *Applied Catalysis A*: General, v. 257, n. 1, p. 97-106, 10 jan. 2004. Disponível em: https://doi.org/10.1016/S0926-860X(03)00637-9. Acesso em: 17 jul. 2024.

CHEN, L. *et al*. Study on Cu-Fe/CeO_2 bimetallic catalyst for reverse water gas shift reaction. *Journal Of Environmental Chemical Engineering*, v. 9, n. 3, p. 1-7, jun. 2021. Disponível em: https://doi.org/10.1016/j.jece.2021.105183. Acesso em: 22 jun. 2024.

CHEN, X. *et al*. Recent Advances in Supported Metal Catalysts and Oxide Catalysts for the Reverse Water-Gas Shift Reaction. *Frontiers In Chemistry*, v. 8, n. 709, p. 1-21, ago. 2020. Disponível em: https://doi.org/10.3389/fchem.2020.00709. Acesso em: 22 jun. 2024.

CHEN, X. *et al*. Theoretical Insights and the Corresponding Construction of Supported Metal Catalysts for Highly Selective CO_2 to CO Conversion. *ACS Catalysis*, v. 7, n. 7, p. 4613-4620, 14 jun. 2017. Disponível em: http://dx.doi.org/10.1021/acscatal.7b00903. Acesso em: 18 jul. 2024.

CHOU, C.-Y.; LOILAND, J. A.; LOBO, R. F. Reverse Water-Gas Shift Iron Catalyst Derived from Magnetite. *Catalysts*, v. 9, n. 9, p. 773, 14 set. 2019. Disponível em: http://dx.doi.org/10.3390/catal9090773. Acesso em: 16 jul. 2024.

CHU, Z. *et al*. Surfactant-assisted preparation of $Cu/ZnO/Al_2O_3$ catalyst for methanol synthesis from syngas. *Journal Of Molecular Catalysis A*: Chemical, v. 366, p. 48-53. jan. 2013. Disponível em: http://dx.doi.org/10.1016/j.molcata.2012.09.007. Acesso em: 28 jul. 2024.

CLIMATE WATCH. *World Greenhouse Gas Emissions in 2019 by Sector, End Use and Gases (static)*. Washington, DC: World Resources Institute, 2022a. Disponível

em: https://www.climatewatchdata.org/key-visualizations?visualization=4. Acesso em: 10 dez. 2023.

CLIMATE WATCH. *Historical GHG Emissions*. Washington, DC: World Resources Institute, 2022b. Disponível em: https://www.climatewatchdata.org/ghg-emissions?breakBy=sector&chartType=percentage&end_year=2020&gases=all-ghg&regions=WORLD&source=Climate%20Watch&start_year=1990. Acesso em: 06 jan. 2024.

DAI, B. *et al*. Reduction of CO_2 to CO via reverse water-gas shift reaction over CeO_2 catalyst. *Korean Journal Of Chemical Engineering*, v. 35, p. 421-427, dez. 2017. Disponível em: https://link.springer.com/article/10.1007/s11814-017-0267-y. Acesso em: 22 jun. 2024.

DASIREDDY, V. D. B. C. *et al*. Effect of alkaline earth metal oxide (MO) $Cu/MO/Al_2O_3$ catalysts on methanol synthesis activity and selectivity via CO_2 reduction. *Fuel*, v. 233, p. 103-112, dez. 2018. Disponível em: https://doi.org/10.1016/j.fuel.2018.06.046. Acesso em: 12 set. 2024.

DAZA, Y. A. *et al*. More Cu, more problems: decreased CO_2 conversion ability by Cu-doped $La_{0.75}Sr_{0.25}FeO_3$ perovskite oxides. *Surface Science*, v. 648, p. 92-99. jun. 2016. Disponível em: http://dx.doi.org/10.1016/j.susc.2015.11.017. Acesso em: 08 jun. 2024.

DAZA, Y. A.; KUHN, J. N. CO_2 conversion by reverse water gas shift catalysis: comparison of catalysts, mechanisms and their consequences for CO_2 conversion to liquid fuels. *RSC Advances*, v. 6, n. 55, p. 49675-49691, abr. 2016. Disponível em: https://doi.org/10.1039/C6RA05414E. Acesso em: 08 jun. 2024.

DEHGHANPOOR, S. *et al*. A Feasibility Study of the Conversion of Petrochemical Off-Gas Streams to Methanol Over $CuO/ZnO/Al_2O_3$ Catalyst. *Topics In Catalysis*, v. 67, p. 1-11, jan. 2022. Disponível em: https://doi.org/10.1007/s11244-022-01570-0. Acesso em: 23 nov. 2023.

DESGAGNÉS, A.; ILIUTA, M. C. Intensification of CO_2 hydrogenation by in-situ water removal using hybrid catalyst-adsorbent materials: effect of preparation method and operating conditions on the RWGS reaction as a case study. *Chemical Engineering Journal*, v. 454, n. 140214, p. 1-14, fev. 2023. Disponível em: https://doi.org/10.1016/j.cej.2022.140214. Acesso em: 22 jun. 2024.

DIETZ, L.; PICCININ, S.; MAESTRI, M. Mechanistic Insights into CO_2 Activation via Reverse Water–Gas Shift on Metal Surfaces. *The Journal Of Physical Chemistry C*, v. 119, n. 9, p. 4959-4966, fev. 2015. Disponível em: http://dx.doi.org/10.1021/jp512962c. Acesso em: 18 jul. 2024.

DUPRAT, F. Light-off curve of catalytic reaction and kinetics. *Chemical Engineering Science*, v. 57, n. 6, p. 901-911, mar. 2002. Disponível em: http://dx.doi.org/10.1016/s0009-2509(01)00409-2. Acesso em: 04 jul. 2024.

ELSERNAGAWY, O. Y. H. *et al*. Thermo-economic analysis of reverse water-gas shift process with different temperatures for green methanol production as a hydrogen carrier. *Journal Of CO_2 Utilization*, v. 41, n. 101280, p. 1-10, out. 2020. Disponível em: https://doi.org/10.1016/j.jcou.2020.101280. Acesso em: 08 jun. 2024.

ERNST, K; CAMPBELL, C. T.; MORETTI, G. Kinetics of the reverse water-gas shift reaction over Cu(110). *Journal Of Catalysis*, v. 134, n. 1, p. 66-74, mar. 1992. Disponível em: https://doi.org/10.1016/0021-9517(92)90210-9. Acesso em: 18 jul. 2024.

GALHARDO, T. S. *et al*. Optimizing Active Sites for High CO Selectivity during CO_2 Hydrogenation over Supported Nickel Catalysts. *Journal Of The American Chemical Society*, v. 143, n. 11, p. 4268-4280, abr. 2021. Disponível em: https://doi.org/10.1021/jacs.0c12689. Acesso em: 22 jun. 2024.

GANDARA-LOE, J. *et al*. K-Promoted Ni-Based Catalysts for Gas-Phase CO_2 Conversion: catalysts design and process modelling validation. *Frontiers In Chemistry*, v. 9, n. 785571, p. 1-13, nov. 2021. Disponível em: https://doi.org/10.3389/fchem.2021.785571. Acesso em: 22 jun. 2024.

GHODOOSI, F.; KHOSRAVI-NIKOU, M. R.; SHARIATI, A. Mathematical Modeling of Reverse Water-Gas Shift Reaction in a Fixed-Bed Reactor. *Chemical Engineering & Technology*, v. 40, n. 3, p. 598-607, fev. 2017. Disponível em: https://doi.org/10.1002/ceat.201600220. Acesso em: 08 jun. 2024.

GINÉS, M. J. L.; MARCHI, A. J.; APESTEGUÍA, C. R. Kinetic study of the reverse water-gas shift reaction over CuO/ZnO/Al_2O_3 catalysts. *Applied Catalysis A*: General, v. 154, n. 1-2, p. 155-171, jun. 1997. Disponível em: https://doi.org/10.1016/S0926-860X(96)00369-9. Acesso em: 17 jul. 2024.

GONZALEZ, G. G. *Ácido acético a partir de etanol na ausência de O2 sobre catalisadores de Cu, ZnO, ZrO_2 e Al_2O_3*. 2017. 90 f. Dissertação (Mestrado em Engenharia Química) – Instituto de Química, Universidade do Estado do Rio de Janeiro, Rio de Janeiro, 2017. Disponível em: https://www.bdtd.uerj.br:8443/bitstream/1/18913/2/Disserta%C3%A7%C3%A3o%20-%20Guilherme%20Gouart%20Gonzalez%20-%202017%20-%20Completa%20.pdf. Acesso em: 28 jul. 2024.

GONZÁLEZ-CASTAÑO, M.; DORNEANU, B.; ARELLANO-GARCÍA, H. The reverse water gas shift reaction: a process systems engineering perspective. *Reaction Chemistry & Engineering*, v. 6, n. 6, p. 954-976, mar. 2021. Disponível em: http://dx.doi.org/10.1039/d0re00478b. Acesso em: 18 jul. 2024.

GRAAF, G. H. *et al*. Chemical equilibria in methanol synthesis. *Chemical Engineering Science*, v. 41, n. 11, p. 2883-2890, 1986. Disponível em: https://doi.org/10.1016/0009-2509(86)80019-7. Acesso em: 27 jul. 2024.

GRAAF, G. H.; STAMHUIS, E. J.; BEENACKERS, A. A. C. M. Kinetics of low-pressure methanol synthesis. *Chemical Engineering Science*, v. 43, n. 12, p. 3185-

3195, 1988. Disponível em: https://doi.org/10.1016/0009-2509(88)85127-3. Acesso em: 29 maio 2024.

GU, M. *et al*. Structure–Activity Relationships of Copper- and Potassium-Modified Iron Oxide Catalysts during Reverse Water–Gas Shift Reaction. *ACS Catalysis*, v. 11, n. 20, p. 12609-12619, 30 set. 2021. Disponível em: https://doi.org/10.1021/acscatal.1c03792. Acesso em: 18 jul. 2024.

HERMAN, R. G. *et al*. Catalytic synthesis of methanol from CO/H_2: I. Phase composition, electronic properties, and activities of the $Cu/ZnO/M_2O_3$ catalysts. *Journal of Catalysis*, v. 56, n. 3, p. 407-429, mar. 1979. Disponível em: https://doi.org/10.1016/0021-9517(79)90132-5. Acesso em: 09 set. 2024.

HERWIJNEN, T. van; JONG, W A. de. Kinetics and mechanism of the CO shift on Cu/ZnO1. Kinetics of the forward and reverse CO shift reactions. *Journal Of Catalysis*, v. 63, n. 1, p. 83-93, maio 1980. Disponível em: https://doi.org/10.1016/0021-9517(80)90061-5. Acesso em: 02 ago. 2024.

IBP. *Tecnologias de Captura e Armazenamento de Carbono (CCUS) e sua Importância para a Transição Energética no Brasil.* [S. l.: s.n.], 2023. Disponível em: https://www.ibp.org.br/personalizado/uploads/2023/06/ccus.pdf. Acesso em: 07 jan. 2024.

IEA. *The Oil and Gas Industry in Net Zero Transitions*. Paris: IEA, 2023. Disponível em: https://www.iea.org/reports/the-oil-and-gas-industry-in-net-zero-transitions. Acesso em: 06 jan. 2024.

IPCC. Sections. In: IPCC. *Climate Change 2023*: Synthesis Report. Contribution of Working Groups I, II and III to the Sixth Assessment Report of the Intergovernmental Panel on Climate Change. Genebra: [s. n.], 2023.

JADHAV, S. G.; JOSHI, H. M.; VAIDYA, P. D. Novel synthesis of RWGS catalysts ZnO/Al_2O_3 and $CuO/ZnO/Al_2O_3$ for improved methanol production via CAMERE process. *Catalysis In Green Chemistry And Engineering*, v. 3, n. 1, p. 57-65, 2020. Disponível em: http://dx.doi.org/10.1615/catalgreenchemeng.2020034930. Acesso em: 17 jul. 2024.

JADHAV, S. G.; VAIDYA, P. D. KINETICS OF REVERSE WATER-GAS SHIFT REACTION OVER $CuO/ZnO/Al_2O_3$ CATALYST. *Catalysis In Green Chemistry And Engineering*, v. 3, n. 2, p. 141-151, 2020. Disponível em: http://dx.doi.org/10.1615/catalgreenchemeng.2020036423. Acesso em: 17 jul. 2024.

JURKOVIĆ, D. L. *et al*. Effect of Copper-based Catalyst Support on Reverse Water-Gas Shift Reaction (RWGS) Activity for CO_2. *Chemical Engineering & Technology*, v. 40, n. 5, p. 973-980, 28 mar. 2017. Disponível em: http://dx.doi.org/10.1002/ceat.201600594. Acesso em: 17 jul. 2024.

KAISER, P. *et al*. Production of Liquid Hydrocarbons with CO_2 as Carbon Source based on Reverse Water-Gas Shift and Fischer-Tropsch Synthesis. *Chemie*

Ingenieur Technik, v. 85, n. 4, p. 489-499, mar. 2013. Disponível em: https://doi.org/10.1002/cite.201200179. Acesso em: 08 jun. 2024.

KAMKENG, A. D. N. *et al*. Transformation technologies for CO_2 utilisation: current status, challenges and future prospects. *Chemical Engineering Journal*, v. 409, n. 128138, p. 1-29, abr. 2021. Disponível em: https://doi.org/10.1016/j.cej.2020.128138. Acesso em: 08 jun. 2024.

LALINDE, J. A. H. *et al*. CO_2 methanation and reverse water gas shift reaction. Kinetic study based on in situ spatially-resolved measurements. *Chemical Engineering Journal*, v. 390, n. 124629, p. 1-19, jun. 2020. Disponível em: http://dx.doi.org/10.1016/j.cej.2020.124629. Acesso em: 16 jul. 2024.

LIU, L. *et al*. $LaNiO_3$ as a precursor of Ni/La_2O_3 for reverse water-gas shift in DBD plasma: effect of calcination temperature. *Energy Conversion And Management*, v. 206, n. 112475, p. 1-12, fev. 2020a. Disponível em: https://doi.org/10.1016/j.enconman.2020.112475. Acesso em: 22 jun. 2024.

LIU, L. *et al*. Low temperature catalytic reverse water-gas shift reaction over perovskite catalysts in DBD plasma. *Applied Catalysis B*: Environmental, v. 265, n. 118573, p. 1-14, maio 2020b. Disponível em: https://doi.org/10.1016/j.apcatb.2019.118573. Acesso em: 22 jun. 2024.

LIU, X. *et al*. Effective and Highly Selective CO Generation from CO_2 Using a Polycrystalline α-Mo_2C Catalyst. *ACS Catalysis*, v. 7, p. 4323-4335. 16 maio 2017. Disponível em: https://doi.org/10.1021/acscatal.7b00735. Acesso em: 22 jun. 2024.

MELLO, N. M. *Estudo cinético da reação de redução do NO pelo CO em catalisador de paládio suportado em alumina*. 2017. 125 f. Dissertação (Mestrado em Engenharia Química) – Instituto de Química, Universidade do Estado do Rio de Janeiro, Rio de Janeiro, 2017. Disponível em: https://www.bdtd.uerj.br:8443/bitstream/1/12075/1/Nathalli%20Meorlluw%20Mello.pdf. Acesso em: 06 jul. 2024.

MENG, F. *et al*. CO hydrogenation combined with water-gas-shift reaction for synthetic natural gas production: a thermodynamic and experimental study. *International Journal Of Coal Science & Technology*, v. 5, n. 4, p. 439-451, 28 jul. 2017. Disponível em: https://doi.org/10.1007/s40789-017-0177-y. Acesso em: 16 jul. 2024.

NEZAM, I. *et al*. Direct aromatization of CO_2 via combined CO_2 hydrogenation and zeolite-based acid catalysis. *Journal Of CO_2 Utilization*, v. 45, n. 101405, p. 1-21, mar. 2021. Disponível em: https://doi.org/10.1016/j.jcou.2020.101405. Acesso em: 08 jun. 2024.

NIST. *Fundamental Physical Constants from NIST*. 2024. Disponível em: https://physics.nist.gov/cuu/Constants/index.html. Acesso em: 26 jul. 2024.

OJEDA, A. N. E. *Síntese de Fischer-Tropsch*: influência das propriedades texturais e parâmetros de reações sobre o desempenho do catalisador do tipo núcleo-casca

Co@SiO_2. 2022. 88 f. Dissertação (Mestrado em Engenharia Química) – Instituto Alberto Luiz Coimbra de Pós-Graduação e Pesquisa de Engenharia, Universidade Federal do Rio de Janeiro, Rio de Janeiro, 2022. Disponível em: http://portal.peq.coppe.ufrj.br/images/documentos/Teses_e_disserta%C3%A7%C3%B5es/08_12_2022_MSc_Abigail.pdf. Acesso em: 29 jul. 2024.

OKONKWO, O.; YABLONSKY, G.; BISWAS, P. Thermodynamic analysis of tri-reforming of oxy-fuel combustion exhaust gas. *Journal of CO_2 Utilization*, v. 39, n. 101156, p. 1-10, jul. 2020. Disponível em: https://doi.org/10.1016/j.jcou.2020.101156. Acesso em: 08 jun. 2024.

OSHIMA, K. *et al*. Low temperature catalytic reverse water gas shift reaction assisted by an electric field. *Catalysis Today*, v. 232, p. 27-32. set. 2014. Disponível em: http://dx.doi.org/10.1016/j.cattod.2013.11.035. Acesso em: 08 jun. 2024.

PAHIJA, E. *et al*. Experimental and Computational Synergistic Design of Cu and Fe Catalysts for the Reverse Water–Gas Shift: a review. *ACS Catalysis*, v. 12, n. 12, p. 6887-6905, maio 2022. Disponível em: https://doi.org/10.1021/acscatal.2c01099. Acesso em: 08 jun. 2024.

PARK, N. *et al*. Kinetic modeling of methanol synthesis over commercial catalysts based on three-site adsorption. *Fuel Processing Technology*, v. 125, p. 139-147, set. 2014. Disponível em: https://doi.org/10.1016/j.fuproc.2014.03.041. Acesso em: 26 jul. 2024.

PASTOR-PÉREZ, L. *et al*. CO_2 valorisation via Reverse Water-Gas Shift reaction using advanced Cs doped Fe-Cu/Al_2O_3 catalysts. *Journal Of CO_2 Utilization*, v. 21, p. 423-428, out. 2017. Disponível em: https://doi.org/10.1016/j.jcou.2017.08.009. Acesso em: 18 jul. 2024.

PÉREZ-ALONSO, F. J. *et al*. Carbon dioxide hydrogenation over Fe–Ce catalysts. *Catalysis Communications*, v. 9, p. 1945-1948. maio 2008. Disponível em: https://doi.org/10.1016/j.catcom.2008.03.024. Acesso em: 08 jun. 2024.

PÖHLMANN, F.; JESS, A. Influence of Syngas Composition on the Kinetics of Fischer–Tropsch Synthesis of using Cobalt as Catalyst. *Energy Technology*, v. 4, n. 1, p. 55-64, jan. 2016. Disponível em: https://doi.org/10.1002/ente.201500216. Acesso em: 08 jun. 2024.

POYNTING, M.; RIVAULT, E. *2023 é confirmado como ano mais quente já registrado*: 2024 pode bater esse recorde? [S. l.: s.n.], 2024. Disponível em: https://www.bbc.com/portuguese/articles/ced7pl4l74vo#:~:text=2023%20%C3%A9%20confirmado%20como%20ano,2024%20pode%20bater%20esse%20recorde%3F&text=O%20ano%20de%202023%20foi,pelo%20fen%C3%B4meno%20natural%20El%20Ni%C3%B1o.. Acesso em: 10 jan. 2024.

PURNAMA, H. *et al*. CO formation/selectivity for steam reforming of methanol with a commercial CuO/ZnO/Al_2O_3 catalyst. *Applied Catalysis A*: General, v. 259, n. 1, p. 83-94, mar. 2004. Disponível em: https://doi.org/10.1016/j.apcata.2003.09.013. Acesso em: 25 jul. 2024.

RAVANCHI, M. T.; SAHEBDELFAR, S. Catalytic conversions of CO_2 to help mitigate climate change: recent process developments. *Process Safety And Environmental Protection*, v. 145, p. 172-194. jan. 2021. Disponível em: https://doi.org/10.1016/j.psep.2020.08.003. Acesso em: 08 jun. 2024.

REINA, T. R.; ODRIOZOLA, J. A.; ARELLANO-GARCIA, H. *Engineering Solutions for CO_2 Conversion*. Weinheim: Wiley-VCH, 2021.

REINIKAINEN, M. *et al*. Two-Step Conversion of CO_2 to Light Olefins: laboratory-scale demonstration and scale-up considerations. *Chemengineering*, v. 6, n. 6, p. 1-15, 6 dez. 2022. Disponível em: https://doi.org/10.3390/chemengineering6060096. Acesso em: 18 jul. 2024.

RIQUELME, P. F. R. *Study of the kinetic model and plant steady-state simulation for the synthesis of methanol from syngas on a synthetic Cu/ZnO/Al_2O_3 catalyst*. 2020. 53 f. Dissertação (Mestrado em Engenharia Química) – Scuola di Ingegneria Industriale e dell'Informazione, Politecnico di Milano, Milano, 2020. Disponível em: https://hdl.handle.net/10589/153311. Acesso em: 26 jul. 2024.

SANTOS, M. F. *et al*. Carbon dioxide conversion via reverse water-gas shift reaction: reactor design. *Journal of Environmental Management*, v. 345, n. 118822, p. 1-8, nov. 2023. Disponível em: http://dx.doi.org/10.1016/j.jenvman.2023.118822. Acesso em: 18 jul. 2024.

SHEKARI, A. *et al*. Conversion of CO_2 by reverse water gas shift (RWGS) reaction using a hydrogen oxyflame. *Fuel*, v. 344, n. 127947, p. 1-11, jul. 2023. Disponível em: https://doi.org/10.1016/j.fuel.2023.127947. Acesso em: 08 jun. 2024.

STONE, F. S.; WALLER, D. Cu–ZnO and Cu–ZnO/Al_2O_3 Catalysts for the Reverse Water-Gas Shift Reaction. The Effect of the Cu/Zn Ratio on Precursor Characteristics and on the Activity of the Derived Catalysts. *Topics In Catalysis*, v. 22, n. 3, p. 305-318, abr. 2003. Disponível em: http://dx.doi.org/10.1023/A:1023592407825. Acesso em: 17 jul. 24.

STORN, R.; PRICE, K. Differential Evolution – A Simple and Efficient Heuristic for global Optimization over Continuous Spaces. *Journal Of Global Optimization*, v. 11, n. 4, p. 341-359, dez. 1997. Disponível em: https://doi.org/10.1023/A:1008202821328. Acesso em: 27 jul. 2024.

SU, X. *et al*. Designing of highly selective and high-temperature endurable RWGS heterogeneous catalysts: recent advances and the future directions. *Journal Of Energy Chemistry*, v. 26, p. 854-867, set. 2017. Disponível em: https://doi.org/10.1016/j.jechem.2017.07.006. Acesso em: 22 jun. 2024.

SUESCUM-MORALES, D.; JIMÉNEZ, J. R.; FERNÁNDEZ-RODRÍGUEZ, J. M. Review of the Application of Hydrotalcite as CO_2 Sinks for Climate Change Mitigation. *ChemEngineering*, v. 6, n. 50, p. 1-18, jul. 2022. Disponível em: https://doi.org/10.3390/chemengineering6040050. Acesso em: 08 jun. 2024.

TAWALBEH, M. *et al*. The novel contribution of non-noble metal catalysts for intensified carbon dioxide hydrogenation: recent challenges and opportunities. *Energy Conversion And Management*, v. 279, n. 116755, p. 1-24, mar. 2023. Disponível em: https://doi.org/10.1016/j.enconman.2023.116755. Acesso em: 08 jun. 2024.

UNITED STATES GLOBAL CHANGE RESEARCH PROGRAM. *Climate Science Special Report*: Fourth National Climate Assessment, Volume I. Washington, D.C.: [s. n.], 2017.

VILLORA-PICÓ, J. J. *et al*. A review on high-pressure heterogeneous catalytic processes for gas-phase CO_2 valorization. *Environmental Research*, v. 240, n. 1, p. 1-15, jan. 2024. Disponível em: https://doi.org/10.1016/j.envres.2023.117520. Acesso em: 18 jul. 2024.

VU, T. T. N. *et al*. Development of highly efficient Cu-based catalyst derived from a metallurgical waste for the reverse water-gas shift reaction. *International Journal Of Hydrogen Energy*, v. 47, n. 90, p. 38170-38184, nov. 2022. Disponível em: https://doi.org/10.1016/j.ijhydene.2022.09.001. Acesso em: 18 jul. 2024.

WANG, Y. *et al*. Catalytic Processes to Accelerate Decarbonization in a Net-Zero Carbon World. *Chemsuschem*, v. 15, n. 24, p. 1-17, nov. 2022. Disponível em: https://doi.org/10.1002/cssc.202201290. Acesso em: 08 jun. 2024.

WOLF, A.; JESS, A.; KERN, C. Syngas Production via Reverse Water-Gas Shift Reaction over a Ni-Al_2O_3 Catalyst: catalyst stability, reaction kinetics, and modeling. *Chemical Engineering & Technology*, v. 39, n. 6, p. 1040-1048, 29 fev. 2016. Disponível em: http://dx.doi.org/10.1002/ceat.201500548. Acesso em: 16 jul. 2024.

YAMAOKA, Masaki *et al*. Efficient reverse water gas shift reaction at low temperatures over an iron supported catalyst under an electric field. *Scientific Reports*, v. 14, n. 10216, p. 1-7, 3 maio 2024. Disponível em: https://doi.org/10.1038/s41598-024-61017-2. Acesso em: 16 jul. 2024.

YANG, L. *et al*. Highly efficient Ni/CeO_2-Al2O_3 catalysts for CO_2 upgrading via reverse water-gas shift: effect of selected transition metal promoters. *Applied Catalysis B*: Environmental, v. 232, p. 464-471. set. 2018. Disponível em: https://doi.org/10.1016/j.apcatb.2018.03.091. Acesso em: 16 jul. 2024.

YOSHIHARA, J.; CAMPBELL, C. T. Methanol Synthesis and Reverse Water–Gas Shift Kinetics over Cu(110) Model Catalysts: structural sensitivity. *Journal Of Catalysis*, v. 161, n. 2, p. 776-782, jul. 1996. Disponível em: https://doi.org/10.1006/jcat.1996.0240. Acesso em: 02 ago. 2024.

ZHANG, M. *et al*. How to Measure the Reaction Performance of Heterogeneous Catalytic Reactions Reliably. *Joule*, v. 3, n. 12, p. 2876-2883, dez. 2019. Disponível em: https://doi.org/10.1016/j.joule.2019.11.005. Acesso em: 27 set. 2024.

ZHANG, Q. *et al*. CO_2 Conversion via Reverse Water Gas Shift Reaction Using Fully Selective Mo–P Multicomponent Catalysts. *Industrial & Engineering Chemistry*

Research, v. 61, n. 34, p. 12857-12865, 19 ago. 2022. Disponível em: https://doi.org/10.1021/acs.iecr.2c00305. Acesso em: 18 jul. 2024.

ZHU, M.; GE, Q.; ZHU, X. Catalytic Reduction of CO_2 to CO via Reverse Water Gas Shift Reaction: recent advances in the design of active and selective supported metal catalysts. *Transactions Of Tianjin University*, v. 26, n. 3, p. 172-187, 13 abr. 2020. Disponível em: https://doi.org/10.1007/s12209-020-00246-8. Acesso em: 18 jul. 2024.

APPENDIX A – Deduction of dimensionless models

A.1 **Model of Ginés, Marchi and Apesteguía (1997)**

The reactor model in terms of Ginés, Marchi and Apesteguía rate equation is, in principle, expressed as:

$$\frac{dF_{CO_2}}{dW} = -\frac{k_1 L_0 \left(P_{CO_2} P_{H_2} - \frac{P_{CO}^2}{K_1}\right)}{P_{H_2} + \sqrt{K_8^*} \cdot P_{H_2}^{1.5} + \frac{1}{K_8^* K_{24}^*} \cdot P_{CO}} \tag{110}$$

$$\frac{dF_{H_2}}{dW} = -\frac{k_1 L_0 \left(P_{CO_2} P_{H_2} - \frac{P_{CO}^2}{K_1}\right)}{P_{H_2} + \sqrt{K_8^*} \cdot P_{H_2}^{1.5} + \frac{1}{K_8^* K_{24}^*} \cdot P_{CO}} \tag{111}$$

$$\frac{dF_{CO}}{dW} = \frac{k_1 L_0 \left(P_{CO_2} P_{H_2} - \frac{P_{CO}^2}{K_1}\right)}{P_{H_2} + \sqrt{K_8^*} \cdot P_{H_2}^{1.5} + \frac{1}{K_8^* K_{24}^*} \cdot P_{CO}} \tag{112}$$

$$\frac{dF_{H_2O}}{dW} = \frac{k_1 L_0 \left(P_{CO_2} P_{H_2} - \frac{P_{CO}^2}{K_1}\right)}{P_{H_2} + \sqrt{K_8^*} \cdot P_{H_2}^{1.5} + \frac{1}{K_8^* K_{24}^*} \cdot P_{CO}} \tag{113}$$

$$\frac{dF_{He}}{dW} = 0 \tag{114}$$

Given hypothesis (f) of ideal gas conditions, the molar flow rates are calculated through ideal gas law:

$$P \cdot V = n \cdot R \cdot T \tag{115}$$

where *P* is the pressure in atm, *V* is the volume in L, *n* is the number of moles in mol, *R* is the universal gas constant in L atm K^{-1} mol^{-1}, and *T* is the temperature in K. This equation can also be expressed for flow rates:

$$P \cdot q = F_T \cdot R \cdot T \tag{116}$$

in which q is the volumetric flow rate in L h^{-1}, and F_T is the total molar flow rate in mol h^{-1}, that thereby can be calculated by:

$$F_T = \frac{P \cdot q}{R \cdot T} \tag{117}$$

The molar flow rate of species i is determined by equation (118), where y_i is the molar fraction of species i in the gas phase (dimensionless):

$$F_i = y_i \cdot F_T \tag{118}$$

Therefore, molar flow rates can be expressed in terms of partial pressures:

$$F_i = \frac{P_i \cdot q}{R \cdot T} \tag{119}$$

And the equation (110) becomes:

$$\frac{d\left(\frac{P_{CO_2} \cdot q}{R \cdot T}\right)}{dW} = -\frac{k_1 L_0 \left(P_{CO_2} P_{H_2} - \frac{P_{CO}^2}{K_1}\right)}{P_{H_2} + \sqrt{K_8^*} \cdot P_{H_2}^{1.5} + \frac{1}{K_8^* K_{24}^*} \cdot P_{CO}} \tag{120}$$

$$\frac{q}{R \cdot T} \cdot \frac{dP_{CO_2}}{dW} = -\frac{k_1 L_0 \left(P_{CO_2} P_{H_2} - \frac{P_{CO}^2}{K_1}\right)}{P_{H_2} + \sqrt{K_8^*} \cdot P_{H_2}^{1.5} + \frac{1}{K_8^* K_{24}^*} \cdot P_{CO}} \tag{121}$$

$$\frac{dP_{CO_2}}{dW} = -\frac{\frac{R \cdot T}{q} \cdot k_1 L_0 \left(P_{CO_2} P_{H_2} - \frac{P_{CO}^2}{K_1}\right)}{P_{H_2} + \sqrt{K_8^*} \cdot P_{H_2}^{1.5} + \frac{1}{K_8^* K_{24}^*} \cdot P_{CO}} \tag{122}$$

Multiplying both sides of equation (122) by W_0/P:

$$\frac{dP_{CO_2}}{dW}\cdot\frac{W_0}{P}=-\frac{\frac{W_0}{P}\cdot\frac{R\cdot T}{q}\cdot k_1L_0\left(P_{CO_2}P_{H_2}-\frac{P_{CO}^2}{K_1}\right)}{P_{H_2}+\sqrt{K_8^*}\cdot P_{H_2}^{1.5}+\frac{1}{K_8^*K_{24}^*}\cdot P_{CO}} \tag{123}$$

$$\frac{d\left(\frac{P_{CO_2}}{P}\right)}{d\left(\frac{W}{W_0}\right)}=-\frac{\frac{k_1L_0\cdot R\cdot T\cdot W_0}{q}\cdot\frac{1}{P}\left(P_{CO_2}P_{H_2}-\frac{P_{CO}^2}{K_1}\right)}{P_{H_2}+\sqrt{K_8^*}\cdot P_{H_2}^{1.5}+\frac{1}{K_8^*K_{24}^*}\cdot P_{CO}} \tag{124}$$

Applying equations (83), (84), (85) and (87):

$$\frac{dy_{CO_2}}{dm}=-\frac{A\cdot\left(\frac{P_{CO_2}}{P}\cdot P_{H_2}-\frac{P_{CO}}{P}\cdot\frac{P_{CO}}{K_1}\right)}{P_{H_2}+\sqrt{K_8^*}\cdot y_{H_2}^{1.5}\cdot P^{1.5}+D\cdot P_{CO}} \tag{125}$$

Multiplying the right side of the equation (125) by $\frac{\frac{1}{P}}{\frac{1}{P}}$:

$$\frac{dy_{CO_2}}{dm}=-\frac{A\cdot\frac{1}{P}\left(y_{CO_2}\cdot P_{H_2}-y_{CO}\cdot\frac{P_{CO}}{K_1}\right)}{\frac{P_{H_2}}{P}+\sqrt{K_8^*}\cdot y_{H_2}^{1.5}\cdot\frac{P^{1.5}}{P}+D\cdot\frac{P_{CO}}{P}} \tag{126}$$

$$\frac{dy_{CO_2}}{dm}=-\frac{A\cdot\left(y_{CO_2}\cdot y_{H_2}-\frac{y_{CO}^2}{K_1}\right)}{y_{H_2}+\sqrt{K_8^*}\cdot y_{H_2}^{1.5}\cdot\sqrt{P}+D\cdot y_{CO}} \tag{127}$$

Applying equation (86):

$$\frac{dy_{CO_2}}{dm}=-\frac{A\cdot\left(y_{CO_2}\cdot y_{H_2}-\frac{y_{CO}^2}{K_1}\right)}{y_{H_2}+B\cdot y_{H_2}^{1.5}+D\cdot y_{CO}} \tag{128}$$

Performing a similar procedure for equations (111) to (114), the dimensionless model is obtained:

$$\frac{dy_{CO_2}}{dm}=-\frac{A\cdot\left(y_{CO_2}\cdot y_{H_2}-\frac{y_{CO}^2}{K_1}\right)}{y_{H_2}+B\cdot y_{H_2}^{1.5}+D\cdot y_{CO}} \tag{68}$$

$$\frac{dy_{H_2}}{dm} = -\frac{A \cdot \left(y_{CO_2} \cdot y_{H_2} - \frac{y_{CO}^2}{K_1}\right)}{y_{H_2} + B \cdot y_{H_2}^{1.5} + D \cdot y_{CO}} \tag{69}$$

$$\frac{dy_{CO}}{dm} = \frac{A \cdot \left(y_{CO_2} \cdot y_{H_2} - \frac{y_{CO}^2}{K_1}\right)}{y_{H_2} + B \cdot y_{H_2}^{1.5} + D \cdot y_{CO}} \tag{70}$$

$$\frac{dy_{H_2O}}{dm} = \frac{A \cdot \left(y_{CO_2} \cdot y_{H_2} - \frac{y_{CO}^2}{K_1}\right)}{y_{H_2} + B \cdot y_{H_2}^{1.5} + D \cdot y_{CO}} \tag{71}$$

$$\frac{dy_{He}}{dm} = 0 \tag{72}$$

A.2 **Model of Vanden Bussche and Froment (1996)**

Applying an initial procedure analogous to that carried out for the Ginés, Marchi, and Apesteguía (1997) model, denoted by equations (116) to (119), the Vanden Bussche and Froment (1996) model is expressed in terms of partial pressures:

$$\frac{dP_{CO_2}}{dW} = \frac{-\left(\frac{R \cdot T}{q}\right) \cdot k_1 \cdot P_{CO_2} \cdot \left(1 - \left(\frac{1}{K_1}\right) \cdot \left(\frac{P_{H_2O} \cdot P_{CO}}{P_{CO_2} \cdot P_{H_2}}\right)\right)}{\left(1 + \left(\frac{K_{H_2O}}{K_{15}^* K_{16}^* K_{H_2}}\right)\left(\frac{P_{H_2O}}{P_{H_2}}\right) + \sqrt{K_{H_2} \cdot P_{H_2}} + K_{H_2O} \cdot P_{H_2O}\right)} \tag{129}$$

$$\frac{dP_{H_2}}{dW} = \frac{-\left(\frac{R \cdot T}{q}\right) \cdot k_1 \cdot P_{CO_2} \cdot \left(1 - \left(\frac{1}{K_1}\right) \cdot \left(\frac{P_{H_2O} \cdot P_{CO}}{P_{CO_2} \cdot P_{H_2}}\right)\right)}{\left(1 + \left(\frac{K_{H_2O}}{K_{15}^* K_{16}^* K_{H_2}}\right)\left(\frac{P_{H_2O}}{P_{H_2}}\right) + \sqrt{K_{H_2} \cdot P_{H_2}} + K_{H_2O} \cdot P_{H_2O}\right)} \tag{130}$$

$$\frac{dP_{CO}}{dW} = \frac{\left(\frac{R \cdot T}{q}\right) \cdot k_1 \cdot P_{CO_2} \cdot \left(1 - \left(\frac{1}{K_1}\right) \cdot \left(\frac{P_{H_2O} \cdot P_{CO}}{P_{CO_2} \cdot P_{H_2}}\right)\right)}{\left(1 + \left(\frac{K_{H_2O}}{K_{15}^* K_{16}^* K_{H_2}}\right)\left(\frac{P_{H_2O}}{P_{H_2}}\right) + \sqrt{K_{H_2} \cdot P_{H_2}} + K_{H_2O} \cdot P_{H_2O}\right)} \tag{131}$$

$$\frac{dP_{H_2O}}{dW} = \frac{\left(\frac{R \cdot T}{q}\right) \cdot k_1 \cdot P_{CO_2} \cdot \left(1 - \left(\frac{1}{K_1}\right) \cdot \left(\frac{P_{H_2O} \cdot P_{CO}}{P_{CO_2} \cdot P_{H_2}}\right)\right)}{\left(1 + \left(\frac{K_{H_2O}}{K_{15}^* K_{16}^* K_{H_2}}\right)\left(\frac{P_{H_2O}}{P_{H_2}}\right) + \sqrt{K_{H_2} \cdot P_{H_2}} + K_{H_2O} \cdot P_{H_2O}\right)} \tag{132}$$

$$\frac{dP_{He}}{dW} = 0 \tag{133}$$

Multiplying equation (129) by W_0/P:

$$\frac{dP_{CO_2}}{dW} \cdot \frac{W_0}{P} = \frac{-\left(\frac{R \cdot T}{q}\right) \cdot k_1 \cdot P_{CO_2} \cdot \left(1 - \left(\frac{1}{K_1}\right) \cdot \left(\frac{P_{H_2O} \cdot P_{CO}}{P_{CO_2} \cdot P_{H_2}}\right)\right) \frac{W_0}{P}}{\left(1 + \left(\frac{K_{H_2O}}{K_{15}^* K_{16}^* K_{H_2}}\right)\left(\frac{P_{H_2O}}{P_{H_2}}\right) + \sqrt{K_{H_2} \cdot P_{H_2}} + K_{H_2O} \cdot P_{H_2O}\right)} \tag{134}$$

Applying the correction factor f_P on the right-hand side to transfer the unit of k_1 to mol kg^{-1} s^{-1} Pa^{-1}, and using equation (89):

$$\frac{d\left(\frac{P_{CO_2}}{P}\right)}{d\left(\frac{W}{W_0}\right)} = - \frac{\frac{k_1 \cdot R \cdot T \cdot W_0 \cdot f_P}{q} \cdot \frac{P_{CO_2}}{P}\left(1 - \left(\frac{1}{K_1}\right) \cdot \left(\frac{P_{H_2O} P_{CO}}{P_{CO_2} P_{H_2}}\right)\right)}{\left(1 + G\left(\frac{P_{H_2O}}{P_{H_2}}\right) + \sqrt{K_{H_2} P_{H_2}} + K_{H_2O} P_{H_2O}\right)} \tag{135}$$

Applying equations (83), (84), and (88), and multiplying all terms on the right side systematically for P/P:

$$\frac{dy_{CO_2}}{dm} = - \frac{E \cdot y_{CO_2}\left(1 - \left(\frac{1}{K_1}\right) \cdot \left(\frac{P_{H_2O}}{P} \cdot \frac{P}{P_{CO_2}} \cdot \frac{P_{CO}}{P_{H_2}}\right)\right)}{\left(1 + G\left(\frac{P_{H_2O}}{P} \cdot \frac{P}{P_{H_2}}\right) + \sqrt{K_{H_2} P_{H_2}} \cdot \left(\frac{\sqrt{P}}{\sqrt{P}}\right) + K_{H_2O} \cdot P \cdot \frac{P_{H_2O}}{P}\right)} \tag{136}$$

Applying equation (91), and multiplying the right-hand numerator by P/P again:

$$\frac{dy_{CO_2}}{dm} = - \frac{E \cdot y_{CO_2}\left(1 - \left(\frac{1}{K_1}\right) \cdot \left(\frac{y_{H_2O}}{y_{CO_2}} \cdot \frac{P_{CO}}{P_{H_2}} \cdot \frac{P}{P}\right)\right)}{\left(1 + G\left(\frac{y_{H_2O}}{y_{H_2}}\right) + \sqrt{K_{H_2} P} \cdot \left(\frac{\sqrt{P_{H_2}}}{\sqrt{P}}\right) + I \cdot \frac{P_{H_2O}}{P}\right)} \tag{137}$$

$$\frac{dy_{CO_2}}{dm} = - \frac{E \cdot y_{CO_2}\left(1 - \left(\frac{1}{K_1}\right) \cdot \left(\frac{y_{H_2O}}{y_{CO_2}} \cdot \frac{P_{CO}}{P} \cdot \frac{P}{P_{H_2}}\right)\right)}{\left(1 + G\left(\frac{y_{H_2O}}{y_{H_2}}\right) + \sqrt{K_{H_2} P} \cdot \sqrt{y_{H_2}} + I \cdot y_{H_2O}\right)} \tag{138}$$

Using equation (90), and applying an analogous procedure to equations (130) to (133), the dimensionless model is obtained:

$$\frac{dy_{CO_2}}{dm} = -\frac{E \cdot y_{CO_2}\left(1-\left(\frac{1}{K_1}\right)\cdot\left(\frac{y_{H_2O}\cdot y_{CO}}{y_{CO_2}\cdot y_{H_2}}\right)\right)}{\left(1+G\left(\frac{y_{H_2O}}{y_{H_2}}\right)+H\cdot\sqrt{y_{H_2}}+I\cdot y_{H_2O}\right)} \tag{73}$$

$$\frac{dy_{H_2}}{dm} = -\frac{E \cdot y_{CO_2}\left(1-\left(\frac{1}{K_1}\right)\cdot\left(\frac{y_{H_2O}\cdot y_{CO}}{y_{CO_2}\cdot y_{H_2}}\right)\right)}{\left(1+G\left(\frac{y_{H_2O}}{y_{H_2}}\right)+H\cdot\sqrt{y_{H_2}}+I\cdot y_{H_2O}\right)} \tag{74}$$

$$\frac{dy_{CO}}{dm} = \frac{E \cdot y_{CO_2}\left(1-\left(\frac{1}{K_1}\right)\cdot\left(\frac{y_{H_2O}\cdot y_{CO}}{y_{CO_2}\cdot y_{H_2}}\right)\right)}{\left(1+G\left(\frac{y_{H_2O}}{y_{H_2}}\right)+H\cdot\sqrt{y_{H_2}}+I\cdot y_{H_2O}\right)} \tag{75}$$

$$\frac{dy_{H_2O}}{dm} = \frac{E \cdot y_{CO_2}\left(1-\left(\frac{1}{K_1}\right)\cdot\left(\frac{y_{H_2O}\cdot y_{CO}}{y_{CO_2}\cdot y_{H_2}}\right)\right)}{\left(1+G\left(\frac{y_{H_2O}}{y_{H_2}}\right)+H\cdot\sqrt{y_{H_2}}+I\cdot y_{H_2O}\right)} \tag{76}$$

$$\frac{dy_{He}}{dm} = 0 \tag{77}$$

A.3 **Model of Graaf, Stamhuis and Beenackers (1988)**

Applying the hypothesis of ideal gas conditions, the fugacity of components is replaced by partial pressure, then the rate equation of Graaf, Stamhuis and Beenackers becomes (Dehghanpoor *et al*., 2022):

$$r_{RWGS} = \frac{k_1 \cdot K_{CO_2}\cdot\left(P_{CO_2}\cdot P_{H_2}-\frac{P_{H_2O}\cdot P_{CO}}{K_1}\right)}{\left(1+K_{CO}\cdot P_{CO}+K_{CO_2}\cdot P_{CO_2}\right)\left(P_{H_2}^{0.5}+P_{H_2O}\cdot\left(\frac{K_{H_2O}}{K_{H_2}^{0.5}}\right)\right)} \tag{139}$$

Thus, it is possible to employ the initial procedure described by equations (116) to (119) to obtain the reactor model in terms of partial pressures:

$$\frac{dP_{CO_2}}{dW} = -\left(\frac{R \cdot T}{q}\right) \cdot \frac{k_1 \cdot K_{CO_2} \cdot \left(P_{CO_2} \cdot P_{H_2} - \frac{P_{H_2O} \cdot P_{CO}}{K_1}\right)}{\left(1 + K_{CO} \cdot P_{CO} + K_{CO_2} \cdot P_{CO_2}\right)\left(P_{H_2}^{0.5} + P_{H_2O} \cdot \left(\frac{K_{H_2O}}{K_{H_2}^{0.5}}\right)\right)} \quad (140)$$

$$\frac{dP_{H_2}}{dW} = -\left(\frac{R \cdot T}{q}\right) \cdot \frac{k_1 \cdot K_{CO_2} \cdot \left(P_{CO_2} \cdot P_{H_2} - \frac{P_{H_2O} \cdot P_{CO}}{K_1}\right)}{\left(1 + K_{CO} \cdot P_{CO} + K_{CO_2} \cdot P_{CO_2}\right)\left(P_{H_2}^{0.5} + P_{H_2O} \cdot \left(\frac{K_{H_2O}}{K_{H_2}^{0.5}}\right)\right)} \quad (141)$$

$$\frac{dP_{CO}}{dW} = \left(\frac{R \cdot T}{q}\right) \cdot \frac{k_1 \cdot K_{CO_2} \cdot \left(P_{CO_2} \cdot P_{H_2} - \frac{P_{H_2O} \cdot P_{CO}}{K_1}\right)}{\left(1 + K_{CO} \cdot P_{CO} + K_{CO_2} \cdot P_{CO_2}\right)\left(P_{H_2}^{0.5} + P_{H_2O} \cdot \left(\frac{K_{H_2O}}{K_{H_2}^{0.5}}\right)\right)} \quad (142)$$

$$\frac{dP_{H_2O}}{dW} = \left(\frac{R \cdot T}{q}\right) \cdot \frac{k_1 \cdot K_{CO_2} \cdot \left(P_{CO_2} \cdot P_{H_2} - \frac{P_{H_2O} \cdot P_{CO}}{K_1}\right)}{\left(1 + K_{CO} \cdot P_{CO} + K_{CO_2} \cdot P_{CO_2}\right)\left(P_{H_2}^{0.5} + P_{H_2O} \cdot \left(\frac{K_{H_2O}}{K_{H_2}^{0.5}}\right)\right)} \quad (143)$$

$$\frac{dy_{He}}{dW} = 0 \quad (144)$$

Multiplying equation (140) by W_0/P:

$$\frac{dP_{CO_2}}{dW} \cdot \frac{W_0}{P} = \frac{-\left(\frac{R \cdot T}{q}\right) \cdot k_1 \cdot \frac{W_0}{P} \cdot K_{CO_2} \cdot \left(P_{CO_2} \cdot P_{H_2} - \frac{P_{H_2O} \cdot P_{CO}}{K_1}\right)}{\left(1 + K_{CO} \cdot P_{CO} + K_{CO_2} \cdot P_{CO_2}\right)\left(P_{H_2}^{0.5} + P_{H_2O} \cdot \left(\frac{K_{H_2O}}{K_{H_2}^{0.5}}\right)\right)} \quad (145)$$

Applying the correction factor f_P for pressure on the right-hand side, and using equations (83) and (84):

$$\frac{d\left(\frac{P_{CO_2}}{P}\right)}{d\left(\frac{W}{W_0}\right)} = -\frac{\frac{k_1 \cdot R \cdot T \cdot f_P \cdot W_0}{q \cdot P} \cdot K_{CO_2} \cdot \left(P_{CO_2} \cdot P_{H_2} - \frac{P_{H_2O} \cdot P_{CO}}{K_1}\right)}{\left(1 + K_{CO} \cdot P_{CO} + K_{CO_2} \cdot P_{CO_2}\right)\left(P_{H_2}^{0.5} + P_{H_2O} \cdot \left(\frac{K_{H_2O}}{K_{H_2}^{0.5}}\right)\right)} \quad (146)$$

Multiplying the numerator and denominator by $\frac{\sqrt{P}}{P}$:

$$\frac{dy_{CO_2}}{dm} = -\frac{\frac{k_1 \cdot R \cdot T \cdot f_P \cdot W_0}{q \cdot P} \cdot K_{CO_2} \cdot \left(P_{CO_2} \cdot P_{H_2} - \frac{P_{H_2O} \cdot P_{CO}}{K_1}\right) \cdot \frac{\sqrt{P}}{P}}{\left(1 + K_{CO} \cdot P_{CO} + K_{CO_2} \cdot P_{CO_2}\right)\left(P_{H_2}^{0.5} + P_{H_2O} \cdot \left(\frac{K_{H_2O}}{K_{H_2}^{0.5}}\right)\right) \cdot \frac{\sqrt{P}}{P}} \tag{147}$$

$$\frac{dy_{CO_2}}{dm} = \frac{-\frac{k_1 \cdot R \cdot T \cdot f_P \cdot W_0 \cdot \sqrt{P}}{q \cdot P} \cdot K_{CO_2} \cdot \left(P_{CO_2} \cdot P_{H_2} - \frac{P_{H_2O} \cdot P_{CO}}{K_1}\right) \cdot \frac{1}{P}}{\left(1 + K_{CO} \cdot P_{CO} + K_{CO_2} \cdot P_{CO_2}\right)\left(\frac{P_{H_2}^{0.5} \cdot \sqrt{P}}{\sqrt{P} \cdot \sqrt{P}} + \frac{P_{H_2O}}{P} \cdot \left(\frac{K_{H_2O} \cdot \sqrt{P}}{K_{H_2}^{0.5}}\right)\right)} \tag{148}$$

Applying equations (92) and (95):

$$\frac{dy_{CO_2}}{dm} = -\frac{J \cdot K_{CO_2} \cdot \left(\frac{P_{CO_2}}{P} \cdot P_{H_2} - \frac{P_{H_2O}}{P} \cdot \frac{P_{CO}}{K_1}\right)}{\left(1 + K_{CO} \cdot P_{CO} + K_{CO_2} \cdot P_{CO_2}\right)\left(\sqrt{y_{H_2}} + y_{H_2O} \cdot Q\right)} \tag{149}$$

Multiplying the numerator and denominator by *P*/*P*:

$$\frac{dy_{CO_2}}{dm} = -\frac{J \cdot K_{CO_2} \cdot P \cdot \left(y_{CO_2} \cdot P_{H_2} - y_{H_2O} \cdot \frac{P_{CO}}{K_1}\right) \cdot \frac{1}{P}}{\left(1 + K_{CO} \cdot P_{CO} + K_{CO_2} \cdot P_{CO_2}\right) \cdot \frac{P}{P}\left(\sqrt{y_{H_2}} + y_{H_2O} \cdot Q\right)} \tag{150}$$

Applying equation (94):

$$\frac{dy_{CO_2}}{dm} = -\frac{J \cdot N \cdot \left(y_{CO_2} \cdot \frac{P_{H_2}}{P} - \frac{y_{H_2O} \cdot P_{CO}}{P \cdot K_1}\right)}{\left(\frac{P}{P} + K_{CO} \cdot P \cdot \frac{P_{CO}}{P} + K_{CO_2} \cdot P \cdot \frac{P_{CO_2}}{P}\right)\left(\sqrt{y_{H_2}} + y_{H_2O} \cdot Q\right)} \tag{151}$$

Using equation (93):

$$\frac{dy_{CO_2}}{dm} = -\frac{J \cdot N \cdot \left(y_{CO_2} \cdot y_{H_2} - \frac{y_{H_2O} \cdot y_{CO}}{K_1}\right)}{\left(1 + L \cdot y_{CO} + N \cdot y_{CO_2}\right)\left(\sqrt{y_{H_2}} + y_{H_2O} \cdot Q\right)} \tag{152}$$

Applying an analogous procedure to equations (141) to (144) the dimensionless model is obtained:

$$\frac{dy_{CO_2}}{dm} = -\frac{J \cdot N \cdot \left(y_{CO_2} \cdot y_{H_2} - \frac{y_{H_2O} \cdot y_{CO}}{K_1}\right)}{\left(1 + L \cdot y_{CO} + N \cdot y_{CO_2}\right)\left(\sqrt{y_{H_2}} + y_{H_2O} \cdot Q\right)} \tag{78}$$

$$\frac{dy_{H_2}}{dm} = -\frac{J \cdot N \cdot \left(y_{CO_2} \cdot y_{H_2} - \frac{y_{H_2O} \cdot y_{CO}}{K_1}\right)}{\left(1 + L \cdot y_{CO} + N \cdot y_{CO_2}\right)\left(\sqrt{y_{H_2}} + y_{H_2O} \cdot Q\right)} \tag{79}$$

$$\frac{dy_{CO}}{dm} = \frac{J \cdot N \cdot \left(y_{CO_2} \cdot y_{H_2} - \frac{y_{H_2O} \cdot y_{CO}}{K_1}\right)}{\left(1 + L \cdot y_{CO} + N \cdot y_{CO_2}\right)\left(\sqrt{y_{H_2}} + y_{H_2O} \cdot Q\right)} \tag{80}$$

$$\frac{dy_{H_2O}}{dm} = \frac{J \cdot N \cdot \left(y_{CO_2} \cdot y_{H_2} - \frac{y_{H_2O} \cdot y_{CO}}{K_1}\right)}{\left(1 + L \cdot y_{CO} + N \cdot y_{CO_2}\right)\left(\sqrt{y_{H_2}} + y_{H_2O} \cdot Q\right)} \tag{81}$$

$$\frac{dy_{He}}{dW} = 0 \tag{82}$$

APPENDIX B – Equilibrium conversion calculation

Let X_{eq} be the CO_2 conversion at equilibrium, given by:

$$X_{eq} = \frac{P^0_{CO_2} - P^{eq}_{CO_2}}{P^0_{CO_2}} \tag{153}$$

in which P^0_{CO2} is the partial pressure of CO_2 at the inlet in atm, and P^{eq}_{CO2} is the partial pressure of CO_2 at equilibrium in atm.

Therefore:

$$P^{eq}_{CO_2} = P^0_{CO_2} \cdot \left(1 - X_{eq}\right) \tag{154}$$

While the partial pressures of the other components at equilibrium are given by:

$$P^{eq}_{H_2} = P^0_{H_2} - P^0_{CO_2} \cdot X_{eq} \tag{155}$$

$$P^{eq}_{CO} = P^0_{CO_2} \cdot X_{eq} \tag{156}$$

$$P^{eq}_{H_2O} = P^0_{CO_2} \cdot X_{eq} \tag{157}$$

being P^0_{H2} the partial pressure of H_2 at the inlet in atm, and P^{eq}_i is the partial pressure of component *i* at equilibrium in atm.

Then the equilibrium constant K_1 is equal to:

$$K_1 = \frac{P^{eq}_{CO} \cdot P^{eq}_{H_2O}}{P^{eq}_{CO_2} \cdot P^0_{H_2}} = \frac{P^0_{CO_2} \cdot X_{eq} \cdot P^0_{CO_2} \cdot X_{eq}}{P^0_{CO_2} \cdot \left(1 - X_{eq}\right) \cdot \left(P^0_{H_2} - P^0_{CO_2} \cdot X_{eq}\right)} \tag{158}$$

However, at a given temperature *T*, the equilibrium constant for the RWGS reaction can be calculated by equation (28):

$$K_1 = 10^{\left(-\frac{2073}{T} + 2.029\right)} \tag{28}$$

Thus, knowing the temperature and the partial pressures of CO_2 and H_2 at the inlet, X_{eq} is the value capable of zeroing the value of the objective function f^{Xeq}_{obj}:

$$f_{obj}^{X_{eq}} = 10^{\left(-\frac{2073}{T}+2.029\right)} - \frac{P_{CO_2}^0 \cdot X_{eq} \cdot P_{CO_2}^0 \cdot X_{eq}}{P_{CO_2}^0 \cdot \left(1 - X_{eq}\right) \cdot \left(P_{H_2}^0 - P_{CO_2}^0 \cdot X_{eq}\right)} \quad (159)$$

APPENDIX C – Experimental data from tests at fixed temperatures

Table 16 – Average of experimental CO_2 conversion values in tests at temperature levels with a H_2/CO_2 molar ratio of 1:1

Temperature (°C)	Space velocity ($m^3\ kg^{-1}\ h^{-1}$)		
	18	30	42
330	3.73	3.05	2.42
380	9.13	7.77	7.43
430	17.1	15.3	14.1

Source: The author, 2024.

Table 17 – Average of experimental CO_2 conversion values in tests at temperature levels with a H_2/CO_2 molar ratio of 2.5:1

Temperature (°C)	Space velocity ($m^3\ kg^{-1}\ h^{-1}$)		
	18	30	42
330	4.42	3.15	2.43
380	13.5	10.8	7.44
430	24.0	19.7	16.4

Source: The author, 2024.

Table 18 – Average of experimental CO_2 conversion values in tests at temperature levels with a H_2/CO_2 molar ratio of 4:1

Temperature (°C)	Space velocity ($m^3\ kg^{-1}\ h^{-1}$)		
	18	30	42
330	8.81	7.06	5.65
380	20.0	16.6	13.7
430	32.2	28.9	25.3

Source: The author, 2024.

APPENDIX D – Experimental data from temperature ramp tests

Table 19 – Light-off test at 30 $m^3\ kg^{-1}\ h^{-1}$ with H_2/CO_2 molar ratio of 1:1

Temperature (°C)	CO_2 conversion (%)
27	0.00
99	0.00
164	0.00
232	0.23
304	1.23
370	6.47
444	16.9
500	25.0

Source: The author, 2024.

Table 20 – Light-off test at 30 $m^3\ kg^{-1}\ h^{-1}$ with H_2/CO_2 molar ratio of 2.5:1

Temperature (°C)	CO_2 conversion (%)
29	0.00
72	0.00
105	0.00
171	0.76
240	1.15
308	2.52
378	9.67
447	23.7
499	35.0

Source: The author, 2024.

Table 21 – Light-off test at 30 $m^3\ kg^{-1}\ h^{-1}$ with H_2/CO_2 molar ratio of 4:1

Temperature (°C)	CO_2 conversion (%)
28	0.00
102	0.00
168	0.00
234	0.00
303	3.37
373	13.2
440	29.7
500	43.7

Source: The author, 2024.

ANNEX – Results of simulations from literature

Figure 18 – Evaluation of the effect of different operational parameters on the equilibrium composition

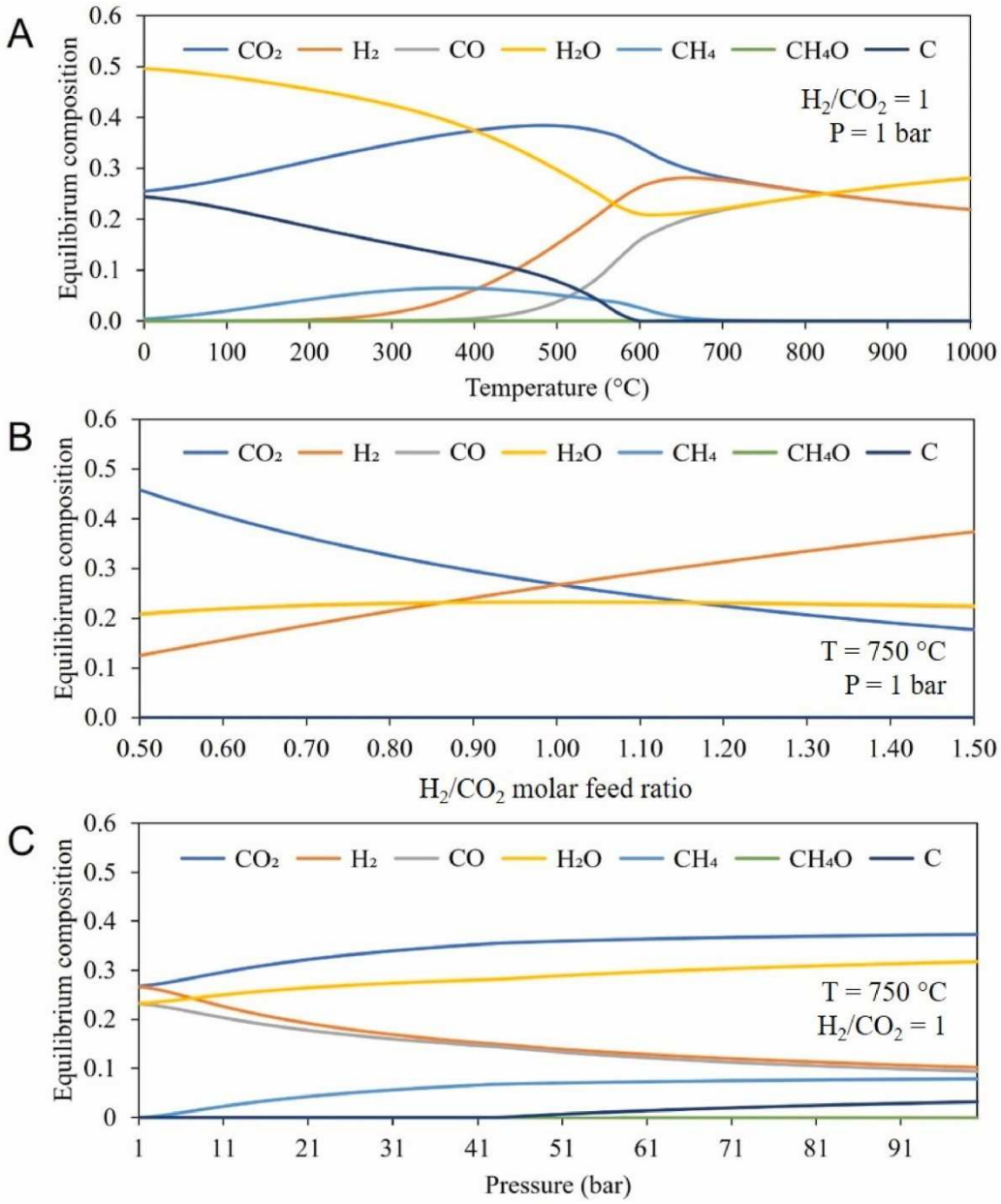

Legend: (a) – Effect of temperature; (b) – Effect of H_2/CO_2 molar feed ratio; (c) – Effect of pressure.

Source: Santos *et al.*, 2023.

Figure 19 – CO_2 conversion in the RWGS reactor as a function of GHSV at 850 °C

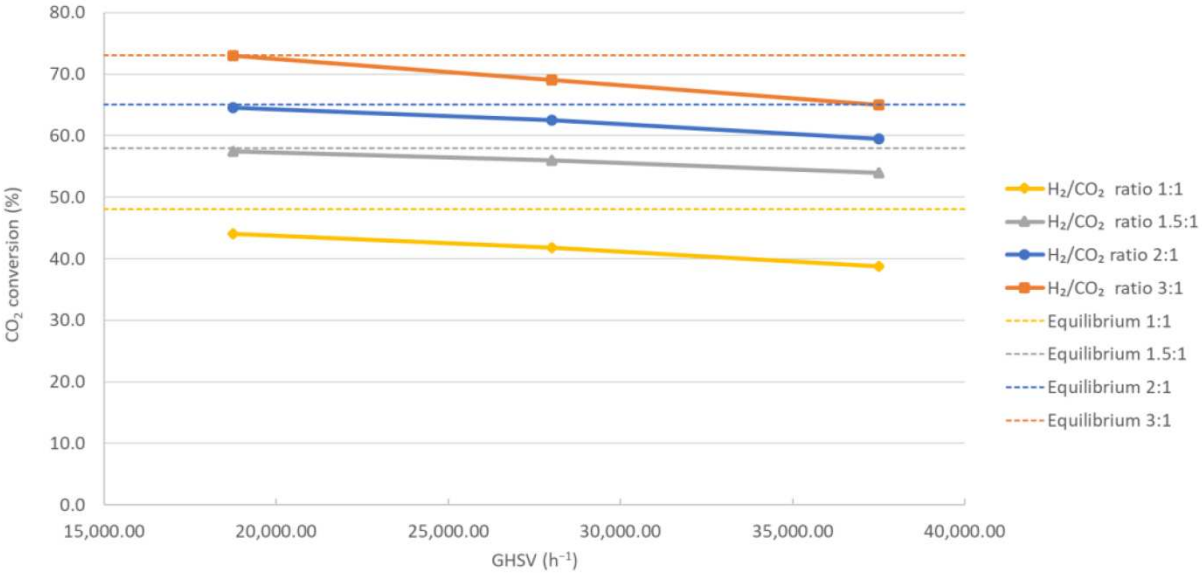

Source: Reinikainen *et al.*, 2022.